Climate and climate processes during the Upper Miocene - Sensitivity studies with coupled general circulation models

Dissertation

zur Erlangung des Grades eines Doktors der Naturwissenschaften

der Geowissenschaftlichen Fakultät
der Eberhard-Karls Universität Tübingen

vorgelegt von
Anke Steppuhn
aus Bad Oldesloe

2002

Tag der mündlichen Prüfung: 28. Juni 2001

Dekan: Prof. Dr. Dr.h.c. M. Satir

1. Berichterstatter: Prof. Dr. V. Mosbrugger

2. Berichterstatter: Prof. Dr. Ch. Hemleben

Contents

Abstract

The climate of the early Neogene differs basically from today's situation by a distinct warmer climate on the Northern Hemisphere. By using palaeoclimate reconstructions it can be proofed on the basis of both terrestrial and marine proxy data that the averaged temperatures were higher in the mid and high latitudes. In order to resolve the causes for this climatic shift outlined above, a time slice experiment for the Upper Miocene (Tortonian ≈ 8 MaBP) was performed in this work. Therefore general circulation models were used which consider a coupling of the ocean and the atmosphere. For several experiments the models ECHAM4/ML and CLIMBER-2 were utilized in order to describe the atmospheric circulation pattern. A validation of this pattern is possible with terrestrial climatic specifications from proxy data. Additionally, several sensitivity studies were performed in order to analyse atmospheric changes caused by slight differences in boundary conditions. For a better understanding of climate processes of the selected time slice, models of different complexity were chosen. In order to adapt the models to the Tortonian situation, the boundary conditions were modified with respect to the orography (world-wide reduction of mountains), continental ice sheets (an ice-free Greenland shield) and the oceanic heat transport (reduction). The variation of the oceanic heat transport is based on marine δ^{18}O data of planktic foraminifera and was implemented into the model ECHAM4/ML. The simulation results of ECHAM show that the reduction of the oceanic heat transport generally is in conformity with marine proxy data. The results of the standard Tortonian run represent a warmer climate at high latitudes. The temperature rises, however, are far below the values which are suggested by proxy data. The comparison of precipitation and temperature data of the ECHAM results with quantitative terrestrial proxy data shows that a doubling of the atmospheric carbon dioxide is necessary in order to simulate the reconstructed warmer climates in mid-latitudes. In contrast to the standard Tortonian run, the results of the double CO_2 run yield an intensification of the Asian and African monsoon systems and an increase of the North Atlantic Oscillation. The latter explains the more humid and warmer climate over Europe which is specific for the Tortonian. The results of the simple model CLIMBER indicate a reduction of the Northern Hemisphere sea ice extent, a slight reduction of the seasonality at high latitudes, and a reduced oceanic heat transport. This is in conformity with the high-complex model ECHAM and allows therefore further sensitivity studies with the economical model CLIMBER. The

performed experiments show that slight modifications in the palaeogeography have an enormous influence on the atmospheric circulation. In addition the distribution of the vegetation shows an important role in the monsoonal circulation system and in the polar area. In both regions the vegetation leads to a positive feedback mechanism, which explains partially the higher temperatures for the Neogene.

Zusammenfassung

Das Klima des frühen Neogens unterscheidet sich im wesentlichen von der heutigen Situation durch ein deutlich wärmeres Klima auf der Nordhemisphäre. Paläoklimatische Rekonstruktionsanalysen sowohl aufgrund terrestrischer als auch aufgrund mariner Proxy-Daten belegen durchschnittlich höhere Temperaturen in den mittleren bis hohen Breiten. Um den Ursachen für diese Klimaverschiebung näher zu kommen, wurde in dieser Arbeit eine Zeitscheibensimulation für das Obere Miozän (Torton ≈ 8 MaBP) mit Hilfe von allgemeinen Zirkulationsmodellen durchgeführt, die eine Kopplung von Ozean und Atmosphäre berücksichtigen. Für die Experimente wurden die Modelle ECHAM4/ML und CLIMBER-2 herangezogen. Diese Modelle ermöglichen es, den atmosphärischen Zustand für das Torton zu beschreiben und mit terrestrischen Klimaangaben zu validieren. Darüber hinaus wurden mit den Modellen Sensitivitätsstudien durchgeführt, die einen Überblick über die atmosphärischen Folgen geben, die durch mögliche geringfügige Unterschiede in den Randbedingungen verursacht werden. Für ein besseres Verständnis der zugrunde liegenden klimatischen Prozesse der selektierten Zeitscheibe wurden deshalb Modelle unterschiedlicher Komplexität ausgewählt. Um die Modelle der Situation im Torton anzupassen, wurden die Randbedingungen hinsichtlich der Orographie (weltweite Reduktion der Gebirge), der kontinentalen Vereisung (Eisfreiheit von Grönland) und des ozeanischen Wärmetransports (Reduktion) geändert. Die Variation des ozeanischen Wärmetransports beruht hierbei auf marinen δ^{18}O Daten planktischer Foraminiferen und wurde entsprechend in das hoch aufgelöste Modell ECHAM4/ML implementiert. Die Simulationsergebnisse von ECHAM zeigen, dass die Reduktion des ozeanischen Wärmetransports generell im Einklang mit marinen Proxy-Daten steht. Der Referenzlauf für das Torton ergibt zwar ein wärmeres Klima in höheren Breiten, die Temperaturanstiege liegen jedoch weit unter den aus Proxy-Daten prognostizierten Werten. Der Vergleich von Niederschlags- und Temperaturdaten der ECHAM Ergebnisse mit quantitativen, terrestrischen Proxy-Daten zeigt, dass eine Verdopplung des atmosphärischen Kohlendioxids notwendig ist, um die rekonstuierten wärmeren Klimate in mittleren Breiten zu simulieren. Die Ergebnisse des Laufs mit doppeltem CO_2-Gehalt weisen im Gegensatz zum Referenzlauf zu einer Intensivierung des asiatischen und afrikanischen Monsunsystems und zu einer Erhöhung der Nord-Atlantischen Oszillation hin. Letzteres erklärt das für das Torton spezifische, feuchtere und wärmere Klima über Europa. Die Ergebnisse des einfachen Modells CLIM-

BER weisen im Einklang mit dem hochkomplexen Modell ECHAM eine Reduktion des nordhemisphärischen Meereises, eine leichte Reduktion der Saisonalität in hohen Breiten und einen reduzierten ozeanischen Wärmetransport auf. Diese Übereinstimmungen der Simulationsergebnisse lassen weitere Sensitivitätsstudien mit dem kostengünstigen Modell CLIMBER zu. Die entsprechenden CLIMBER Experimente zeigen, dass geringfügige Änderungen der Paläogeographie einen enormen Einfluss auf die atmosphärische Zirkulation haben. Außerdem spielt die Verteilung der Vegetation eine wichtige Rolle im monsunalen Zirkulationssystem und im polaren Bereich. In beiden Regionen führt die Vegetation zu einem positiven Rückkopplungsmechanismus, der die höheren Temperaturen im Neogen zum Teil erklären kann.

Chapter 1

Introduction

The heated debate about a possible temperature increase of up to 5.8°C for the next century (Working Group I of the IPCC 2001) causes a general interest in predicting how climatic change, such as a temperature increase, will seriously affect our lives. For a complete understanding of our complex climate system and possible changes for the next couple of decades it is important to analyse simulated data validated by empirical data. Several numerical studies have shown that contemporary general circulation models simulate modern climate situation quite well (e.g., Mote and O'Neill 2000). Apart from climate predictions, these models are also useful for reconstructing atmospheric and oceanic circulation patterns for specific time slices (e.g., Dutton and Barron 1996, Upchurch et al. 1999, Haywood et al. 2000, Sellwood et al. 2000). These studies show that there are often significant agreements between proxy data and simulation results. This means that numerical models can be used as a tool for understanding different climates and climatic processes which were driven by different internal and external forcings.

Still, individual components of the climate system, including the hydrosphere, atmosphere, cryosphere, pedosphere and biosphere and their interactions, are not completely understood. Due to the complexity of the climate system a variety of numerical models exist (e.g., Gordon et al. 2000, Herterich and Berger 1993, Roeckner et al. 1993, Petoukhov 2000). These models differ from each other by their choice of modules, their physical description of the radiation transfer, their parametrizations, and their dimensional complexity. In order to understand palaeoclimates, different types of climate models are used to provide a comprehensive analysis of different climate conditions. The strategy of using

models of high and intermediate complexity has been used by Kubatzki et al. (2000) and Montoya (1999). They suggest that their choice of models is not only of advantage for a better understanding for palaeoclimate characteristics, but also for understanding the discrepancies between simulation results and proxy data. Therefore, in this work two models of different complexity were used. First, simulations were performed with the complex model ECHAM4 coupled to a slab ocean, which provides detailed atmospheric information. Due to the model's high resolution its results can be validated with quantitative temperature and precipitation proxy data. Second, simulations were performed with the low resolution model CLIMBER-2 to investigate interactions between large-scale circulation and the biosphere.

Palaeontological and geological data indicate that the earth's climate has varied significantly through geologic time (see fig. 1.1) with notable changes occuring over different time scales. The time period between the interglacials which occurred during the last 1 million years (Pleistocene) are in the order of some 100000 years (e.g., Stocker 1999, Berger et al. 1993). In contrast, the change from a greenhouse climate (e.g., Cretaceous) to a bi-polar-icehouse climate (Neogene which includes the Pliocene and Miocene) occurred over a time period of millions of years (see fig. 1.1). These changes appear to be caused by different internal (e.g., carbon cycle changes and vegetation changes) and external (e.g., change of orbital parameters) forcings. In order to contribute a better understanding of pre-Quaternary climates, our work is concentrated on the time-slice Tortonian (Upper Miocene), which corresponds to a time span of one to four million years (7-11 Ma BP). When applying such a long time span in palaeoclimate modeling, homogeneous boundary conditions such as the orography should be assumed. This also means that for describing changes of the averaged state of the anomalous climate (Tortonian run) in comparison to modern conditions (Control run) the first moment (the means) of some decisive variables are sufficient for our numerical analysis. In order to evaluate deviations on the synoptic scale (weather regimes), the second moments (standard deviations) were also taken into account.

For pre-Quaternary studies there is a special interest in specifying and understanding the forcings for palaeoclimate conditions different from today. The two epochs of the Neogene, which are the Miocene (22-5Ma BP) and the Pliocene (5-2Ma BP) (fig. 1.1),

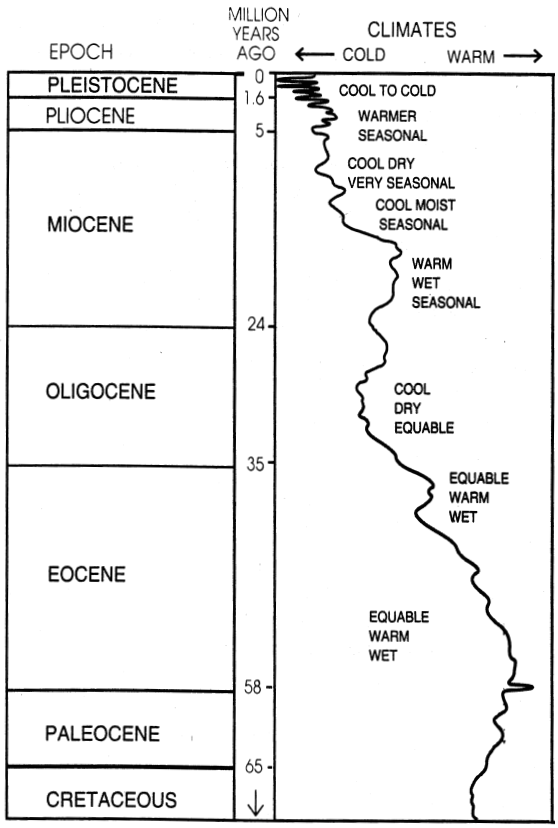

Figure 1.1: *Climatic trend of the Cenozoic based on ratio of heavy and light isotopes measured in the shells from foraminifera. Copied from Partridge et al. 1995*

are characterized by global cooling. The cooling at high to mid-latitudes was combined with an expansion of the cryosphere on the Northern Hemisphere (Kennett 1995). The step by step decrease in temperature begins with the Miocene Climate Optimum, which is dated $\approx$ 16 Ma BP by Flower and Kennett (1994), and ends with the "Ice Climates" during the Pleistocene. Wright and Miller (1996) proposed that several factors were responsible for Cenozoic cooling. A variety of numerical studies have been focused on past warm climates, such as the Cretaceous (e.g., Upchurch et al. 1998, Sellwood et al. 1994), and also on glacials (e.g., Lorenz et al. 1996) and interglacials (Kubatzki et al. 2000) during the last one million years. However, numerical investigations on transitional climates being arranged between "greenhouse" and "icehouse" conditions are quite rare. In spite of this fact, the quantity and reliability of late Neogene terrestrial proxy data has been increased over the past decade (Mosbrugger and Schilling 1992). With regard to the Tortonian time-slice, the density of both marine and terrestrial proxy data is great (e.g., Zahn and Mix 1991 Mai 1995, Utescher et al. 2000, Wolfe 1995). Therefore this work

focuses on Tortonian climate because proxy data are sufficient for the numerical set-up and the validation of results.

With respect to earth history, land-sea distribution during the last 10 million years was not significantly different from today's despite small variations in ocean gateways such like the Panama Strait. This roughly same distribution of land and sea is the basis for the assumption that the general pattern of the atmospheric and oceanic circulation of the Tortonian was almost alike the present-day one. Whereas the intensification of the circulation system is probably different from the Recent one. In contrast to today, the high-latitudinal climate was warmer as suggested by proxy data (e.g., Mai 1995, Utescher et al. 2000, Wolfe 1995). Several investigations have addressed the question of which processes may have lead to such a warm climate during the late Miocene. Dutton and Barron (1996) suggest that higher temperatures at high-latitudes resulted from greater areal extended forest vegetation relative to today. Fluteau et al. (1999) and Ramstein et al. (1997) emphasize that the remains of the Paratethys had a significant influence on the intensification of regional climate circulations (e.g., the Asian monsoon system) during the late Miocene. The above-mentioned studies, however, are based on atmospheric general circulation models with prescribed sea surface temperatures for the Miocene ocean. Thus, the impact of the palaeo-ocean on the atmospheric circulation pattern is not completely considered. In order to minimize this deficiency our studies take the palaeo-ocean into account. Therefore a mixed-layer ocean and a three-dimensional ocean is considered with regard to the models ECHAM and CLIMBER, respectively.

Significant climate changes during the Neogene can be linked to variations in the oceanic conveyer belt (e.g., Mikolajewicz et al. 1993, Mikolajewicz and Crowley 1997). These variations are caused by the closures of seaways between Atlantic and Pacific Ocean (Panama Strait) and between Pacific and Indian Ocean (e.g., Collins et al. 1996, Tsuchi 1997). It is proposed that these closures of ocean gateways induced an intensification of North Atlantic and Pacific ocean currents during the last 20 Ma (Barron and Peterson 1991, Haug and Tiedemann 1998, Tsuchi 1997). Numerical simulations (e.g., Bice et al. 2000, Maier-Raimer et al. 1990, Mikolajewicz et al. 1993, Mikolajewicz and Crowley 1997) support this fact. Therefore in this study a qualitatively changed oceanic heat transport is assumed for the Upper Miocene time slice. In order to calculate a different heat transport

in the ocean, palaeo sea surface temperatures are derived from oxygen isotope values in planktonic foraminifera. And used to compute the meridional temperature gradient. The slope of the latitudinal temperature gradient is assumed to be a measure for the oceanic heat transport. Hence a comparison of Recent and palaeo-temperature gradients generates a basis for the variation of the oceanic heat transport. The corresponding approach is explained in detail in chapter 2.

One problem to be investigated by palaeoclimatic modeling of the Tortonian are the climatic forcings that provided high latitudes with warmer conditions. Although it is still not known with certainty which mechanisms are most important for warm polar and mid-latitudinal temperatures, two main hypotheses have been proposed.

- The first hypothesis proposes changes in heat transport in the climate system. As there is a gain of heat at the tropics and a deficiency at high latitudes, the fluids atmosphere and ocean are transferring heat from the equator towards the poles. The intensity of the heat transport, however, is different for both systems and varies with time. With regard to the ocean, changes in heat transport are mainly caused by variations in the geography (e.g., Bice et al. 2000, Haug and Tiedemann 1998, Flower and Kennett 1994, Wright and Miller 1996, Woodruff and Savin 1989). The impact, however, of such changes on the atmosphere is still not completely understood (Crowley 1996). Thus one main topic in our palaeoclimate study is the consideration of the palaeo-ocean.

- The second hypothesis proposes variations in the global earths' energy budget. Changes can be caused by a different constellation of the earth to the sun (e.g., Berger et al. 1998), by different compositions of greenhouse gases in the atmosphere (e.g., Cerling et al. 1997), or by a different planetary albedo, which can be varied due to a change of the polar ice cover, the land-sea distribution, or the vegetation cover (e.g., Dutton and Barron 1997, Upchurch et al. 1998).

In order to analyse climate processes for the Upper Miocene, sensitivity studies with both the complex model ECHAM and the simple model CLIMBER are performed with regard

to the above mentioned hypotheses. Therefore experimental runs considering a changed oceanic heat transport in the ocean, different CO_2 forcing, and slight variations in palaeogeography are investigated. The results of the simulations are described in chapter 2 and 3 for ECHAM and CLIMBER, respectively. Our investigations show that an increase in atmospheric carbon dioxide can explain warmer climates at mid and high-latitudes with respect to the Northern Hemisphere for the Tortonian time-slice. Sensitivity runs show that slight changes in palaeogeography cause a significant change in atmospheric circulation which is of importance for understanding regional circulation systems. Finally, the Tortonian climate reconstruction is discussed with regard to terrestrial proxy data and responsible boundary forcings as proposed in the two previously mentioned hypotheses.

Chapter 2

Simulations with ECHAM4/ML

2.1 The model ECHAM4/ML

The atmospheric global circulation model used in this work is the ECHAM4 model, which was initially developed at the European Center for Medium Range Weather Forecast in Reading (UK). Later it was modified at the Max-Planck-Institut für Meteorologie in Hamburg (Germany) to adjust the model for climate simulations (DKRZ Modellbetreuungsgruppe 1994, DKRZ Modellbetreuungsgruppe 1997, Roeckner et al. 1996, Reockner et al. 1992). The model is coupled to a mixed-layer ocean model with a depth of 50 m (Reockner pers. comm.). In this work the T30 version was used, which corresponds to a spatial resolution of approximately 3.75° in latitude and longitude.

The mixed-layer ocean model used for this work includes the heat budget of an oceanic mixed-layer with a constant depth of h_o of 50 m. Via the heat flux in the ocean the currents can be described without including a velocity field. The energy budget at the ocean surface can be written in the form

$$C_o \frac{\partial T_m}{\partial t} = H_a - divT_o \qquad , \tag{2.1}$$

where T_m, the temperature of the mixed-layer, is equivalent with the SST (Sea Surface Temperature) because of the depth-independent temperature profile. H_a represents the net heat flux at the sea surface, $divT_o$ is the divergence of the oceanic heat transport, and $C_o = \rho_o h_o c_o$ describes the effective heat capacity of the oceanic mixed-layer, whereas ρ_o is the density of water and c_o the specific heat capacity of water. The climatological average of $divT_o$ represents the divergence of the ocean heat transport. It can also be interpreted

as the time-independent flux correction FC of the mixed-layer ocean model. Because the oceanic heat transfer is strongly dependent on the insolation rate, the flux correction contains a climatological seasonal cycle represented by monthly means. The term $divT_o$ was reconstructed from different ECHAM4 runs forced with observed SSTs. These runs provided the net heat flux H_a and the time evolution of the temperature T_m so that the divergence of oceanic heat flux could be calculated. These previous made calculations of the flux correction are used for this work.

Dependent on the property of the surface, the heat divergence must be determined for water and ice surfaces separately, as ice could be built on climatological water points (grid points which correspond to water points in the specified time span). Therefore an ice and water correction term is considered using

$$C_o \frac{\partial T_m}{\partial t} = H_a - FC(SST) - FC(ICE) \quad . \tag{2.2}$$

An ice sheet could grow and melt dependent on the water temperature. Thus the sea-ice model is thermodynamic only. There is no treatment of ice dynamics in this model. Freezing and melting rates are calculated from local imbalance between the atmospheric and oceanic heat fluxes. The phase changes are described by the following equations considering temperature differences between the ice top and the water below the ice sheet.

Growth of ice at the bottom of the sheet occurs when the skin temperature of the thin ice sheet T_s is smaller than the temperature at the bottom of the ice sheet T_b, with $T_b = -1.8°C$. Ice melts at the bottom of the ice sheet, however, if $T_s > T_b$ and $T_s \leq 0°C$. Thus the heat flux through the ice sheet is balanced by a phase change at the bottom of the ice sheet and could be expressed by

$$-L_f \rho_i \partial h_i / \partial t = H_i - FC(ICE) - FC(SST) \quad . \tag{2.3}$$

Hereby H_i is the heat flux through the ice sheet given by $H_i = k \cdot (T_s - T_b)/h_i$, whereas h_i represents the thickness of ice, k the thermal conductivity of ice, L_f the latent heat of fusion of water, and ρ_i the density of ice.

Melting mainly occurs at the top of the ice sheet. Then the skin temperature at the surface T_s reaches 0 °C and additionally the heat flux H_a at the surface is positive. Thus

the heat flux through the ice sheet can be written as

$$-L_f \rho_i \partial h_i / \partial t = H_a - FC(ICE) - FC(SST) \quad . \tag{2.4}$$

Using eq.(2.3) and (2.4) the total variation of the ice sheet is calculated. An increase in water temperature is possible if the ice has completely vanished. In this case the water temperature is calculated using eq.(2.2).

Because the oceanic heat flux pattern is driven by ocean currents, the global heat transport has to be adjusted when performing different time-slice experiments. A method has been established which enables to receive palaeo-flux corrections. The main idea is based on the pole-equator gradient of the SSTs, which can be interpreted as a measure of the heat transfer via water. In the following subsections it is outlined how palaeo-SST gradients can be obtained and how they can be used to determine palaeo-flux correction.

2.2 Setting up the Tortonian run

For the model set-up several changes are performed for representing the Tortonian time-slice situation (Upper Miocene). The topographical changes are derived from geological proxy data representing global changes in orography 10 Ma BP (Kuhlemann pers. comm.). For instance Greenland is made ice-free. Consequently for calculations of its palaeo-height iso-static assumptions have to be considered. Correspondingly Greenlands' Late Miocene orography - apart from its most southern regions - reached about 10 per cent of nowadays height. Likewise the vegetation of the Greenland-shield was changed to tundra. The orography for the Control and the Tortonian run can primarily be distinguished by a noticeable reduction of some high mountain ranges like the Alps, the Greenland shield and the Himalaya mountain range. The uplift of Tibetean Plateau during the Neogene is discussed by several authors (e.g., Wang et al. 1999, Molnar et al. 1993) resulting in different mean heights of the Tibetean Plateau in the latest Miocene. Assumptions of Tibetean Plateau height range between reaching its highest elevation during the late Miocene and as low as 1500 m. In accordance with other authors (e.g., Prell and Kutzbach 1992) the height of Tibetean Plateau for the Tortonian is assumed to have reached about

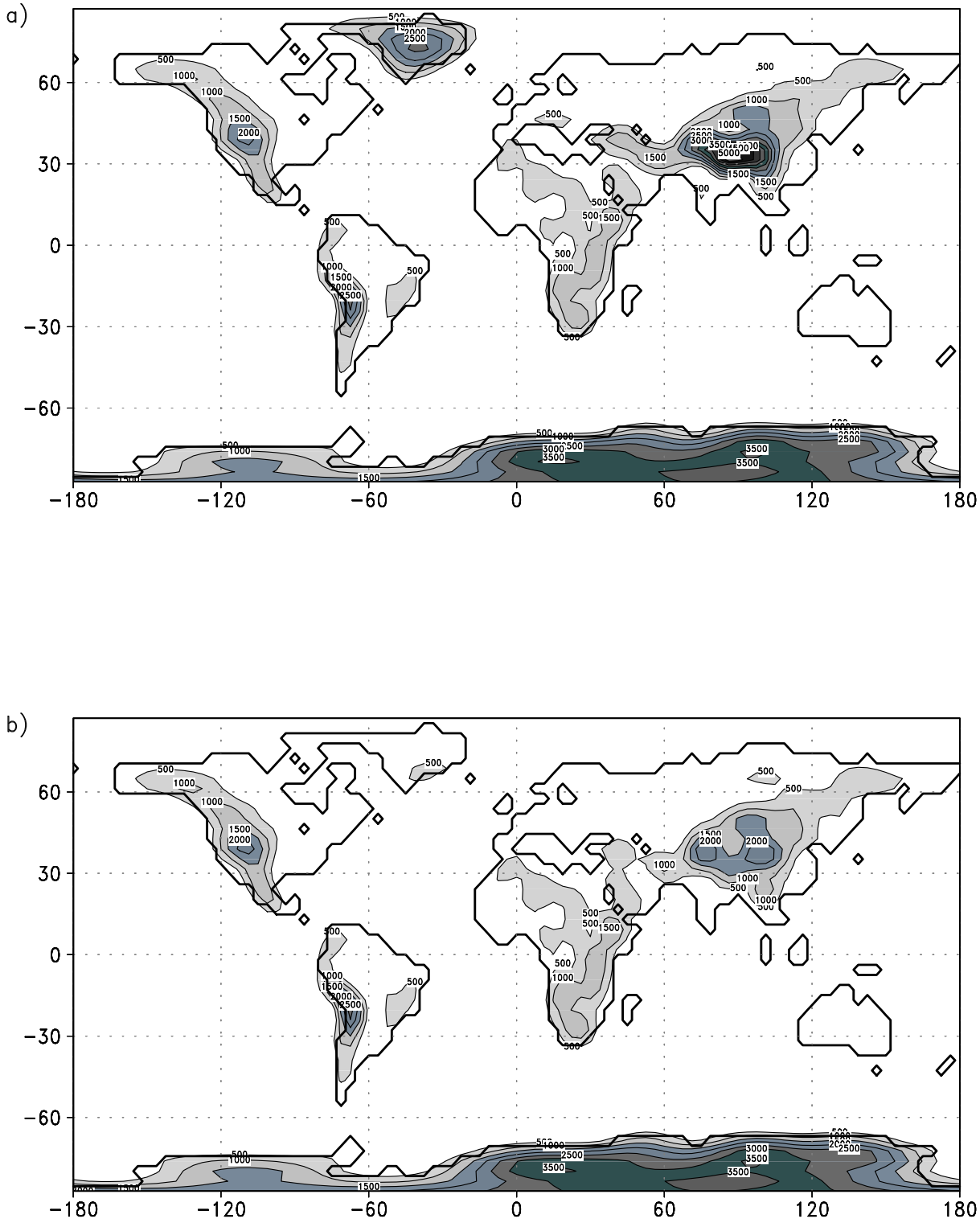

Figure 2.1: *Orography for T30 resolution for ECHAM4 a) Control run and b) Tortonian run with changes based on geological proxy data.*

half of the Recent height. The orography for the Control and Tortonian run can be seen in fig. 2.1 at which only differences of several 100 m and more can be seen. The represented values are Fourier transformed from spectral units to grid ones.

Meridional heat fluxes redress the radiation imbalance by transporting heat from low to high latitudes. In the climate system the oceanic properties like ocean currents, temperature, salinity, air-fluxes of momentum, water substances, and heat play an important role (e.g., Charnock 1994). Focusing on exchange processes of the interface atmosphere-ocean these processes are dominantly influencing both subsystems in the climate system. On these processes belong the momentum flux which drives ocean currents and the heat flux which plays an important role in the global heat budget. This ocean-atmosphere interface is prescribed by the used ECHAM4/ML model in a special manner. In this model heat loss and gain via the heat budget is prescribed for calculating ocean-air heat exchanges. The heat flux can also describe ocean currents and thus the implied oceanic heat transport. In the ECHAM4/ML model, however, all these parameters are corresponding to today's ocean. In changing the amount of oceanic heat transport in the model it is adjusted to the Tortonian situation on the basis of palaeo-SSTs derived from δ^{18}O data. In order to perform this, firstly, the data basis is described. The data base reveals, however, that pre-Quaternary SST information is quite rare on the global scale. In order to obtain sufficient SST information for climate modeling a method is developed which enables to compare highly resolved Recent and sparse palaeo-SSTs. This comparison enables to identify differences in ocean properties like the equator-pole heat transfer. Therefore in varying the oceanic heat transport on the basis of different SST-gradients the heat flux is varied in such way that it fits to the palaeo-situation.

2.2.1 Reconstruction of palaeo-temperatures using δ^{18}O values

So far there is no direct method which can provide exact palaeo-temperatures from fossils. However, the oxygen isotope composition of carbonates offers a good possibility for reconstructing palaeo-temperatures (e.g., Attendorn and Bowen 1997, Faure 1986, Rye and Sommer 1980, Rohling and Cooke 1999). Being interested in palaeo-SSTs the attention of the investigation is focused on the calcareous shells of planktonic organisms (planktic

foraminifera) as they represent best the condition of the uppermost ocean. The technique of reconstructing palaeo-temperatures is based on the oxygen isotope fractionation of ^{18}O and ^{16}O both in the carbonate of the shell and in the ocean water where the carbonate shell was formed. At isotopic equilibrium the $^{18}O/^{16}O$ ratio of both, carbonate minerals and ocean water, is dependent on temperature. It is assumed that the isotope rate at the time of shell formation is recorded in the carbonate and is unaltered through time. In general, with increasing temperature the ^{18}O accumulation in the shell material decreases (e.g., Epstein et al. 1953). Unfortunately an accurate calculation of palaeotemperatures on the basis of isotopes is difficult because there are several causes for an isotopic disequilibrium (Rohling and Cooke 1999). For our studies some crucial uncertainties regarding the palaeothermometry are listed below.

In order to classify measured isotope ratios of the foraminifera shells they are compared with known standards. In general carbonate measurements refer to the PDB-Standard which is related to the **P**ee**D**ee **B**elemnite formation whereas the belemnite is exhausted. The isotopic composition of ocean water, however, often corresponds to the SMOW-Scale (**S**tandard **M**ean **O**cean **W**ater). The isotope ratios are usually expressed in δ-notation in the form

$$\delta = \frac{R_{sample} - R_{standard}}{R_{standard}} \cdot 10^3 \quad \text{in per mil} \tag{2.5}$$

where R is the measured isotope ratio $^{18}O/^{16}O$ of the sample and a standard sample (e.g., Rohling and Cooke 1999). The data base used for this work, which is related to the time-slice at 8 Ma BP, is shown in fig. 2.2. The mapped planktonic $\delta^{18}O$ values are taken from publications based on ODP and DSDP sites (see also appendix A). These data are averaged over a time span of about 1-3 Ma BP corresponding to the Tortonian time-slice (Geiger pers. comm. 1998).

Palaeo-temperatures were calculated using the empirical equation of Erez and Luz (1983):

$$T(in^\circ C) = 17.00 - 4.52(\delta_c - \delta_w) + 0.03(\delta_c - \delta_w)^2 \tag{2.6}$$

where δ_c is the $\delta^{18}O$ of the isotopic composition of the foraminifer carbonate relative to PDB and δ_w is the $\delta^{18}O$ composition of seawater relative to SMOW in which the calcite was precipitated. The formula (2.6) is taken because it approximates the predicted

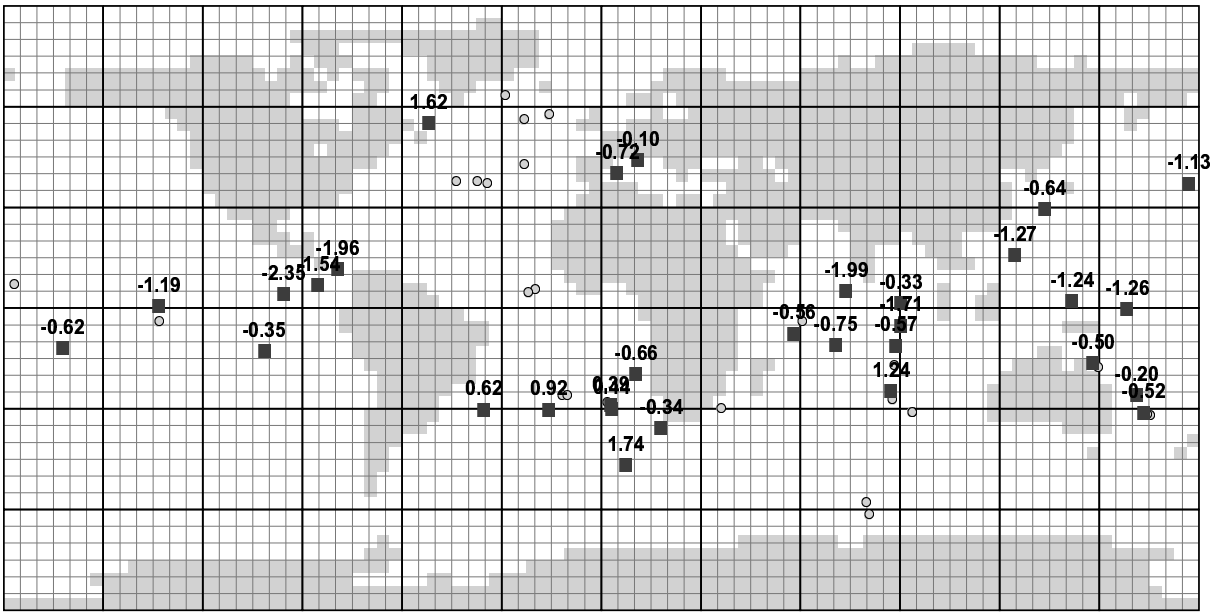

Figure 2.2: *Global distribution of planktonic (squares) and benthic (circles - partly overlapped by squares and not complete) $\delta^{18}O$ data in per mil at 8 Ma BP. Data are from ODP and DSDP sites. (Primarily compiled from Geiger pers. comm. 1998)*

equilibrium values for the modern ocean quite well (Zahn and Mix 1991). Furthermore, Zachos et al. (1994) used this equation for their Palaeogene and Neogene studies which showed that their temperature reconstruction of the Cenozoic ocean is in good agreement with other proxy data.

However there are always systematic errors when using such empirical equations. The most significant deviations are listed below:

- Errors due to measurements and due to the biology of foraminifera (deviations of δ^{18}O of calcite):
  - δ ^{18}O values extracted from calcite samples can be interpreted within an accuracy of about $\pm$ 0.1 per mil which corresponds to a temperature range of $\pm$ 0.5 °C (Erez and Luz 1983, Norris et al. 1994).
  - For this study near-surface dwellers of planktic foraminifera were chosen. For example the species *Globigerinoides sacculifer* preferably lives in the uppermost 100 m of the ocean (Niebler 1995). During the lunar life cycle these foraminifera change their depth habitat which can be in the order of several 10 to 100 m (Hemleben et al. 1989). Similar conditions are valid for *Neogloboquad-*

rina pachyderma which changes to deeper habitat levels during older growth states (Berberich 1996). The variations in depth habitat may suggest calcifications in colder water since temperature decreases with increasing water depth. Therefore temperature values derived from δ_c values are not exactly accurate for representing the oceanic surface temperature. However when assuming a depth independent temperature profile for the mixed layer ocean (e.g., Hartmann 1994), which is applied in the ECHAM4/ML model, one can use the assigned palaeo-temperatures from the carbonate shell as a good estimate of the sea surface temperature (SST).

- Because of the declination of the sun the temperature of tropical ocean water is nearly independent with time whereas water masses closer to the poles undergo more different radiation rates during a year. This could mean that planktonic foraminifera at higher latitudes are reflecting higher annual temperature changes than those at low latitudes. This mechanism is another source of variability in δ_c values derived from calcite shells. Therefore δ_c values can reflect integrated seasonal changes in ocean temperature which vary in latitudinal direction (e.g., Norris et al. 1994).

- It is known that foraminifera may precipitate their shells in isotopic disequilibrium. This behaviour of the organism can be regarded as a vital effect which is assumed to be a constant factor within the own species. For instance the planktonic foraminifer *Globigerinoides sacculifer* exhibits a vital effect of -0.2 to -0.3 per mil (Norris et al. 1994) resulting in a temperature error of about $+1.4°C$ when referring to eq.(2.6).

- Errors due to unknown properties of palaeo-oceans (deviations of $\delta^{18}O$ of water):
  $\delta^{18}O$ values of water for different time-slices can only be determined indirectly. Zachos et al. (1994) used benthic foraminifera as they provide indirectly an evidence for the global ice volume which is mainly stored in polar ice caps. With respect to the Neogene they suggest that oceanic convection rates increase with expansion of polar ice and that the increase of cold surface waters at the ocean bottom can be seen in the derived palaeo-temperatures from benthic foraminifera. Because light oxygen is preferably incorporated into snow or ice, more heavy isotopes are dissolved in ocean water. Therefore the $\delta^{18}O$ value increases with a greater accumulation of ^{16}O

isotopes at the poles in terms of snow and ice. Assuming a Northern and Southern Hemisphere sea ice extent for the Tortonian like nowadays (Wolf and Thiede 1991, Nikolaev et al. 1998) a δ^{18}O value of -1.2 permil is used (see also Nikolaev et al. 1998).

- Errors due to different precipitation and evaporation rates: (deviations in δ^{18}O of water)

  The isotopic composition of water is related to salinity, which is not constant during earth history and not constant for all ocean basins. Salinity is altered not only by changes of the global ice volume, up- or downwelling rates, and ocean currents but also by changes of precipitation and evaporation rates. Because the specification of the land-sea distribution of the Miocene is quite similar to nowadays, it is assumed as a first order approximation that the structure of atmospheric and oceanic circulation is relatively similar to the present-day state. Therefore for the local change of evaporation and precipitation rates over the oceanic areas two different adjustments for δ^{18}O of water can be used:

  - Savin et al. (1985) determine δ^{18}O values of water with respect to different ocean basins. The authors used empirical palaeo-temperature equations from different authors (e.g., Craig and Gordon 1965) where the salinity of the corresponding oceans has to be known. Applying these equations, salinity values for every ocean basin has to be prescribed which is quite difficult for pre-Quaternary time-slices.

  - The studies of Zachos et al. (1994) take into account the latitudinal variation of salinity which is driven by global precipitation and evaporation rates. Typical variations of δ_w values for open ocean amount 1.5 per mil between low and high latitudes (Broecker 1989). For a latitudinal correction of δ_w values they derived an expression which describes the present-day distribution of δ_w values as a third-order polynomial function of latitude:

    $$\delta_w = 0.576 - 0.041y - 0.0017y^2 + 1.35 \cdot 10^{-5}y^3 \quad , \tag{2.7}$$

    where y represents the absolute latitude between 0° and 70°. After Zachos et al. (1994) sensitivity studies for the Recent ocean show a better conformity with observed SSTs using the latitudinal correction than without any adjust-

ments. In contrast to the salinity specifications of the different ocean basins this mathematical model seems to be in agreement with the outlined approach for the ocean heat flux adjustments. Therefore eq. (2.7) is utilized for the palaeo-temperature reconstruction in conjunction with eq. (2.6).

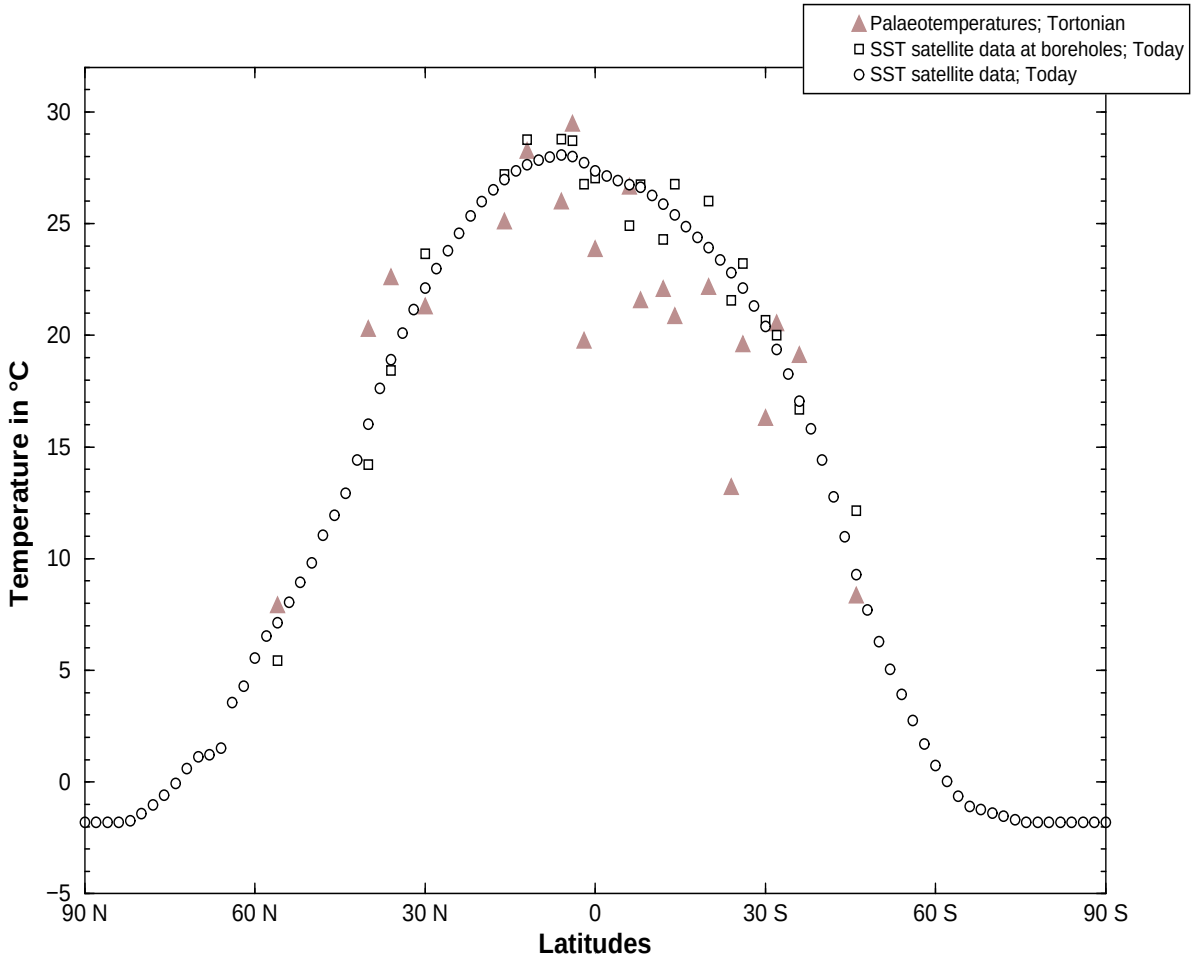

Figure 2.3: *Yearly zonally averaged SSTs from satellite data and palaeo-temperature equations. Circles: satellite data, rectangular: satellite data at the locations where $\delta^{18}O$ values were taken from, triangles: palaeo-SSTs received from equation (2.6).*

For a further comparison with Recent data the palaeo-temperatures are zonally averaged in a 2 degree resolution. Using above mentioned equations (eq. 2.6 and 2.7) the obtained palaeo-temperatures are shown in fig. 2.3.

For a comparison of palaeo-temperature data and Recent SSTs, satellite data were utilized which were analysed by using monthly optimum interpolation (Reynolds 1993, Reynolds and Marsico 1993, Reynolds and Smith 1994, Slutz et al. 1985, Woodruff et al. 1993). The data include the time period from 1979 to 1993 with a horizontal resolution of 2 degrees. This data base is processed and split into several data sets in order to filter yearly and seasonal averages from it. The SSTs are zonally averaged as it was performed for the palaeo-data. Additionally, the Recent SST information at the locations of the palaeo-temperatures were extracted from the satellite data base. The different temperature sets (i.e., the palaeo-temperatures at the locations of the boreholes, Recent temperatures at the locations of the boreholes, and zonally averaged Recent temperatures in 2 degree resolution), are needed to result in a comparison of Recent and palaeo-temperatures. The approach will be explained in the next subsection.

From fig. 2.3 it can be seen that, at high latitudes on the Northern Hemisphere, the palaeo-temperatures are generally higher than the satellite temperatures at the boreholes. Subtropics and tropics, however, tend to be cooler in the Tortonian. It is feasible that the lower temperatures in the tropics can be attributed to the above explained sources of errors in reconstructing palaeo-temperatures for the Neogene on the basis of foraminifera. In order to avoid such failures, our study is focused on the latitudinal temperature gradient rather than using absolute palaeo-temperatures. Nevertheless, a first rough overview shows already a more flattened palaeo-temperature gradient in comparison to the modern one.

2.2.2 Transformations

As it can be seen from fig. 2.2 the palaeo-SST information is scarce on the global scale. In addition, most boreholes are situated between 30° northern and southern latitude. And unlike Recent data sets, the palaeo-SSTs show an irregular distribution of the locations of the boreholes. With regard to climate modeling, however, SSTs must be globally determined at a specific spatial resolution. In order to fill the horizontal gap of palaeo-SSTs, a comparison of Recent and palaeo-SSTs is performed in which the zonal averages are calculated and the best fit Gaussian curves over the latitudes are computed. It is assumed that the zonal averages of the temperatures are well represented by a Gaussian

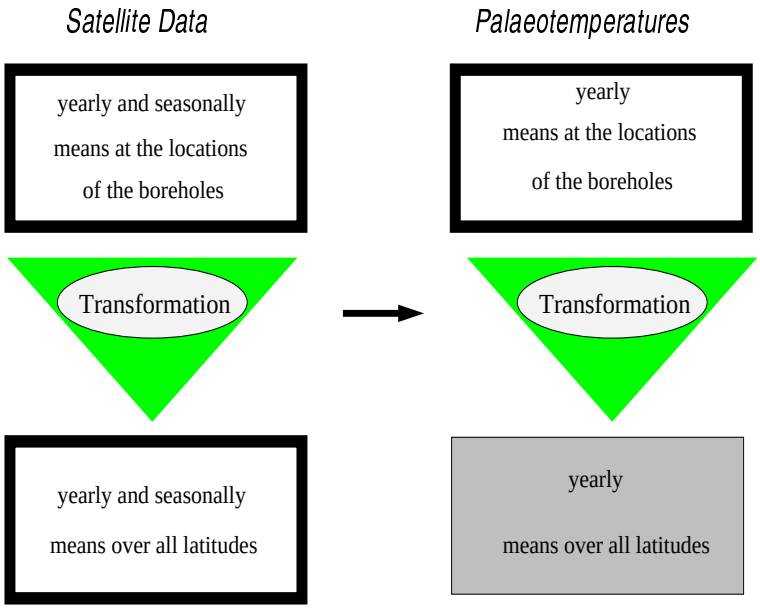

Figure 2.4: *Schematic diagram of transformations of the Gauss curves. Thick bounded rectangles represent data sets which exist and the shaded box represents the needed data set for implementation in the climate model.*

curve, as the satellite data from surface temperatures (fig. 2.3) are indeed similar to a Gauss curve. In search of the best fit Gaussian curve the method of the least squares was used. Additionally the Gaussian curve is constrained by setting the minimum value to -1.8°C as the minimum temperature of sea water is constrained to about this level. Consequently there remain three independent parameters which describe the Gaussian curve, i.e. the amplitude A, the distance from the maximum value to the turning points σ, and the latitudinal shift Δ. The parameters are defined for three sets of data which are:

- Palaeo-temperatures derived from palaeo-temperature equation,
- SSTs over all latitudes in 2° resolution derived from satellite data and
- SSTs at the location of the boreholes derived from satellite data.

The next steps which are applied to the three different categories of data sets are described below and refer to fig. 2.4. In this figure the juxtaposition of Recent and palaeo-data should clarify the reapplication of the same computing procedure on different data sets.

Two main categories partition the data into time and space. Recent data, derived from remote sensing methods, are easily divided into several categories as these data supply both a high horizontal resolution and an annual cycle. The satellite data can be split into

yearly and seasonal averages, whereas the palaeo-SSTs can only refer to yearly means. The latter is due to the coarse time resolution of δ^{18}O information and the applied averaging over some million years for representing a mean of a specific time-slice. Recent data can additionally be limited in space by only including the data at the locations of the boreholes corresponding to the palaeo-data positions.

In figure 2.4 the thick bounded rectangles show available data sets, while the shaded box shows the record that is finally needed for the implementation into the climate model. Starting points for the temperature reconstruction are the Recent data sets, which represent yearly and seasonally means at the locations of the boreholes and over all latitudes. Firstly a transformation is found explaining the variation of the Gauss parameters A, σ and Δ of the Recent data set including the borehole locations in comparison to the Gauss parameters of the Recent data set including all latitudes. This has been carried out by comparing the yearly and seasonal means of the SSTs over all latitudes with those restricted to the locations of the boreholes. For all three parameters p of the Gaussian curve linear dependencies in the form $p|_{all} = a + b \cdot p|_{loc}$ were chosen which represents the transformation equation. The small indices show if the Gaussian parameter p belongs to the borehole locations (index $_{loc}$) or if it is representative for all latitudes (index $_{all}$). The constants a and b were found by establishing 5 equations corresponding to four seasonal means and one yearly mean referring to the Recent data sets. Applying the same transformation equation on the palaeo-SSTs data this conversion results in yearly mean palaeo-SSTs over all latitudes (shaded box in fig 2.4).

Small deviations in δ^{18}O values have an effect on the computation of palaeo-temperatures. The calculation of palaeo-temperatures depends on the determination of polar or inland glaciation occurrences, vital effects of foraminifera, and different depth habitats of the ocean dwellers. The sensitivity of temperature to small variations of δ_c and δ_w can be seen in fig. 2.6. Explaining the effect of different oxygen isotope composition in the ocean a uni-polar ice-covered world (early Oligocene) is compared to modern conditions. This case study is well represented when assuming a correction factor of -0.4 per mil for the δ_w value (Zachos et al. 1994). There are also taken into account variations in δ_c values of ± 0.3 per mil which is in the order of possible errors due to the vital effect of the organisms. A comparison of these different Gauss curves in fig. 2.6 show at first sight essential

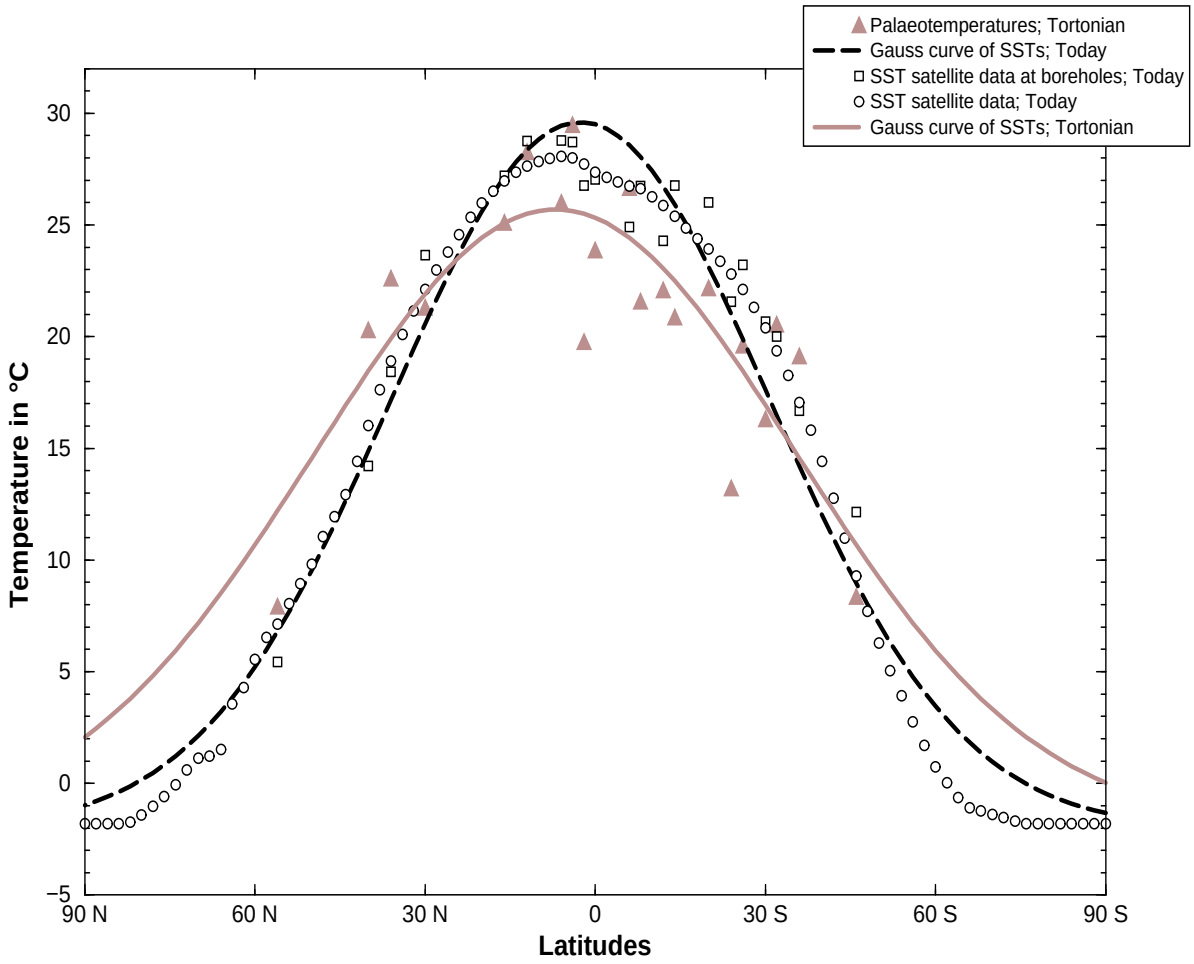

Figure 2.5: *Yearly zonally averaged SSTs from satellite data and palaeo-temperature equations with corrected δ values. (Circles: satellite data, rectangular: satellite data at the locations where $\delta^{18}O$ values were taken from, triangles: palaeo-SSTs received from equation (2.6), long-dashed line: Gaussian curve of satellite data and solid line: Gaussian curve from palaeo-temperatures.)*

differences in the magnitude of the temperatures. However, when comparing their shape they seem to be quite similar.

In the following section a method is applied for calculating the change of oceanic heat transport which takes into account the gradients of the Gauss curves to avoid discrepancies in δ^{18}O specification. It should be noted already that this method is only feasible if the ocean currents do not differ significantly from nowadays. This means that the near-surface ocean circulation pattern has to be basically similar to the Recent one.

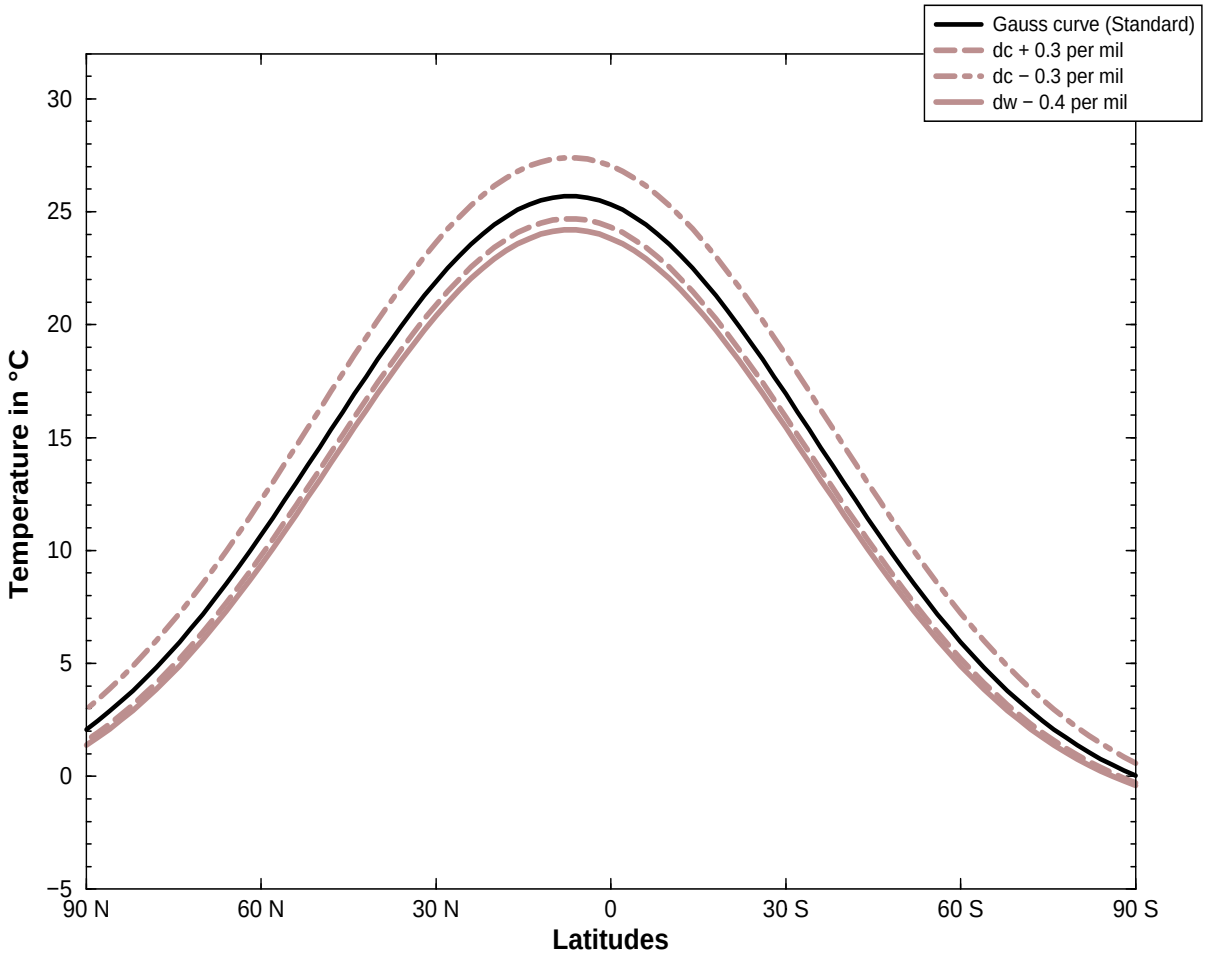

Figure 2.6: *Different Tortonian Gauss curves representing meridional palaeo-temperatures with differences in δ_c and δ_w values relative to the Standard Tortonian temperature curve. (Black curve: Standard curve of the Tortonian time-slice, Solid grey line: an additional correction of -0.4 per mil for δ_w, dashed line: an additional correction of -0.3 per mil for δ_c, dotted-dashed line: an additional correction of 0.3 per mil for δ_c.)*

2.2.3 Variation of the flux correction

The SST gradient can be interpreted as a measure of the heat flux transfer in the ocean. Thus a high gradient value would result in an intensified heat transport from the tropics to the poles or vice versa a small gradient value would yield a moderate oceanic heat transport. With the SST information from the previous section (fig. 2.5) we can see that the SST gradient for the Tortonian time-slice is smaller than today. According to the assumptions this means a weakened oceanic heat transport for the Tortonian in comparison to today. For climate modeling studies of different time-slices a changed ocean heat flux is considered (e.g., Upchurch et al. 1998), however, there are further studies trying to quantify the change in oceanic heat flux for specific time-slices and its change during

geological time (e.g., Bice et al. 2000, Covey and Thompson 1989)

From the previously mentioned generated Gauss curves (fig. 2.5) the corresponding zonal gradients are calculated providing the basis for the variation of the oceanic heat transport for the climate model. Evaluating the gradients has the advantage not being dependent on the absolute values of the reconstructed palaeo-temperatures and therefore on the exact offset of the palaeo-temperature equations.

A comparison of the Recent and palaeo-gradients allows one to determine the alteration of the heat fluxes in the ocean. As a measure of the heat transport the ratio of palaeo-gradients and Recent ones is applied yielding a zonal constant value

$$f_o(y) = \frac{gradSST(y)_{palaeo}}{gradSST(y)_{recent}}, \tag{2.8}$$

where the y coordinate refers to the latitudes. Regarding the alteration of the SST gradients, values of f_o greater than 1 yield an intensification of the flux correction FC, which describes the heat transport in the ocean (see also section 2.1). If $f_o < 1$ the flux correction is weakened. Therefore the Recent flux correction can be simply multiplied by f_o which yields in the palaeo-flux correction

$$FC(t,x,y)_{palaeo} = f_o(y) \cdot FC(t,x,y)_{recent}, \tag{2.9}$$

where the x-coordinate corresponds to the longitudes and t to the monthly changes.

It will be presented in the next section to what extent changes in δ^{18}O values can effect the oceanic heat transport. As this method is simple it can be applied to different time-slices without much effort. Unfortunately the high latitude temperatures are inaccurate due to the lack of information but obviously the greatest advantage is the receipt of global SSTs on the basis of a few.

2.2.4 Oceanic heat transport

The meridional heat transport can be divided into an atmospheric and an oceanic part at which the atmosphere contributes the greatest part as an energy transporter (e.g.,

Trenberth and Solomon 1994). Furthermore studies examining the role of the oceanic heat transport in the climate system show a noticeable atmospheric response (Cohen-Solal and Le Treut 1997, Cohen-Solal and Le Treut 1999). Examining past climates the oceanic heat transport is supposed to be different from nowadays. Therefore in this study the heat flux is altered which consequently effectuates a change in oceanic properties of the mixed-layer.

The results of the calculated palaeo-flux correction using eq. (2.8) and (2.9) can be seen in fig. 2.7. In fig. 2.7 c) the coarse pattern of the altered flux correction of the yearly mean shows a weakening over all latitudes which is attributed to the different gradient trends of the palaeo and Recent SST curves (fig. 2.5). For example the Gulf-Stream between 40 and 60°N in the Tortonian study is less intense providing less energy to high latitudes of the Atlantic Ocean. The maximal reductions are in the order of 25 W/m^2. The reductions for the Kuroshio are in the order of 31 $\mathrm{W/m^2}$ providing a less intense heat transfer to the North-Pacific.

The zonally averaged heat flux represented in fig. 2.8 provides an analysis of the changed flux correction. Positive values correspond to divergence zones and negative to convergence zones of the implied ocean heat transport. In the Tortonian case the heat flux is reduced in the tropics by 7 $\mathrm{W/m^2}$ which is equivalent with a lowering of heat divergence near the equator. In the mid-latitudes the convergence is lowered by 4 $\mathrm{W/m^2}$ in the Northern Hemisphere as a consequence of less heat transport. This is synonymous to a less efficient oceanic heat transport transferring heat from the equator to the poles. The global mean of the perturbations is decreased slightly by -0.02 $\mathrm{W/m^2}$ so the perturbations remove oceanic heat in the global mean term. The changes are constrained by the vanishing of the implied meridional oceanic heat transport at the poles. This means that the heat transport must be equal zero at both poles.

In fig. 2.9 the oceanic heat transport T_0 is calculated by integrating the zonally mean heat fluxes from the south to the north pole (e.g., Carissimo et al. 1985, Hastenrath 1982, Hsiung 1985, Cohen-Solal and Le Treut 1997):

$$T_0(\phi) = \int_{SouthPole}^{\phi} \left(\int_{-\pi}^{\pi} div T_0(\phi, \lambda) R d\lambda \right) \cos(\phi') d\phi', \tag{2.10}$$

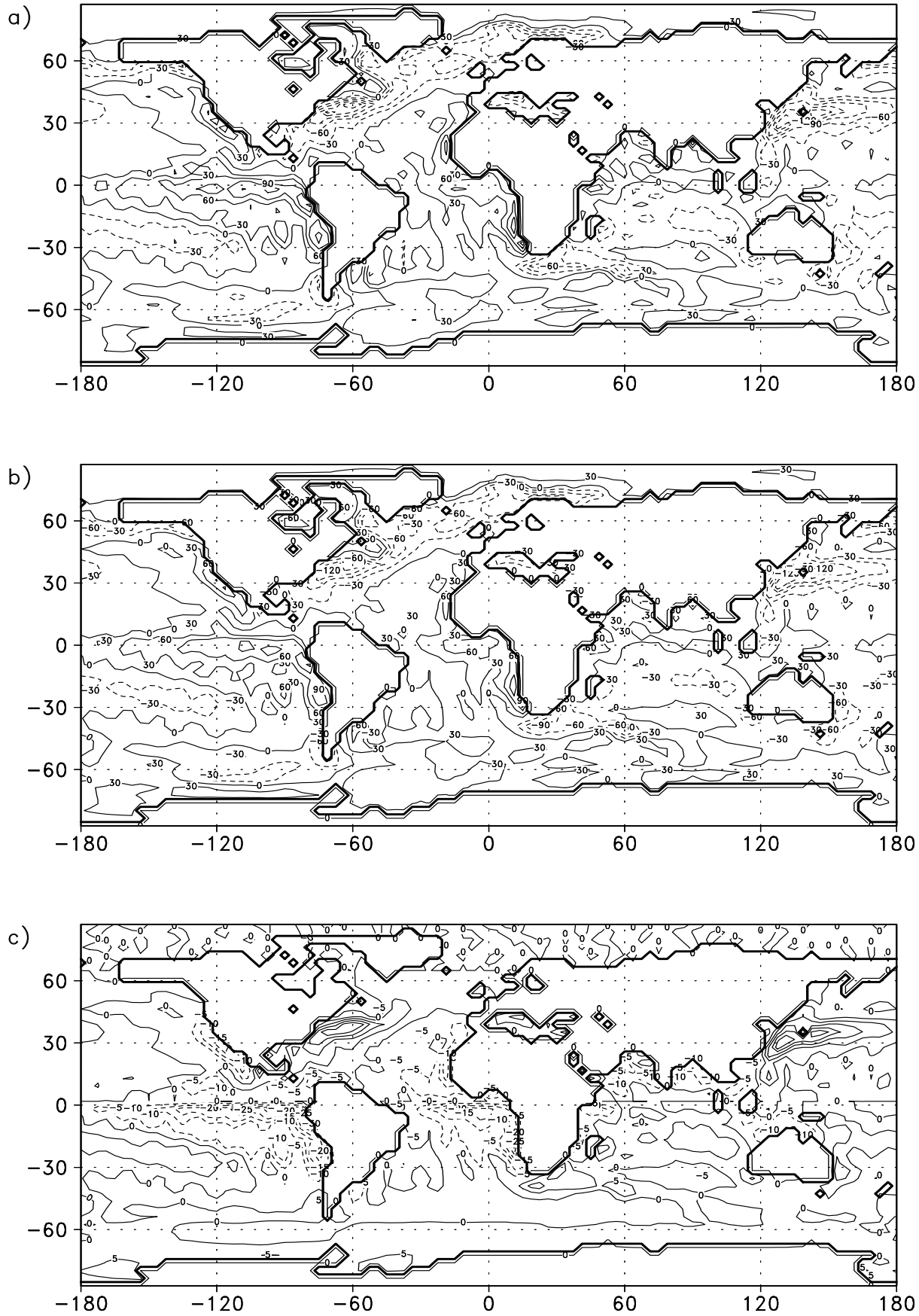

Figure 2.7: *Flux correction in W/m^2 for Control and Tortonian run representing yearly means. a) Control run, b) Tortonian run, c) Difference of Tortonian and Recent run.*

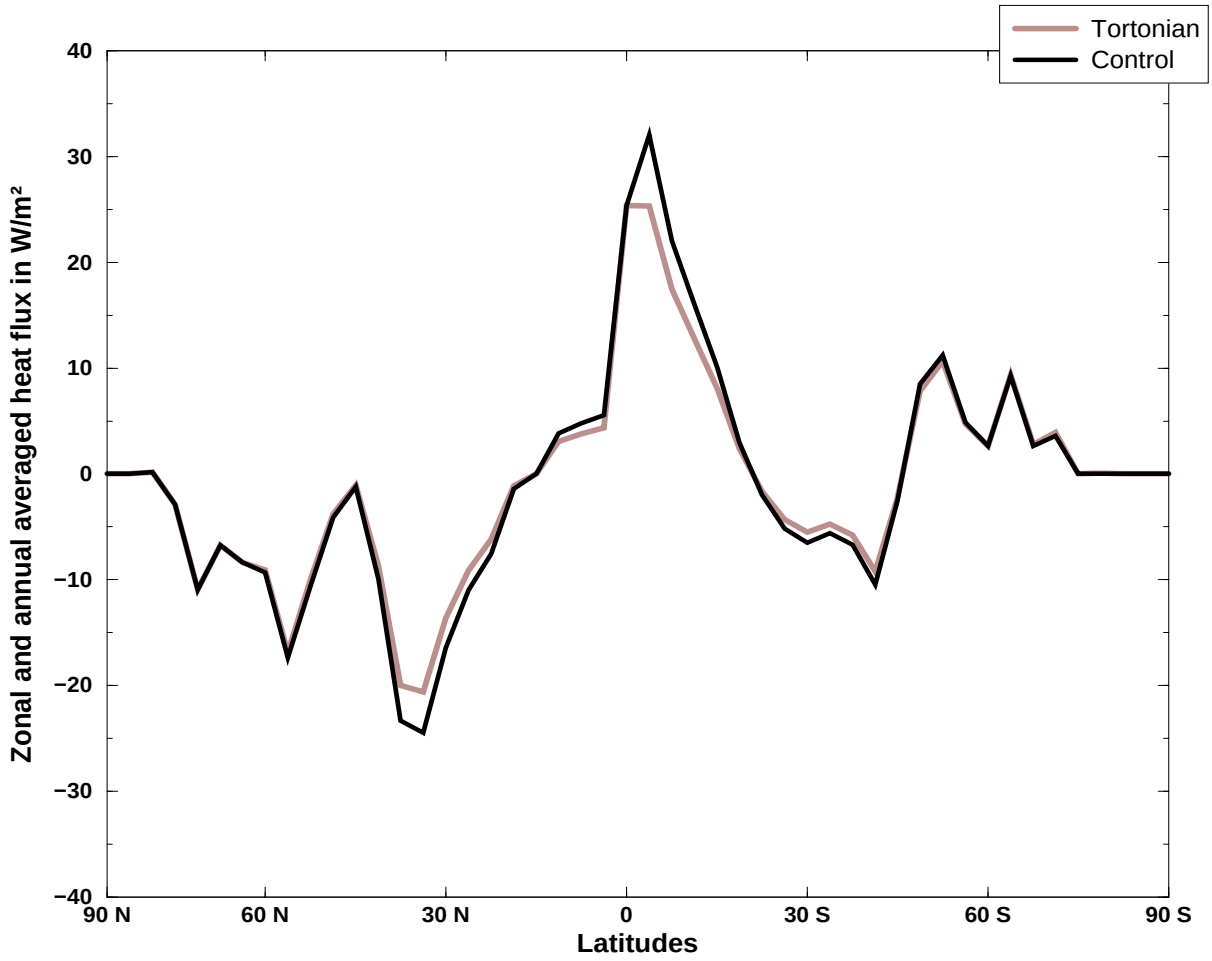

Figure 2.8: *Zonally and yearly mean divergence of oceanic heat transport (Black line: Recent curve, grey line: Tortonian curve)*

where R is the Earth radius. Additionally the oceanic heat transport is constrained by eliminating a spurious offset at the north pole. This implies a constant heat storage in the ocean. The calculated oceanic heat transport (fig. 2.9) demonstrates a maximum around 20 °N. The position of the maximum coincides with that found by other authors (cf. e.g., Carissimo et al. 1985, Gleckler et al. 1995). Eq. (2.10) shows that the implied oceanic heat transport has an additive character that makes it very sensitive to small changes. Estimated values from different authors for the meridional heat transport lie in between 1.5 and 2.5 PW for the world ocean (see e.g., Ganachaud and Wunsch 2000). A value of the order of 1 PW at 24 ° N is suggested by e.g., Roemmich and Wunsch 1985. Fig. 2.9 shows also oceanic heat transports for the Tortonian case (left side). Due to the changed heat flux the northward oceanic heat transport is weakened in comparison to the one of the control run. The maximum values for the world ocean on the Northern Hemisphere

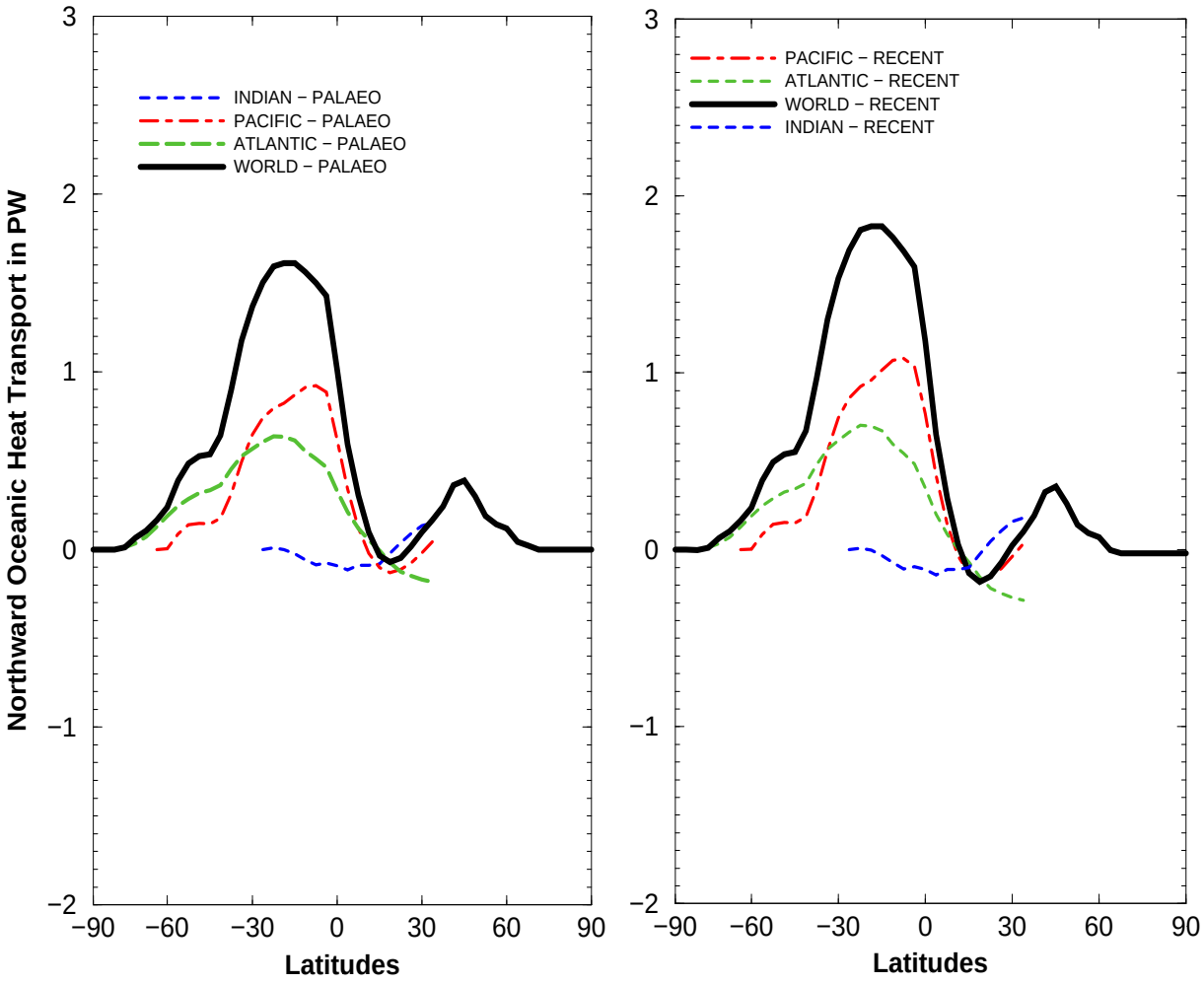

Figure 2.9: *Northward oceanic heat transport in Peta Watts for the world ocean and the main 3 basins splitted into nowadays (right side) and Tortonian (left side) transport.*

are reduced by approximately 0.2 PW resulting in less heat transport from the equatorial region to the pole. Focusing on the North Atlantic there is a reduction of about 0.1 PW in meridional oceanic heat transport. Regarding the Pacific Ocean the differences between Recent and palaeo-curve are of the same order.

Differences in implied oceanic heat transport due to small deviations in δ^{18}O values (cf. fig. 2.6) can be seen in fig. 2.10. In this figure the anomalies of the northward oceanic heat transport are compared to the standard Tortonian data base using the Atlantic Ocean. As shown in fig. 2.6, the temperature curves differ slightly due to uncertainties in δ^{18}O values of calcite and ocean water. An additional decrease/increase of tropical temperatures would decrease/increase the pole-equator gradient. This would imply a less/more intense North-Atlantic heat transport in comparison to the standard Gauss curve. However the

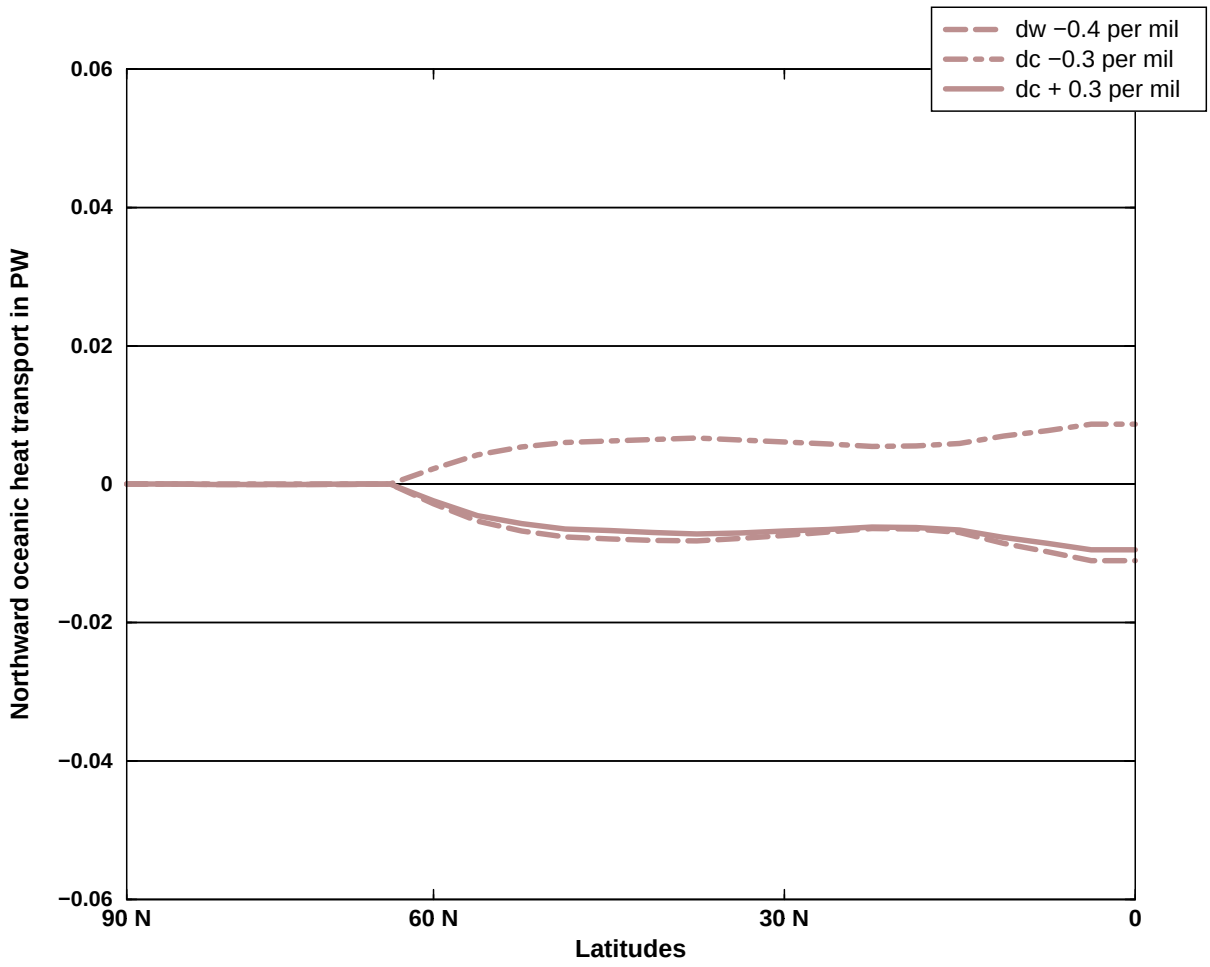

Figure 2.10: *Changes in northward oceanic heat transport of the Atlantic Ocean in comparison to the standard Tortonian data base. Differences belong to deviations in* $\delta^{18}O$ *values: long-dashed line: deviation in* δ_w *of -0.4 per mil, dot-dashed line: deviation in* δ_c *of -0.3 per mil and solid line: deviation in* δ_c *of +0.3 per mil.*

added differences are smaller than $\pm$ 0.01 PW for this ocean basin which is in the order of less than 10 per cent of the specified reduction.

Today both the Gulf-Stream and the Kuroshio current transport extensive heat from mid-latitudes to polar regions. These surface ocean currents are also connected to the thermohaline circulation. The heat transport and downwelling are somehow linked together (e.g., Weaver et al. 1999). In contrast to the present situation it is assumed that during the Miocene the oceanic heat transfer was less efficient due to different seaways. The final closure of the Panama Strait occurred around 3 Ma BP (e.g., Collins et al. 1996) so there was no more water exchange possible between Atlantic and Pacific Ocean. Prior to this event the Central American seaway was temporarily open during the Upper Miocene but with a considerable variation in depth (Collins et al. 1996). While there

was a connection between the ocean basins the much saltier water of the Atlantic was transported to the Pacific. It is suggested by proxy data (e.g., Haug and Tiedemann 1998) and by general circulation models (Barron and Peterson 1991, Maier-Reimer et al. 1990, Mikolajewicz and Crowley 1997) that the heat turnover is intensified with the closing of the Panama Isthmus. While there is a seaway between North- and South-America North Atlantic water is diluted and provides less dense water at high latitudes. Thus the convection rate producing North Atlantic bottom water is reduced. Through the decrease of the impulse of the ocean circulation the Gulf-Stream is also weakened. This explanation coincides with the results of the noticeable reduction of heat flux representing the Gulf-Stream. Likewise there is also evidence for a strengthening of the Kuroshio linked to the closing of the Central American seaway which can also be seen in proxy data (Tsuchi 1997).

As will be outlined in the next chapters, a changed oceanic heat transport for the Upper Miocene can reconstruct the main features of atmospheric processes and they coincide widely with proxy data. However detailed results of the simulations should not be overestimated because small changes in boundary conditions and even the usage of a different mixed-layer ocean model could result in different magnitudes of crucial variables. Nevertheless climate changes represented by the model simulations are in agreement with terrestrial proxy data which will be represented in the following.

2.3 Tortonian run

In this section the results of the 30 year integration run for the Tortonian time slice is presented. This run uses boundary conditions reconstructed from proxy data. These changes mainly represent variations in orography and oceanic heat transport, which were explained in detail in the previous chapter. This run is referred to as the standard Tortonian run. In order to analyse the effect of a reduced oceanic heat transport, first the oceanic properties are investigated. For this purpose the vertical velocities and the barotropic streamfunction are calculated. Subsequently the effect on the atmosphere is examined. Therefore, the focus is set first on the sea ice distribution near both pole caps, then on the mean large scale atmospheric pattern for summer, winter, and the annual mean. Anomalies between Tortonian run and Control run are calculated. The evaluated

data of the Control run are taken from the first 100 years of integration of the experiment called EXP700-run712. Results corresponding to atmospheric variables of the Tortonian run can be found in the appendix B. To make a comparison possible the same atmospheric CO_2 concentrations of 353 ppm are used.

2.3.1 Oceanic mass transport

In order to investigate horizontal and vertical mass transports in the ocean, the surface wind stress field must be considered (fig. 2.11). The annual mean of wind stress of the Control run shows strong correspondence with wind stress data derived from surface wind analysis (Hellermann and Rosenstein 1983, Trenberth et al. 1990). For example, the formation of subtropical gyres related to the trade winds and the strong westerly flow at mid-latitudes are well represented in both hemispheres. However, even small differences in wind stress can have an impact on ocean circulation (Townsend et al. 2000). The comparison between Tortonian and Control run shows that there are small differences in the wind stress pattern (fig. 2.11). In order to evaluate the anomalies between both runs the deviations will be discussed. In fig. 2.11 c) a decrease in wind stress at high mid-latitudes on both hemispheres can be seen. With regard to low mid-latitudes of North Pacific and North Atlantic, an increase in wind stress leads to a strengthening of ocean currents. This is discussed below.

Calculations of several authors (e.g., Danabasoglu 1998, Leetmaa and Bunker 1978, Trenberth et al. 1990, Townsend et al. 2000) show the linkage between the climatological wind stress field at the ocean surface and the wind-driven oceanic circulation. The atmospheric wind stress drives horizontal and vertical movements of ocean water, which are modified by the geometry of the ocean basin. For example the upwelling zone at the eastern boundary of the South Pacific ocean is caused by a strong divergence of horizontal water masses. Compensating this loss of mass, a positive vertical velocity is induced. The vertical velocity at the base of the Ekman-layer, w_E, is described by the wind stress curl using

$$w_E = \frac{\partial}{\partial x}\left(\frac{\partial \tau_y}{\rho_o f}\right) - \frac{\partial}{\partial y}\left(\frac{\partial \tau_x}{\rho_o f}\right) \quad , \tag{2.11}$$

where f is the Coriolis parameter (f=2 Ω sin Φ , where Ω is the rotation velocity of the earth), ρ_o the density of ocean water (1000 kg/m^3 used for this computation) and τ the

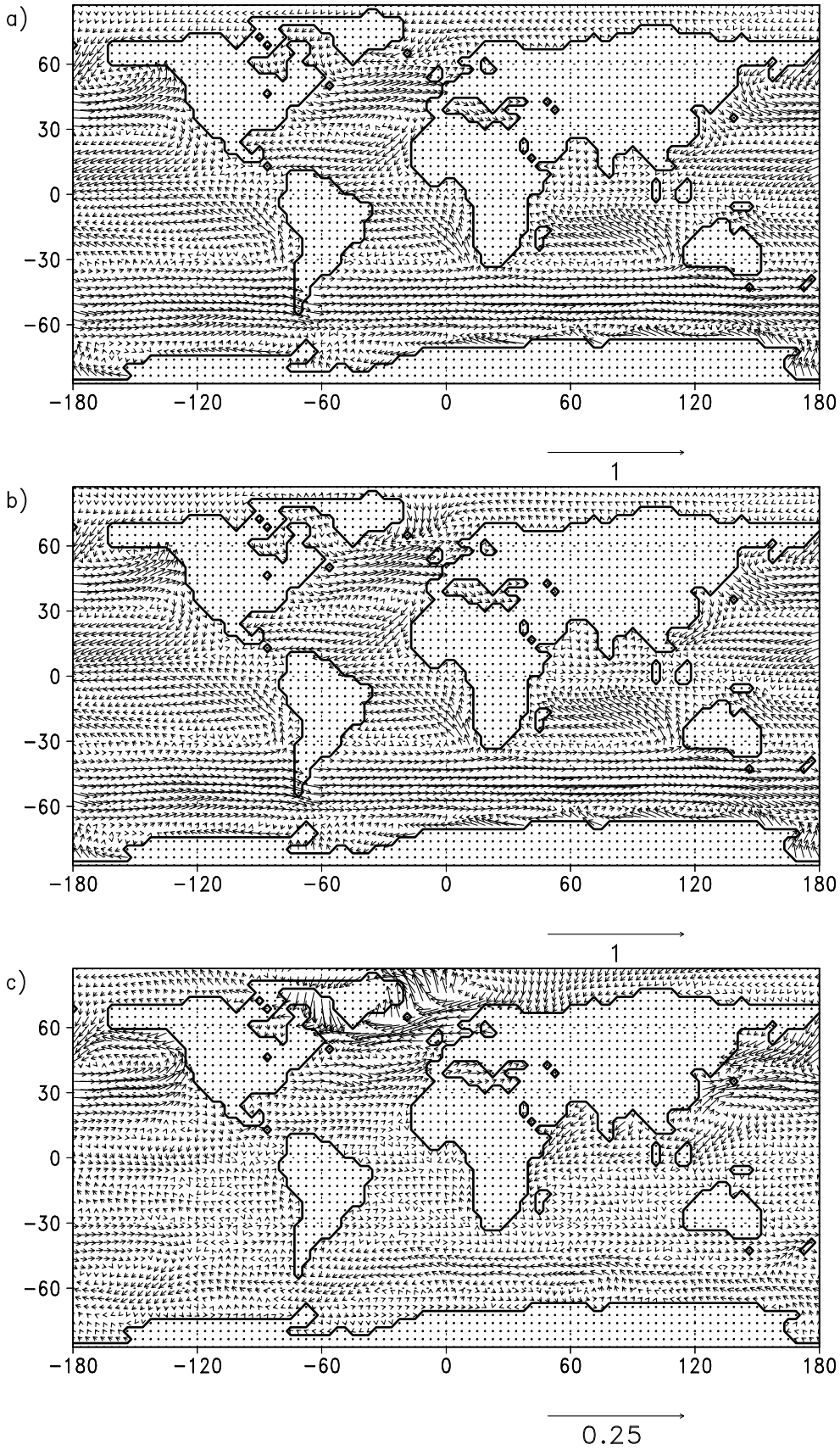

Figure 2.11: *Yearly mean wind stress field over the ocean where a) corresponds to the Tortonian run b) to the Control run, and c) is the difference between both. The magnitude of the reference arrow is 1 m/s for a) and b), and 0.25 m/s for c).*

wind stress in x (longitudinal) and y (latitudinal) direction. For the calculation, values next to land grid points were not considered as the result would be affected unrealistically. Due to the low values of the Coriolis parameter next to the equator the wind stress curl was not determined for the tropical zone. The vertical velocity fields for Tortonian and Control run can be seen in fig. 2.12. For both simulations strong upwelling zones can be identified at the eastern boundaries of the southern ocean basins. And the upwelled water in the tropics is transported downwards in the subtropics. However, vertical velocities at the ice edge around Antarctica, however, cannot realistically be calculated as the wind stress rather represents the movements of ice sheets than ocean water.

For the Tortonian run the vertical velocity field shows small changes (fig. 2.12) for the upwelling zones at the eastern boundaries of the South Atlantic and South Pacific ocean. These regions indicate an increase of upwelling over its central area and significant decreases in upwelling around it. This feature points at a shortening of the eastern boundary currents. Their intensity, however, is locally increased. In the subtropics negative vertical velocities are intensified. This means an increase of downwelling corresponding to the subtropical North Pacific and North Atlantic. This rise is caused by the increased surface wind stress and - due to mass conservation - downwelling is intensified.

The Sverdrup transport is considered as a measure of the oceanic response to atmospheric forcing. Mass transport is calculated via the surface wind stress curl, because the simulation uses a mixed-layer ocean and thus equatorial return flows in intermediate and deep water cannot be calculated. Therefore this Sverdrup transport is not a realistic interpretation of surface ocean currents. The streamfuntion Ψ is written in the form (after Stommel 1978)

$$\Psi(x) = \int_{x_{eastern}}^{x} \frac{curl_z(\tau)}{\beta\rho} dx \qquad , \tag{2.12}$$

where the eastern boundaries $x_{eastern}$ of the oceans are set to zero. The variables ρ, β, and τ are representing the density of the atmosphere, the meridional derivative of the Coriolis parameter, and the horizontal wind stress respectively. The streamfunction value on the western boundary of the ocean basin equals the required flow of Sverdrup transport across a given latitude. This is presumably the Sverdrup portion of the western boundary current.

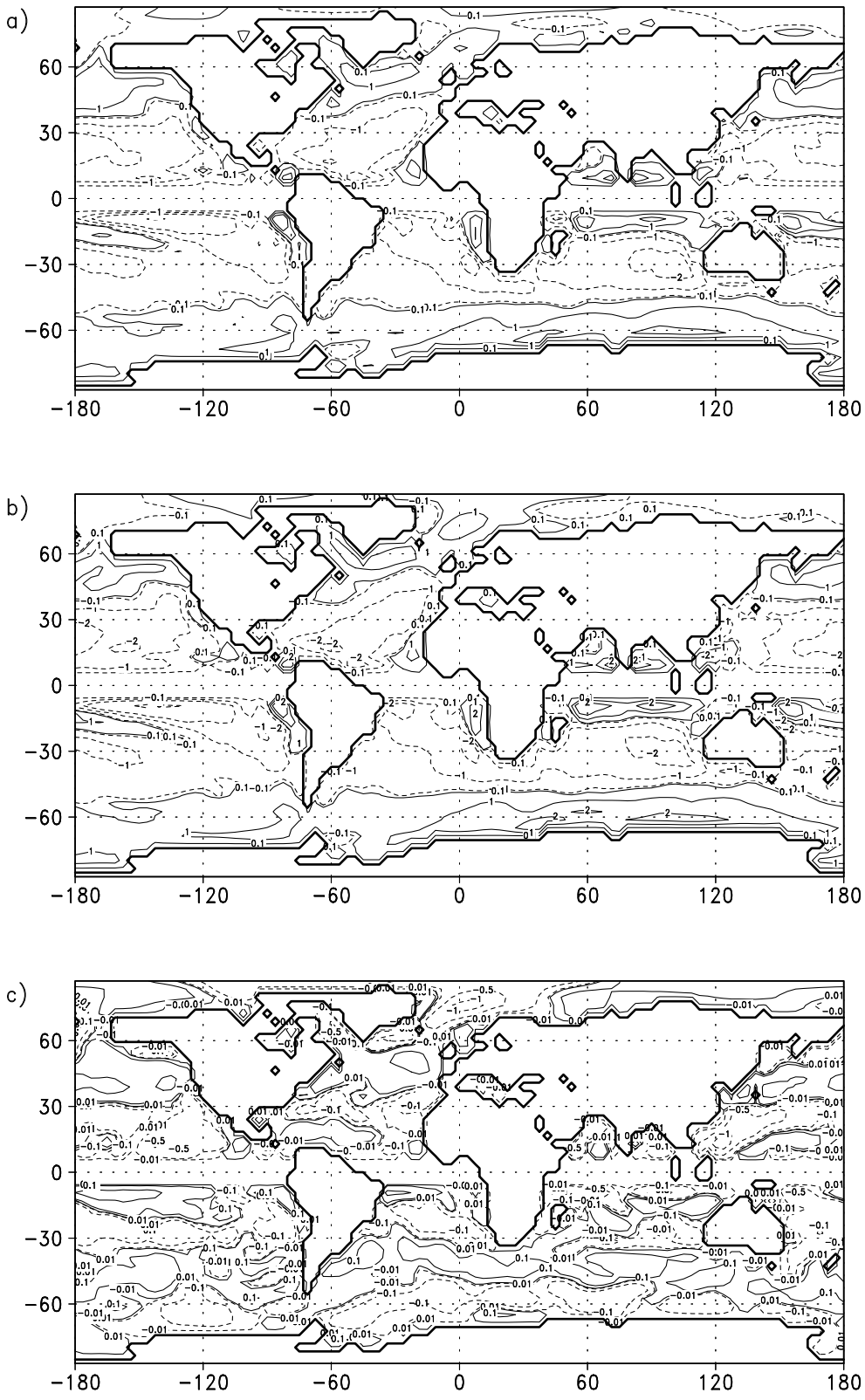

Figure 2.12: *Vertical velocities at the base of the Ekman layer in 10^{-6} m/s. Positive values correspond to upwelling and negative values to downwelling areas. (a) Tortonian run, b) Control run, and c) is the difference between Tortonian and Control run. Contour interval is -5, -2, -1, -0.1, 0.1, 1, 2 and $5 \cdot 10^6$ m/s for a) and b) and -5, -1, -0.5, -0.1, -0.01, 0.01, 0.1, 0.5, 1 and $5 \cdot 10^6$ m/s for c).*

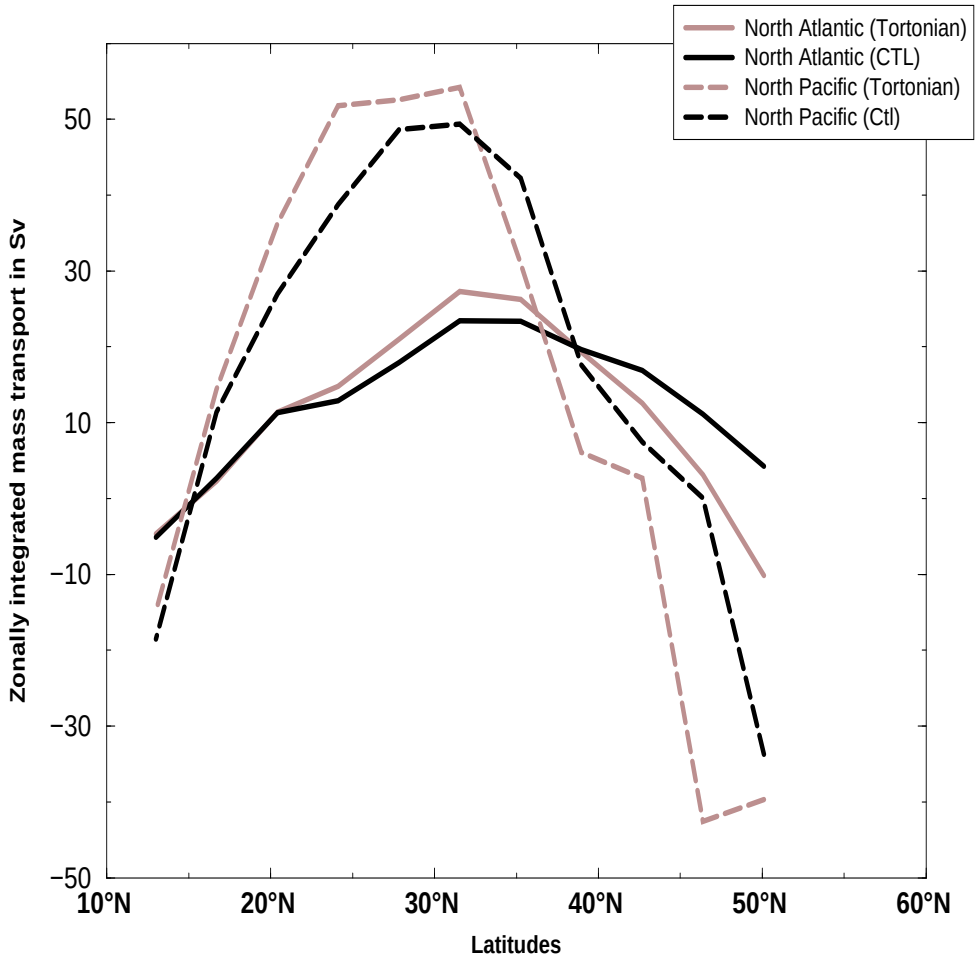

Figure 2.13: *Annual mean sverdrup transport streamfuntion in Sv over the global oceans.*

Here the investigation is focused on the Northern Hemisphere ocean currents, especially the Gulf Stream and Kuroshio. Annual mean values of 23.5 Sv and 49.3 Sv in the Control run are obtained respectively (fig. 2.13). Roughly the same values were also calculated by Townsend et al. (2000) and Harrison (1989). The northward transport of ocean water shows differences between Tortonian and Control run (fig. 2.13). The northward flow of the western boundary currents is strengthened at lower latitudes which is related to an increased surface wind stress in the Tortonian run. At higher latitudes, however, the oceanic mass flux is weakened. The general pattern shows an equatorial shift of maximal transport along western boundaries with a reduction of Sverdrup transport further northwards. This complies with a shortening of the Gulf Stream and the prescribed reduction of oceanic heat transport on the Northern Hemisphere (section 2.2.4).

2.3.2 Global temperature and sea ice

Using weighted areas, the time evolution of the global averaged surface temperature is represented in fig. 2.14. Here the yearly means show no significant differences between Control and Tortonian run. Further experiments with the mixed-layer model, however, have shown that during the first 20 years of integration the mixed-layer model shows

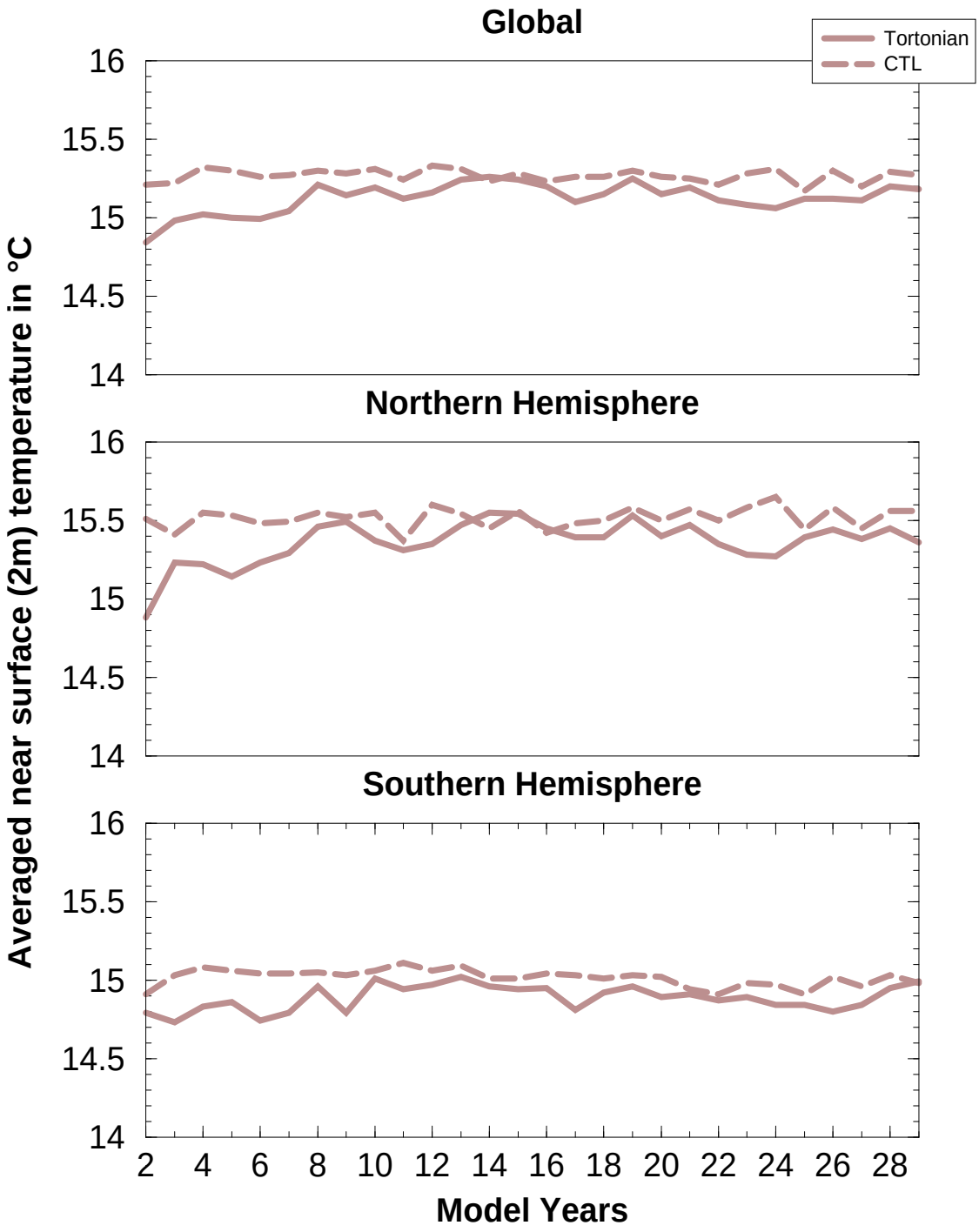

Figure 2.14: *Yearly means of global averaged surface temperature using weighted areas.*

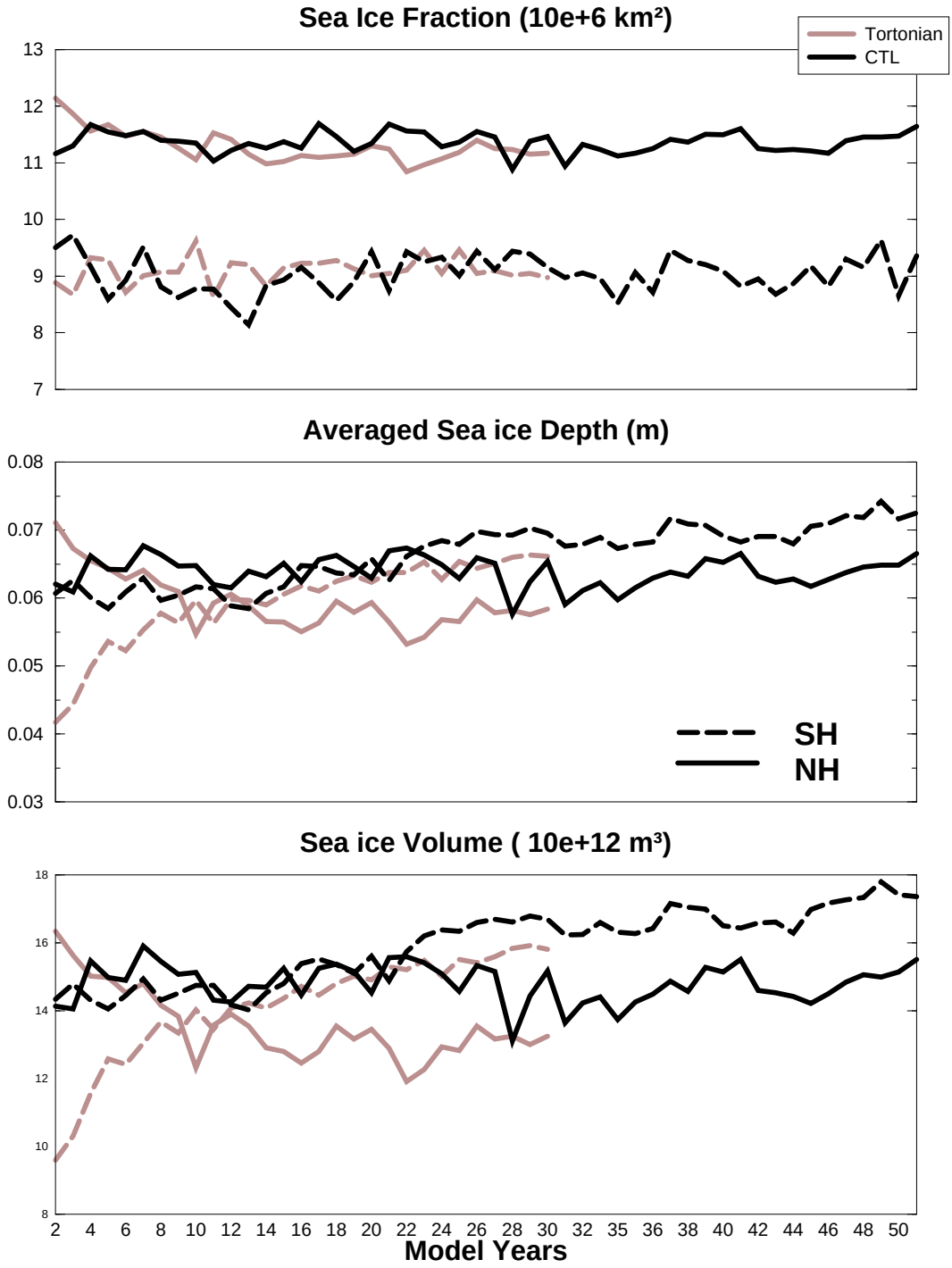

Figure 2.15: *Yearly means of global sea ice fraction, depth, and volume on both hemispheres. (Dashed line: Southern Hemisphere (SH), Solid line: Northern Hemisphere (NH), Black lines: Control run, Grey lines: Tortonian run.)*

noticeable responding features to different boundary forcings. However after 20 years of simulation the model tends to level off in an equilibrium state. Therefore the years 21 to 30 are taken into account for further analysis.

Variation of glaciation can be seen in changes of sea ice volume. Fig. 2.15 shows the annual average of sea ice for the Tortonian and Control run. For both hemispheres there are hardly any variations in sea ice fraction, however, sea ice depth is decreased. This leads to a noticeable reduction of sea ice volume over the North Polar Sea. The elimination of the Greenland ice shield contributes to the diminishment of sea ice.

So far it is uncertain when cooler climates evolved in the Arctic during pre-Miocene time since data from the central Arctic ocean are rare (Thiede et al. 1998). It has been proposed by Wolf and Thiede (1991) that the Arctic Ocean was ice covered before 8 Ma BP. And between 9 and 7 Ma BP cold ocean currents around Greenland started to evolve in strengthening as sediment records indicate. Ice rafting is present in the sediments of the Baffin Sea and the Subpolar Pacific Ocean (Nikolaev et al. 1998). Regarding the spread of sea ice, model output, however, represents a smaller extent for the Tortonian run with a distinct smaller sea ice depth than today. An exact reproduction is demanding as the SST gradients are reconstructed on a poor data basis which is especially poor at high latitudes.

Following the onset of the antarctic ice sheet development, its extent varied significantly during the Neogene. The ice margin even transgressed the Recent limits (Prentice and Matthews 1991). During the middle Miocene (12-14 Ma BP) the east antarctic ice sheet underwent major growth but no major amounts of sea ice occurred (Flower and Kennett 1994). After a short period of warming between 12 and 10 Ma BP, cooler conditions followed, dated with 9 Ma BP (Matthews and Poore 1980, Schoell et al. 1994). Proxy data derived from isotope data suggest a similar ice extent as nowadays (Woodruff et al. 1981) or even smaller than nowadays (Barker et al. 1999). In correspondence with our simulation data, Nikolaev et al. (1998) points out that ice rafting became more intense during the Upper Miocene, effectuating ice rafting at least till Prydz Bay and the Kerguelen plateau (Eastern Antarctica). The glaciation conditions of the Tortonian time-slice prescribed by proxy data can be compared with the obtained simulation data. In order to analyse further climatic changes, the atmospheric pattern is investigated in the following.

2.3.3 Atmospheric pattern

In this section the large scale atmospheric pattern is described as a mean of the last 10 years of integration. Seasonal and annual averages are calculated. The summer means correspond to June, July and August (JJA) and the winter means correspond to December, January, and February (DJF) respectively. For comparison, anomalies are calculated between Tortonian run and Control run. For a comparison, the horizontal plots of the Tortonian results are shown in the appendix B.

Averages of climate variables taken over long periods of time tend to be nearly normal distributed, corresponding to the *Central Limit Theorem*. Using gridded output from climate models, sufficient data are available, both in space and time, for calculating a distribution of a climate variable at any grid point. Here the difference fields of the anomalous climate (Tortonian climate) and the control climate are computed and tested against the null hypothesis, which states that the mean difference of the climate variable at any grid point is zero. For analysing this one sample distribution a local statistical test can provide information about the significance of the mean difference to zero. For this purpose a local "Student t-Test" of one sample, representing the differences of the means, was applied to the climate variables. Assumptions include a normal distribution of the differences and that all differences come from the same distribution. The paired difference test statistic is given by

$$t_S = \frac{\mu}{S/\sqrt{n}} \qquad , \tag{2.13}$$

where μ is the mean difference, n the size of the sample of differences and S the sample variance of the differences. This statistic has a t-distribution with n - 1 degrees of freedom (cf. e.g., von Storch and Zwiers 1999). For the following applications a significance level p of 0.01 is set for the null hypothesis, which says that there is no difference between the mean of differences and zero.

In spite of the unchanged global averaged surface temperatures, significant differences exist in surface temperatures, especially over continental areas (see fig. 2.16). The general pattern of the difference in the yearly mean on the Northern Hemisphere shows an increase in temperatures at high latitudes and a decrease at mid-latitudes (fig. 2.16 c). In the Southern Hemisphere differences are less evident. However, there is also a general pat-

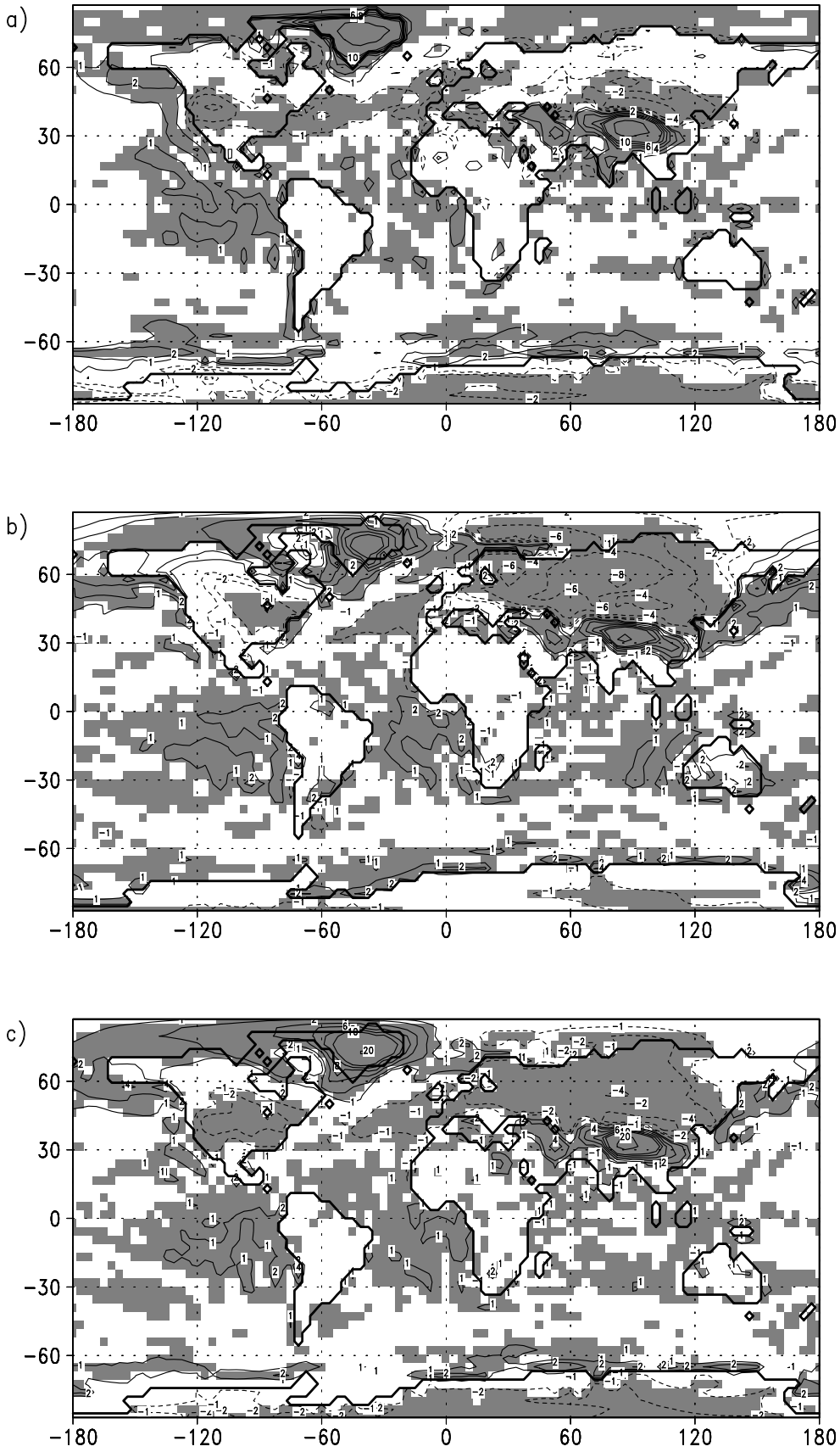

Figure 2.16: *Averaged surface temperature anomalies between Tortonian run and Control for a) JJA, b) DJF, and c) the year. Shaded squares represent "highly significant" anomalies with a local Student t-test ($p < 1\%$).*

tern showing a slight temperature increase in the subtropics and at the margin of sea ice. Over Antarctica a cooling occurs, which is more intense during winter months (fig. 2.16 a).

In accordance with the decrease of sea ice volume in the Northern Hemisphere (fig. 2.15) there is an enormous temperature increase on Greenland and surroundings. This is caused by the removal of the inland ice on the island. However in the Tortonian run, Greenland temperature values are still below zero in the yearly mean (see appendix B). At the ocean points around Greenland the increases in temperature can be attributed to the positive feedback mechanism of the ice-albedo effect. Additionally the changes differ with respect to the season. Regarding near surface temperatures over the polar ocean, the warming during winter months is greater (fig. 2.16 b) than in the summer season (fig. 2.16 a). Thus the annual temperature oscillation is smaller in the Tortonian run. In combination with the temperature rise over Greenland, the precipitation rate is increased over land (fig. 2.17). A precipitation increase of 108 mm is highest in summer season which corresponds to an amplification of 300 %.

In the Tortonian run mid-latitudes are characterized by significantly lower temperatures throughout nearly every longitude (fig. 2.16). A major role in this temperature decrease can be attributed to the change in oceanic heat transport. Nowadays European climate is affected by the Gulf Stream, which transports warmer surface ocean masses from Southern Hemisphere to high latitudes on the Northern Hemisphere. Therefore the ocean current provides 4 °C warmer ocean waters in the North Atlantic than at the same latitudes in the Pacific Ocean (Rahmstorf 1996). In the Tortonian run the northward oceanic heat transport is reduced, resulting in a reduction of the Gulf Stream. Hence less heat is transferred to Northern Europe. By this means the continental areas in Asia are also provided with colder air masses. Because the Gulf Stream is more effective during winter season, a strong cooling during DJF (December, January, February) occurs over continental regions. Therefore the temperature decrease is in agreement with the oceanic heat reduction. Over the North Atlantic the temperature gradient from mid-latitudes to high-latitudes is reduced. This complies with the prescribed oceanic heat transport. However, in the suptropics the temperature gradient is slightly increased leading to an intensified oceanic mass transport (fig 2.13). There is also an amplification of the Iceland Low over the North Atlantic which can be seen in the differences of sea surface pres-

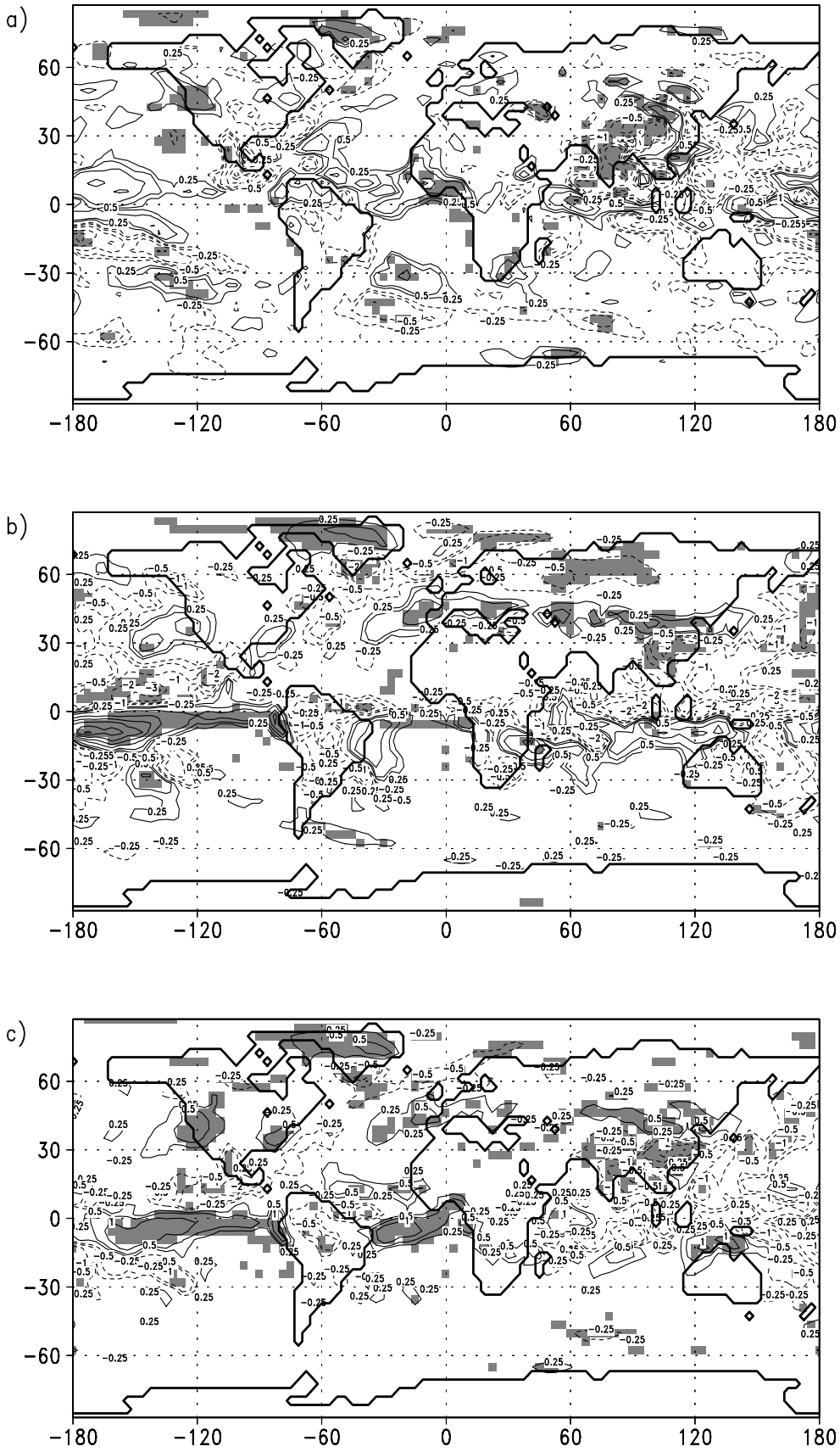

Figure 2.17: *Averaged anomalies of precipitation rates in mm/a between Tortonian run and Control for a) JJA, b) DJF, and c) the year. Shaded squares represent "highly significant" anomalies with a local Student t-Test ($p < 1\%$).*

sure values (fig. 2.19). This indicates particularly during DJF an increased atmospheric cyclonic character. Consequently the surface wind is amplified from the North Atlantic region to Southern Europe (fig. 2.20). As a result the precipitation rate is increased by up to 144 mm/a to 1116 mm/a in Southern Europe as was found in a detailed analysis for Europe.

With regard to the Pacific Ocean, the atmospheric circulation in the Tortonian run differs from the Control run. A changed atmospheric flow is indicated by the yearly mean temperature anomalies (fig. 2.16) in central and eastern Pacific Ocean. These differences correlate with the El Niño-year pattern well known from Recent observations and climate modeling (e.g., Bigg 1999, Latif and Neelin 1994). In general Recent climate measurements show positive temperature anomalies of about 2 to 4°C in the upper 50 m of the ocean during DJF. In contrast to the Tortonian results, these temperature variations occur on a time period of 2-8 years (Timmermann et al. 1999). In the Tortonian run there is a significant warming of ocean water at the eastern boundary of the Pacific Ocean with values greater than 2 °C. The warming occurs in correspondence with a decreased upwelling in this coastal area. Moreover, the atmospheric circulation is also reorganized. As climate models and measurements show, an El-Niño-like pattern is combined with a weakening of the equatorial Walker circulation (e.g., Bigg 1999). Hence equatorial trade winds are weakened which can also be seen in numerical results of the Tortonian run (fig. 2.20). Consequently a convergence zone over the central Pacific Ocean is formed resulting in a highly significant increase of precipitation (fig. 2.17). Furthermore there are drier regions over the eastern and western Pacific. A comparison of Recent and palaeo model output shows that the atmospheric circulation of the Tortonian run over the Pacific Ocean equals a permanent El-Niño phenomenon. As it is analysed by climate model results (e.g., Roeckner et al. 1993) there are aside from tropical atmospheric responses also extratropical climate changes which are somehow related to the El-Niño phenomena (teleconnections). These extratropical atmospheric responses, however, cannot be analysed for the Tortonian run. This is due to the specific Tortonian set-up which considers several different boundary conditions in comparison to the Control run. As there exist different boundary constraints for the palaeo-run several atmospheric response mechanisms are most likely overlapped.

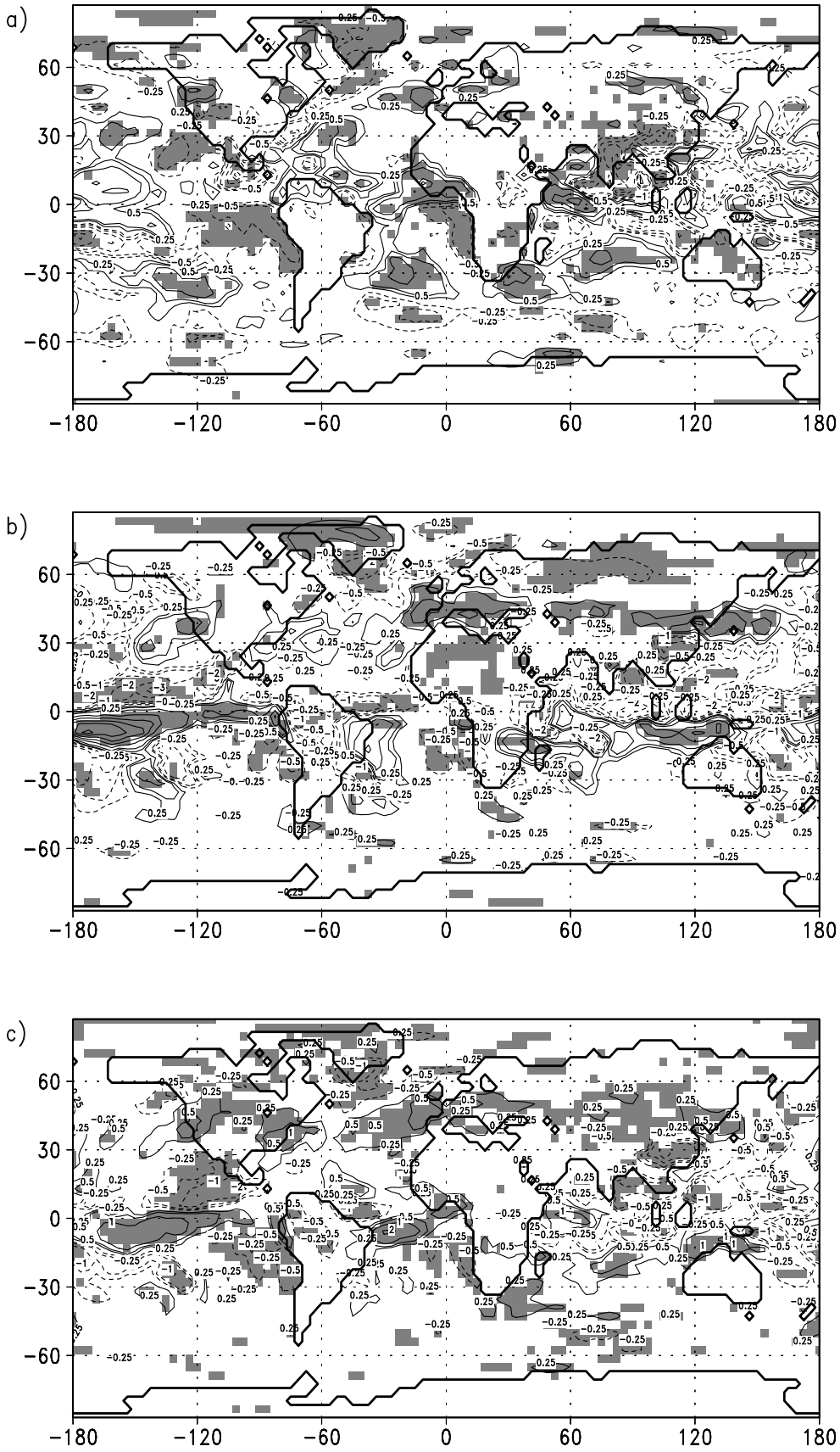

Figure 2.18: *Averaged anomalies of precipitation minus evaporation rates in mm/a between Tortonian run and Control for a) JJA, b) DJF, and c) the year. Shaded squares represent "highly significant" anomalies with a local Student t-Test ($p < 1\%$).*

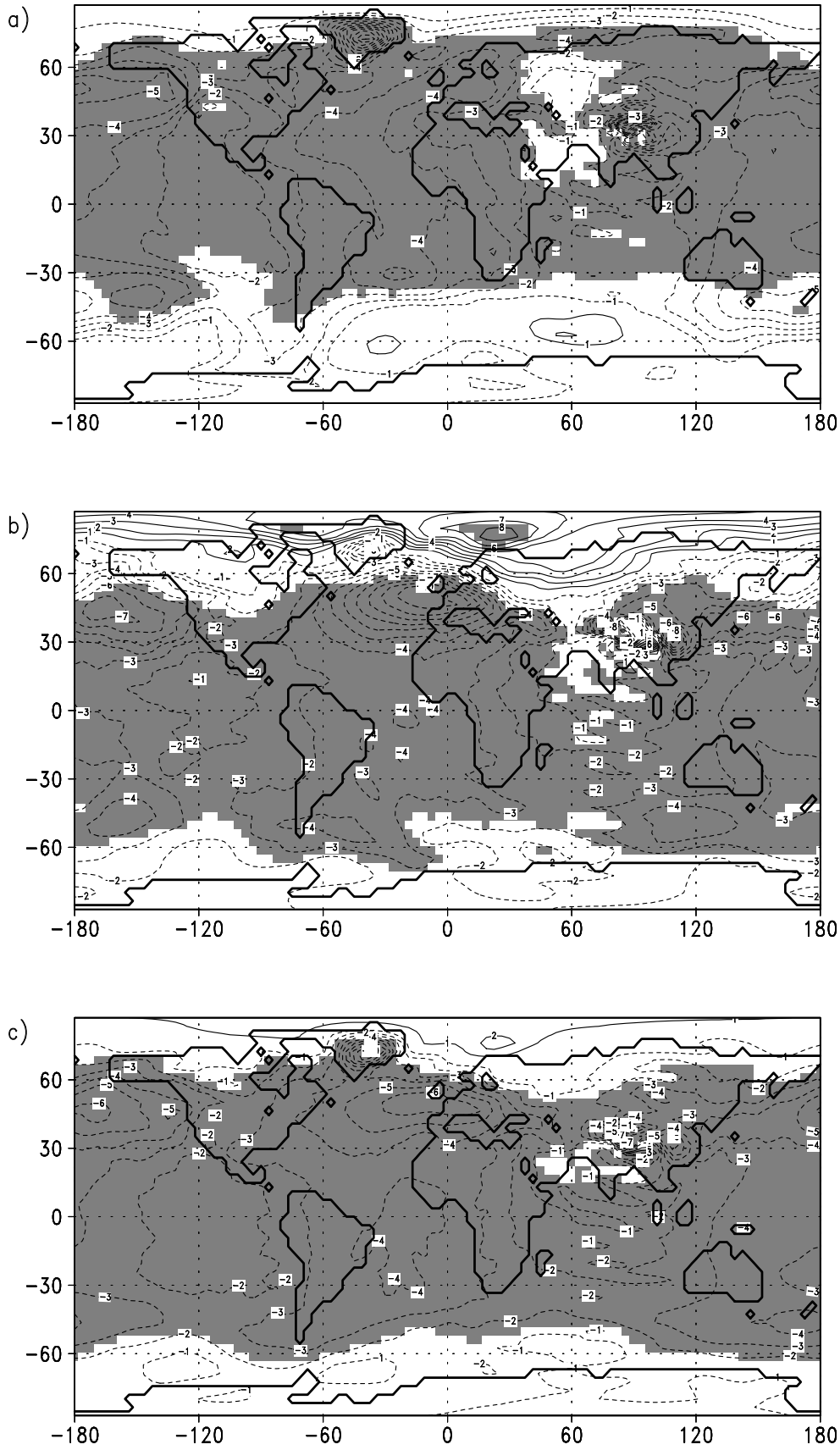

Figure 2.19: *Averaged anomalies surface pressure between Tortonian run and Control for a) JJA, b) DJF, and c) the year. Isoline spacing in 1 hPa. Shaded squares represent "highly significant" anomalies with a local Student t-Test (p <1%).*

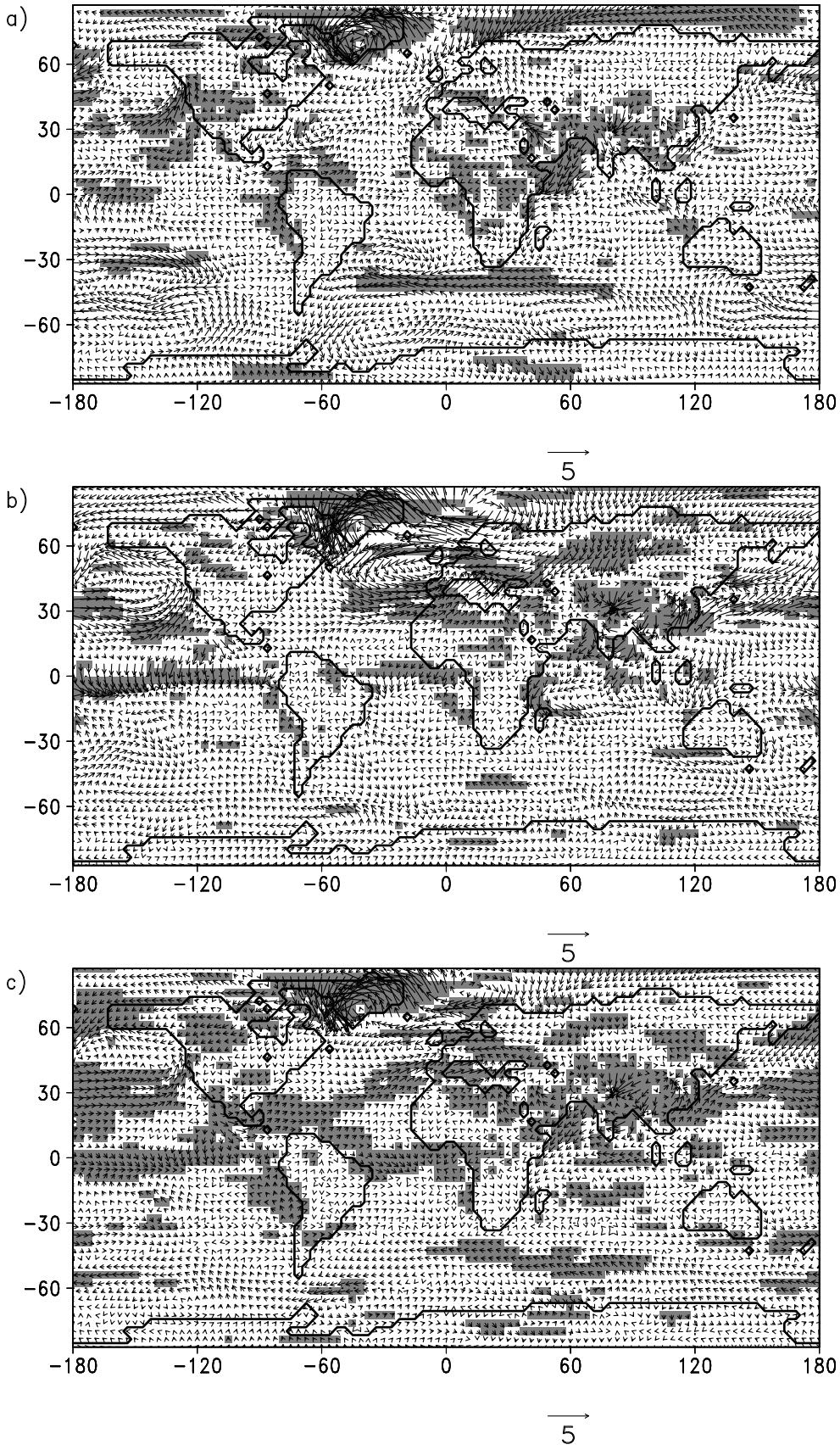

Figure 2.20: *Averaged anomalies of wind vectors between Tortonian run and Control for a) JJA, b) DJF, and c) the year. Reference arrow is representing 5 m/s. Shaded squares represent "highly significant" anomalies with a local Student t-Test ($p < 1\%$).*

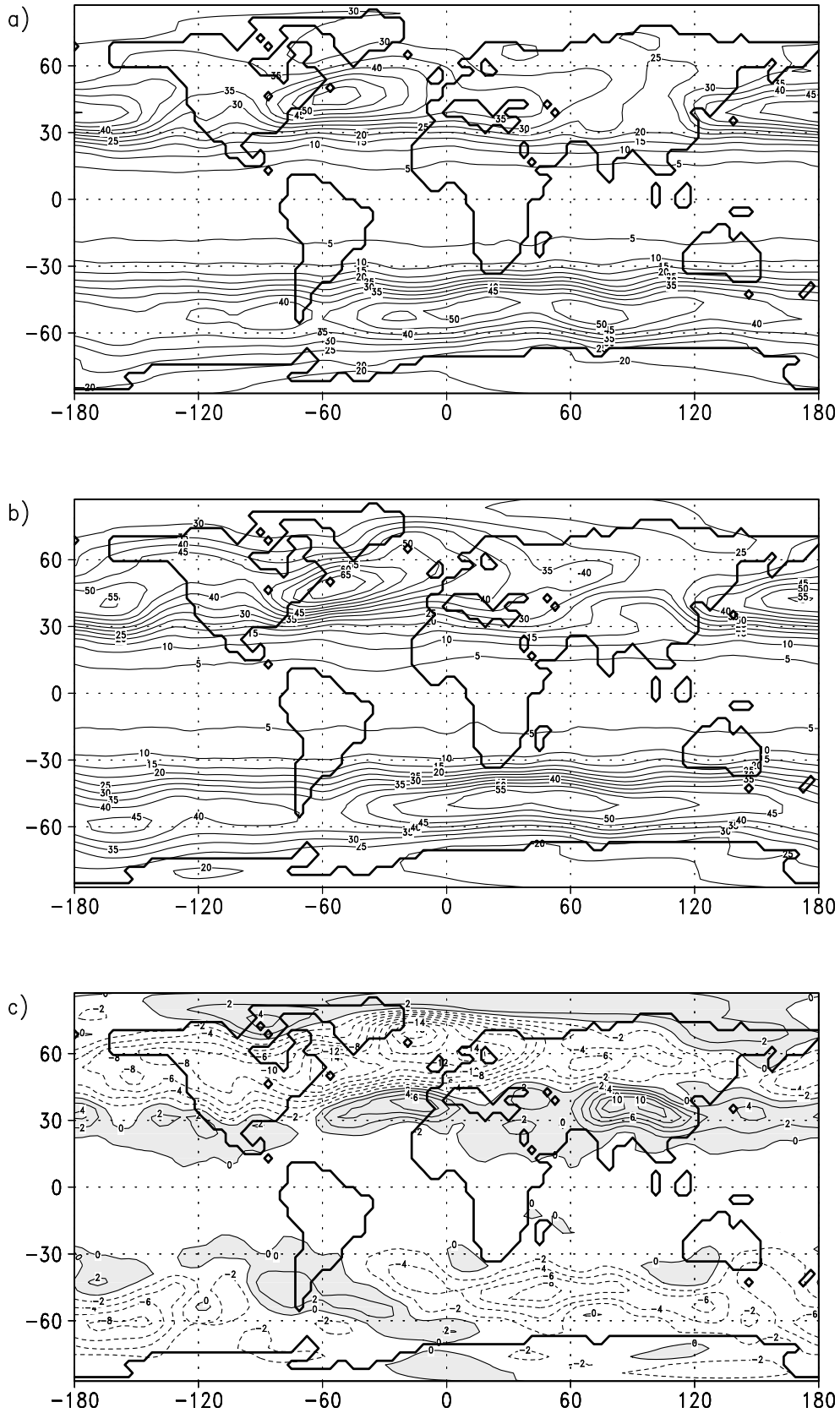

Figure 2.21: *Standard deviation of the geopotential in 500 hPa height during DJF. The geopotential is band-pass filtered. Shaded area represent positive values. a) Tortonian run. Contour interval is 5 gpm, b) Control run. Contour interval is 5 gpm and c) Difference between Tortonian and Control run. Contour interval is 2 gpm.*

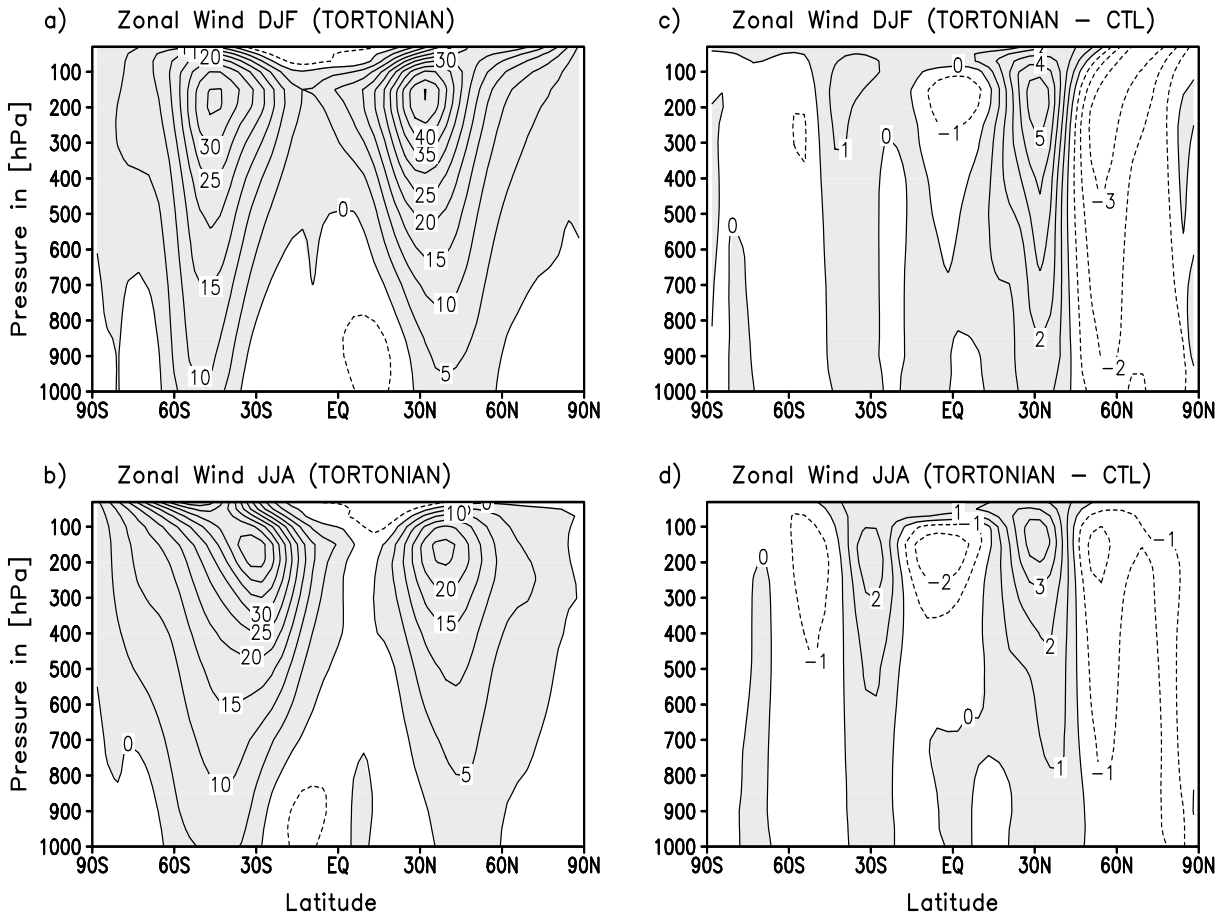

Figure 2.22: *Zonal averaged zonal wind and zonal wind anomalies with height. a) DJF with a contour interval of 5 m/s b) JJA with a contour interval of 5 m/s, c) anomalies between Tortonian and Control run for DJF, contour intervall is 1 m/s, d) anomalies between Tortonian and Control run for JJA, contour interval is 1 m/s. Shaded area represent positive values.*

A further study concentrates on atmospheric variability that is not represented in monthly, seasonal or yearly averages of atmospheric variables. In order to focus on synoptic phenomena at mid-latitudes, the geopotential in 500 hPa height is investigated. The variation of the height of the geopotential in the middle of the atmosphere gives information on directional movements of low pressure areas. Therefore the geopotential height can also describe storm track paths and accordingly it is an indicator of storm track activity. For this purpose the 500 hPa geopotential is time filtered using the baroclinic time filter from Blackmon (1976). This time filter considers changes in a time span of 2.35 to 6.6 days, which is the usual lifetime of a storm. Calculating the standard deviation gives further detail on the variability of low pressure areas and their tracks during their evolution. Areas

with higher variability are a measure of the number of passed storms. As the storm tracks are more frequently during winter time the months DJF were taken into account. In fig. 2.21 the standard deviation is represented showing a reduction of low pressure activity in midlatitudes. There is also an equatorial shift of storm tracks over the North Atlantic and the North Pacific. This indicates a decrease in meridional transient transport which can be ascribed to the diminished oceanic heat transport.

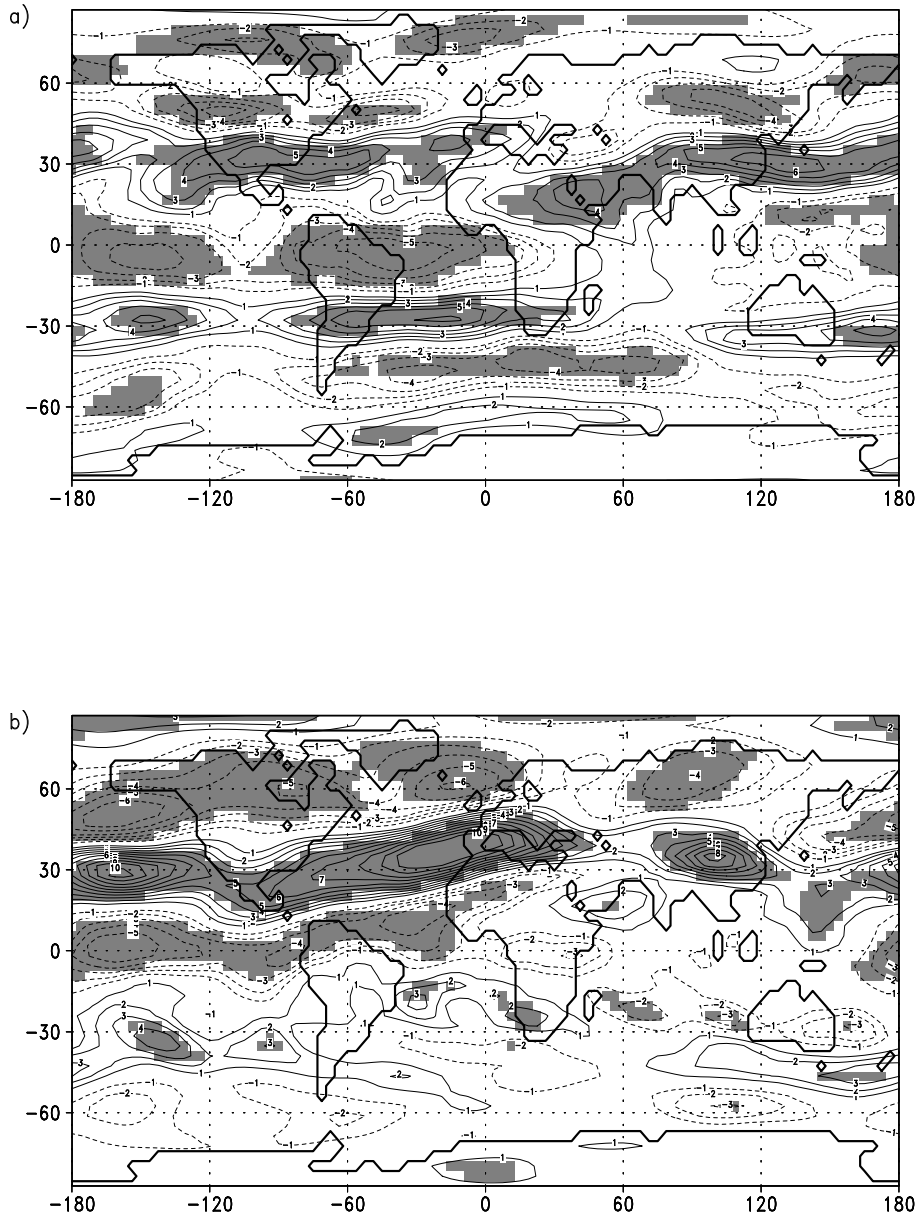

Figure 2.23: *Averaged anomalies of wind in 200 hPa height between Tortonian run and Control for a) JJA, b) DJF. Contour intervals are 1 m/s. Shaded squares represent "highly significant" anomalies with a local Student t-Test (p <1%).*

Both the relocation of storm tracks and the position of the center of the jet-stream in 200 hPa height (fig. 2.22 and fig. 2.23) show an equatorial shifting of the planetary wave. The southward shifting over Asia is enhanced by the reduction of the height of the Tibetean Plateau. Simultaneously there is an intensification of zonal mean mass transport (fig. 2.23).

Another indicator for a change in mid-latitude circulation is the North Atlantic Oscillation Index. In general the North Atlantic Oscillation (NAO) describes an atmospheric phenomenon in the North Atlantic sector as an organized motion of Iceland Low and Azores High. For reasons largely unknown these pressure systems feature a northward shifting with a simultaneously strengthening of both pressure systems. The intensified pressure gradient results in a zonal circulation providing Europe with a higher frequency of storms, an increase in precipitation rates during winter, a warmer climate during winter, and a cooler climate during summer. With regard to North America this strengthened meridional pressure gradient provides a cooler climate during winter. With a reduction of the meridional pressure gradient opposite climatic conditions are found. These different atmospheric conditions are explained in detail by e.g., Osborn et al. (1999) and Paeth et al. (1999). For this study a descriptive investigation of NAO is used instead of an analytical calculation.

A comparison of annual averaged surface anomalies for the Control and Tortonian simulations (fig. 2.19) shows a decrease in meridional pressure gradient and a slight southward shift of the weakened pressure systems for the Tortonian time-slice. As suggested by modern climate modeling results (Mächel et al. 1998) this change induces a more meridional circulation with less advection of warmer air to Europe. This is in agreement with a weakened storm track over the North Atlantic (cf. fig. 2.21) and a less intense zonal wind component in the upper troposphere above this sector (cf. fig. 2.23).

Temperature increases in Southern Asia (fig. 2.16), corresponding to the results of the Tortonian run, can be linked with the enormous reduction of the height of the Tibetean Plateau. The change of mountain heights is supposed to have an influence on both the high tropospheric circulation and the regional climate. Referring to the upper-level circulation, positive temperature anomalies could affect the strength of the jet-stream above

the Tibetean Plateau. The regional climate over Asia is commonly characterized by the monsoonal low-level flow (lowest 200 hPa layers of the atmosphere) over land connected with heavy rainfalls over India and Southeast Asia during JJA. This feature is caused by an intense heating of landmasses during Northern Hemisphere summer producing a warm core structure with a low-level cyclonic circulation. In the upper troposphere, however, an anticyclonic circulation occurs which is associated with the easterly tropical jet (cf. e.g., Barry and Chorley 1992, Holton 1992).

For the Tortonian run a lower mountain range induces a reduced upward vertical motion South of the Tibetean Plateau. This can be seen in the reduction of upper troposphere wind and a less intense low-level flow (cf. fig. 2.20) from Indian Ocean to South Asia. Therefore, less moist air is moved from open ocean surface to Asian landmasses. As a result the precipitation rates are reduced to nearly half of present day values over India (fig. 2.17). This is in qualitative agreement with studies from Prell and Kutzbach (1992), Ruddiman and Kutzbach (1989), and Kutzbach et al. (1989). They calculated a precipitation reduction over Asia of 20 % of present day values. It is suggested by e.g., Ding et al. (1999) that the Tibetean Plateau may have reached a significant height in the Upper Miocene for maintaining the East Asia monsoon system. Also Filippelli (1997) dates with sedimentary and geochemical methods an intensification of the Asian monsoon at 8 Ma BP. Numerical studies by Ramstein et al. (1997) and Fluteau et al. (1999) agree with the results of the standard Tortonian run that there is an indication of a less intense Asian monsoon system during late Miocene in comparison to nowadays.

Due to the rapid rise of the Tibetean Plateau during the Cenozoic, this region is likely to have been sensitive to rapid climatic changes. In the Tortonian run, a weakening of summer Asian monsoonal circulation is associated with a less intense aridification north of the Tibetean Plateau (2.17). Today, the Tibetean Plateau prevents moist air masses from penetrating north of the massive mountain range. However, in the Tortonian the lower height of the Tibetean Plateau leads to a more zonal flow transporting moisture over Asia, which can be seen in the intensified standard deviation of the geopotential height (fig. 2.21). This is in compliance with studies by Broccoli and Manabe (1997) and Ramstein et al. (1997). Additionally, several studies based on the commencement of eolian deposits in central China indicate the beginning of aridification north of the

Tibetean Plateau starting between 5.25 and 7.4 Ma BP (e.g., Ding et al. 1999, Wang et al. 1999). Hence our numerical simulation results with regard to a more humid climate north of Tibetean Plateau are in agreement with proxy data and other numerical studies.

2.4 Tortonian run with double CO_2

Specifying an actual value of remaining carbon dioxide in the atmosphere for the Tortonian time-slice is difficult. There have been a variety of different studies on this topic. Since the beginning of the Phanerozoic carbon dioxide content has decreased permanently due to geological and biological processes (Berner 1991, Berner 1998). The reduction can be attributed to different carbon sinks. During Earth history carbon is stored in plants and sedimentary depositions in ocean and intramontane basins. Due to these different kind of carbon storages there exist a variety of methods which could provide indirect information on the variation of CO_2 over time.

Paleogene time-slices are characterized by a warmer atmosphere with a carbon dioxide content up to a tripling of the preindustrial level. Cerling et al. (1997) suggest an atmospheric carbon dioxide content above about 500 ppm based on the displacement of C_3 plants for the benefit of C_4 ones. This revolution in biomass is supposed to have been occurred at the Miocene/Pliocene boundary. Estimates from palaeosoils suggest less than 700 ppm for late Miocene/Tortonian (Cerling 1991) i.e. also indicating a significant higher value than the present one. Studies based on fossil plants from the Upper Miocene by Van der Burgh et al. (1993) show also in comparison to nowadays a slightly higher atmospheric carbon dioxide concentration in the range of 380 ppm to 400 ppm. However, studies from Pagani et al. (1999) indicate a CO_2 content for the late Tortonian as low as the preindustrial level. Their investigation is based on carbon isotopic analysis of planktonic shells.

Because of disagreement in estimated CO_2 levels for the Late Miocene, a simulation with enhanced CO_2 was performed. The CO_2 content is doubled, which corresponds to the upper limit of previous estimations. All other boundary conditions are kept the same as in the standard Tortonian run. For simulations with increased greenhouse gases warmer climates are expected at high and mid-latitudes, as is well known from greenhouse scenarios of future climate studies (e.g., IPCC scenarios composed by Houghton et al. 1995).

The following results are calculated from the last 8 years of integration of the double CO_2 run for the Tortonian time slice. Model output will be discussed with regard to changes in atmospheric circulation pattern in comparison to the Tortonian run with single carbon dioxide content. In order to analyse the "greenhouse effect", anomalies of both Tortonian runs are represented in the following. For a comparison of absolute values of the discussed variables, results of the standard Tortonian run (single CO_2 content) are shown in appendix B.

A doubling of CO_2 in ECHAM4/ML causes an increase in global surface temperature of about 3 °C (cf. tab. 2.1). This value is comparable to that for Recent climate scenarios using mixed-layer ocean models, which indicate an increase ranging from 2.5 to 4 °C (McGuffie et al. 1999). Due to higher temperatures there is an enormous change in sea ice extension, with reductions of up to 75 % for Artic sea ice during summer and 60 % during winter relative to the Control run (tab. 2.1). Furthermore, the changes tend to reduce seasonal differences in sea ice volume. Because the sea-ice model used in these runs is non-dynamic and prescribed via the heat budget (Roeckner et al. 1996, Modellbetreuungsgrupe 1997), reliable predictions for changes in sea ice volume are not possible.

Table 2.1: *Global and hemispherical averaged values of temperature (T), precipitation (P) and sea ice volume on the Northern and on the Southern Hemisphere .*

	T in °C	P in mm/d	Sea Ice Northern Hemisphere JJA	DJF	Sea Ice in $10^{12}m^3$ Southern Hemisphere JJA	DJF
Control	15.7	2.83	11.3	17.8	17.5	14.8
Tor	15.6	2.82	09.4	16.3	16.6	13.8
Tor ($2xCO_2$)	18.6	2.92	1.5	6.1	12.6	10.2

A doubling in CO_2 for the Tortonian run causes a differential temperature increase over land and oceans. Temperature increases are greater over continents due to different heat capacities of land and ocean (fig. 2.24). The anomalies in temperatures show a great warming at high latitudes due to the snow-albedo positive feedback mechanism (fig. 2.24). This is initialized by a warmer atmosphere, which reduces snow cover at northern parts

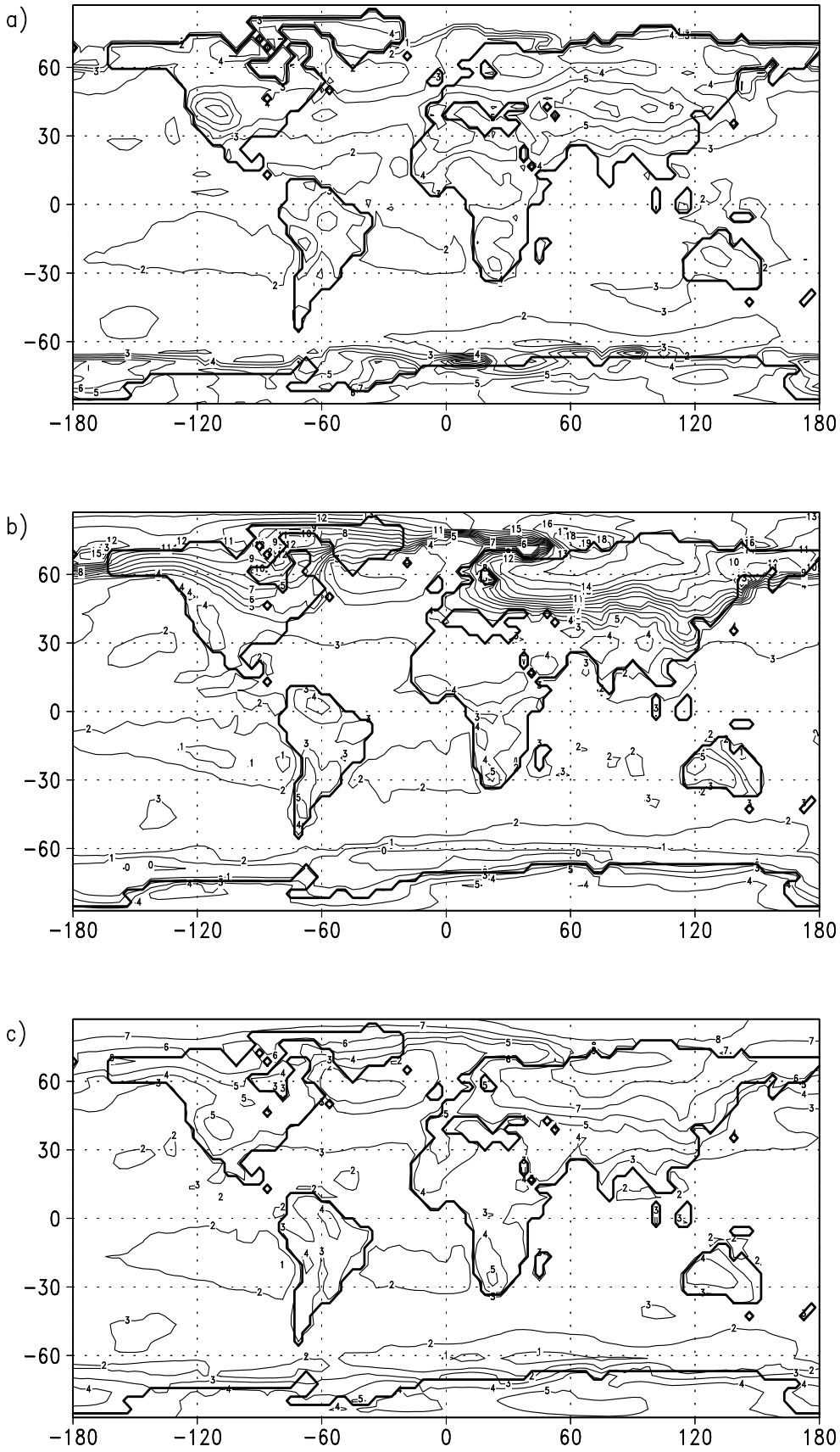

Figure 2.24: *Averaged surface temperature anomalies between double CO_2 Tortonian and single CO_2 Tortonian run a) JJA, b) DJF, and c) the year. Contour interval is 1 ° C.*

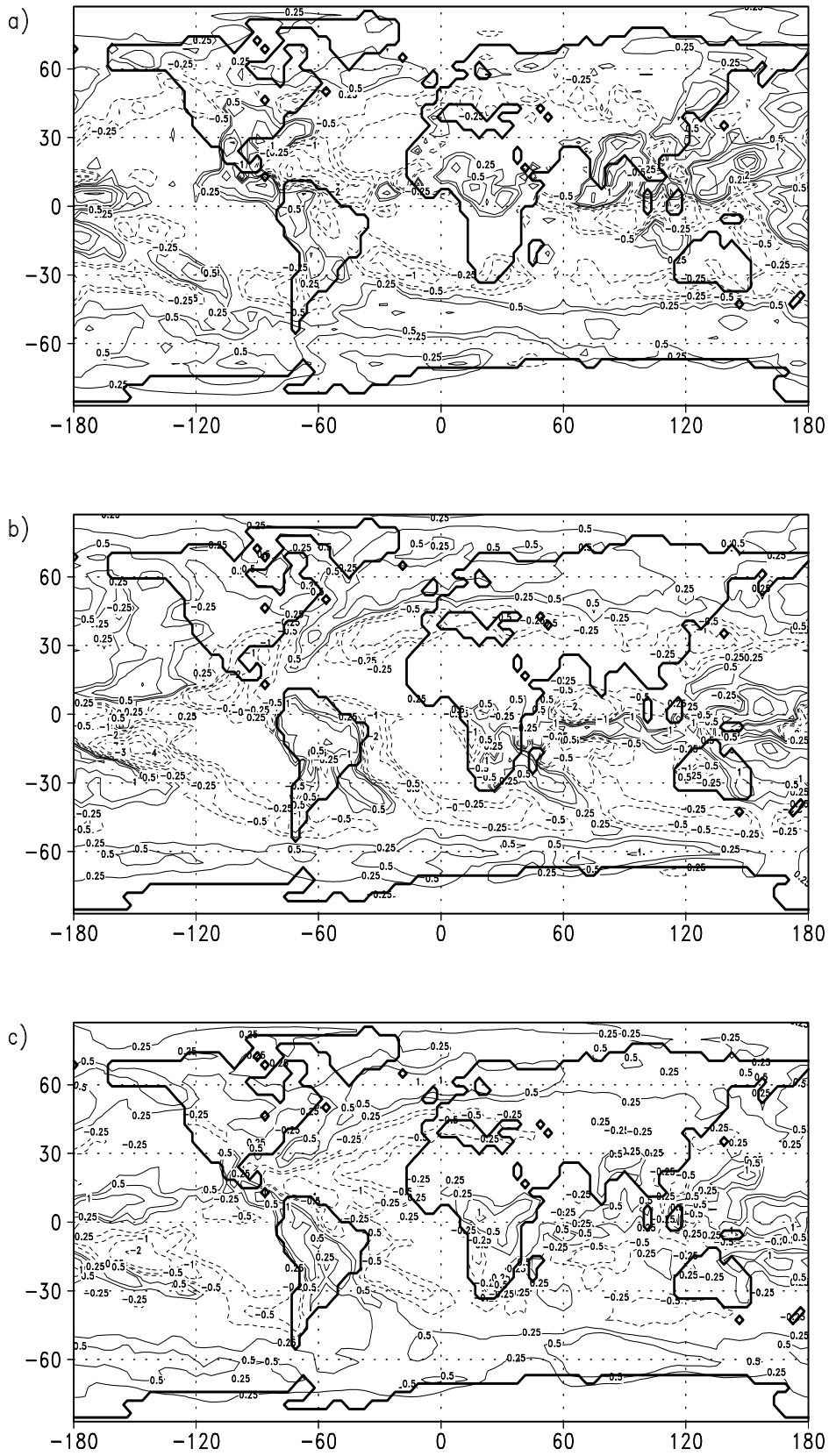

Figure 2.25: *Total precipitation anomalies between double CO_2 Tortonian and single CO_2 Tortonian run a) JJA, b) DJF, and c) the year. Contour interval is 1 mm/d.*

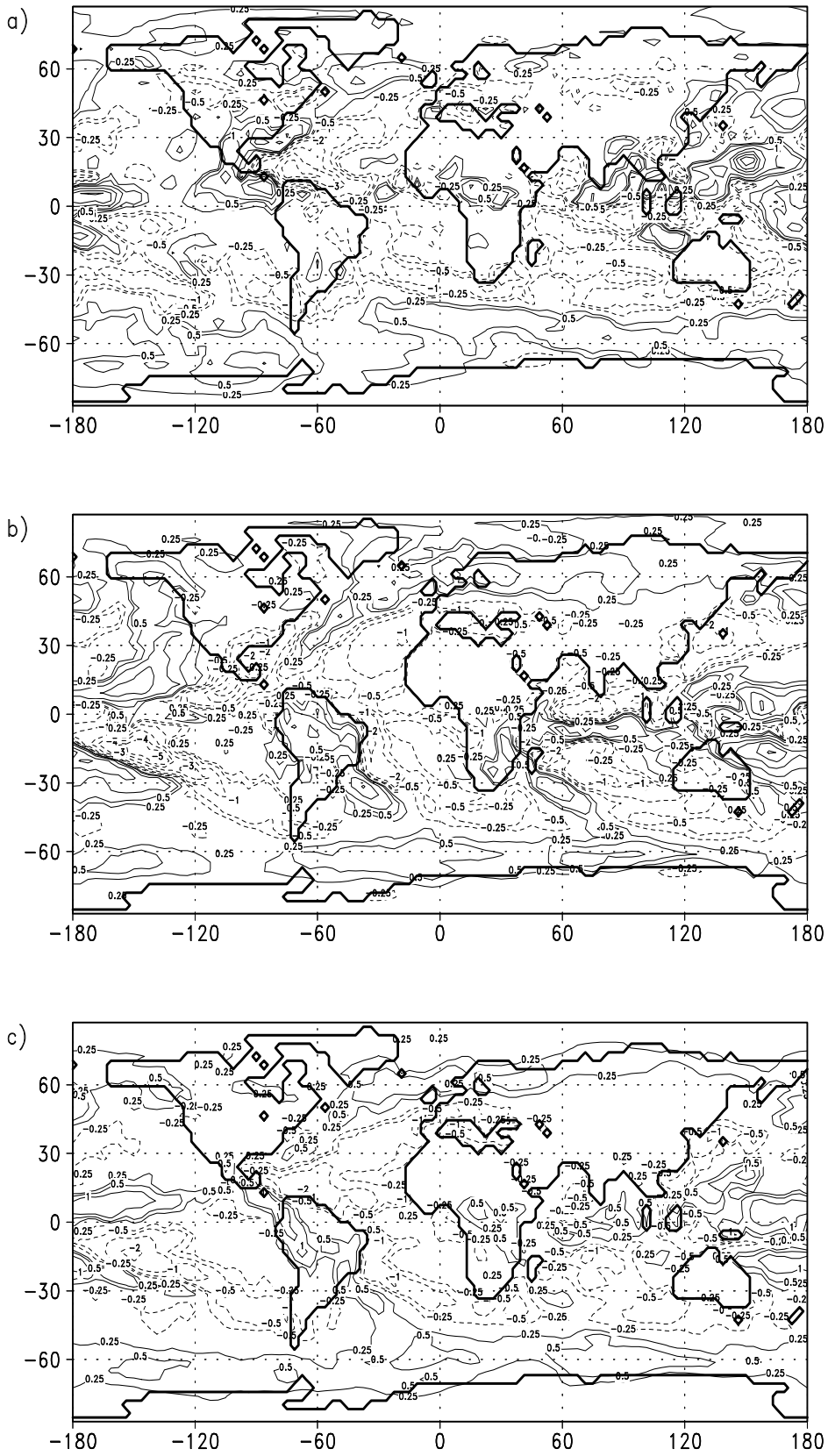

Figure 2.26: *Precipitation minus evaporation anomalies between double CO_2 Tortonian and single CO_2 Tortonian run a) JJA, b) DJF, and c) the year. Contour interval is 1 mm/d.*

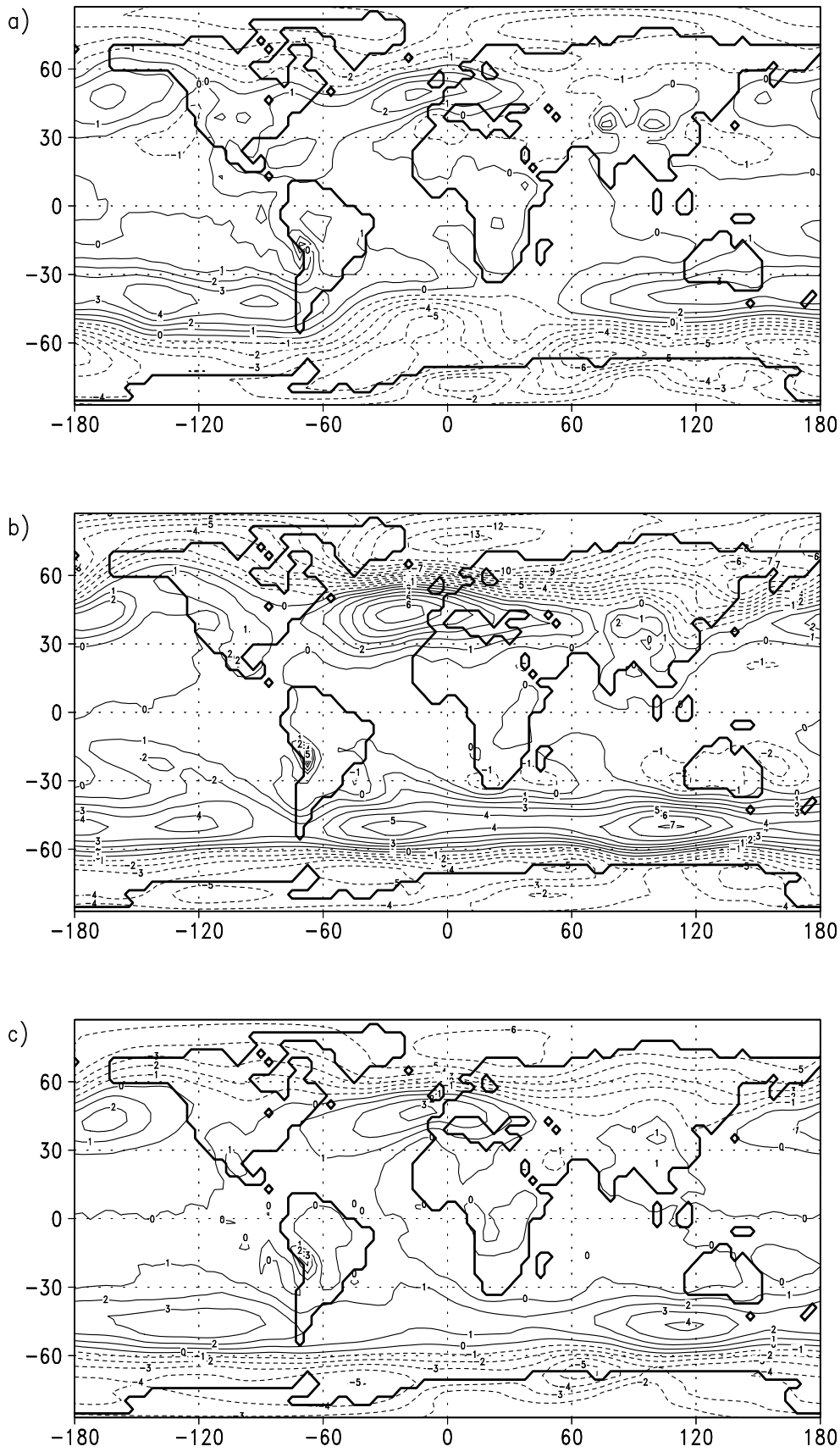

Figure 2.27: *Surface pressure anomalies between double CO_2 Tortonian and single CO_2 Tortonian run a) JJA, b) DJF, and c) the year. Contour interval is 1 hPa.*

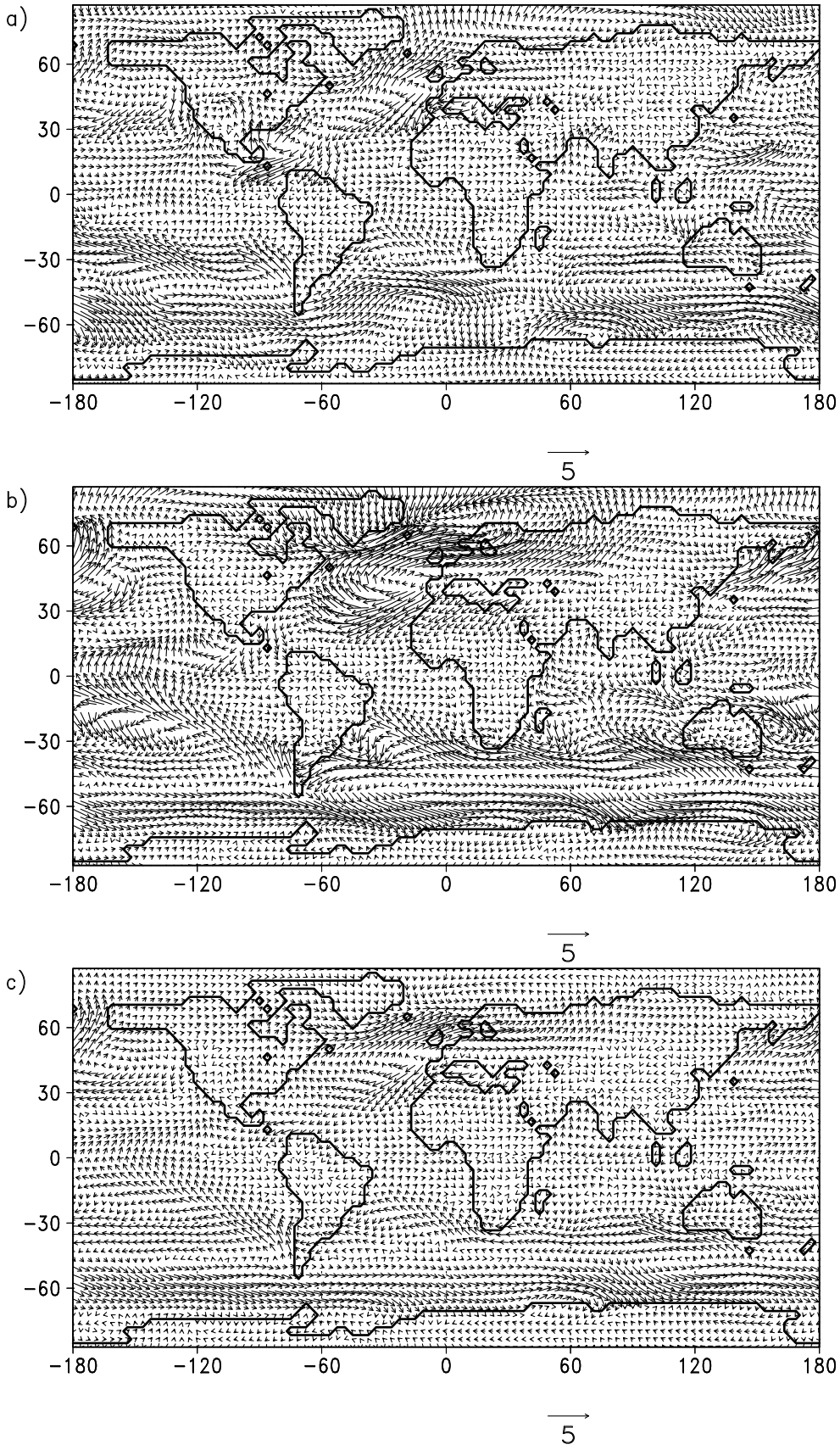

Figure 2.28: *Wind anomalies in 10 m height between double CO_2 Tortonian and single CO_2 Tortonian run a) JJA, b) DJF, and c) the year. Reference arrow represents 5 m/s.*

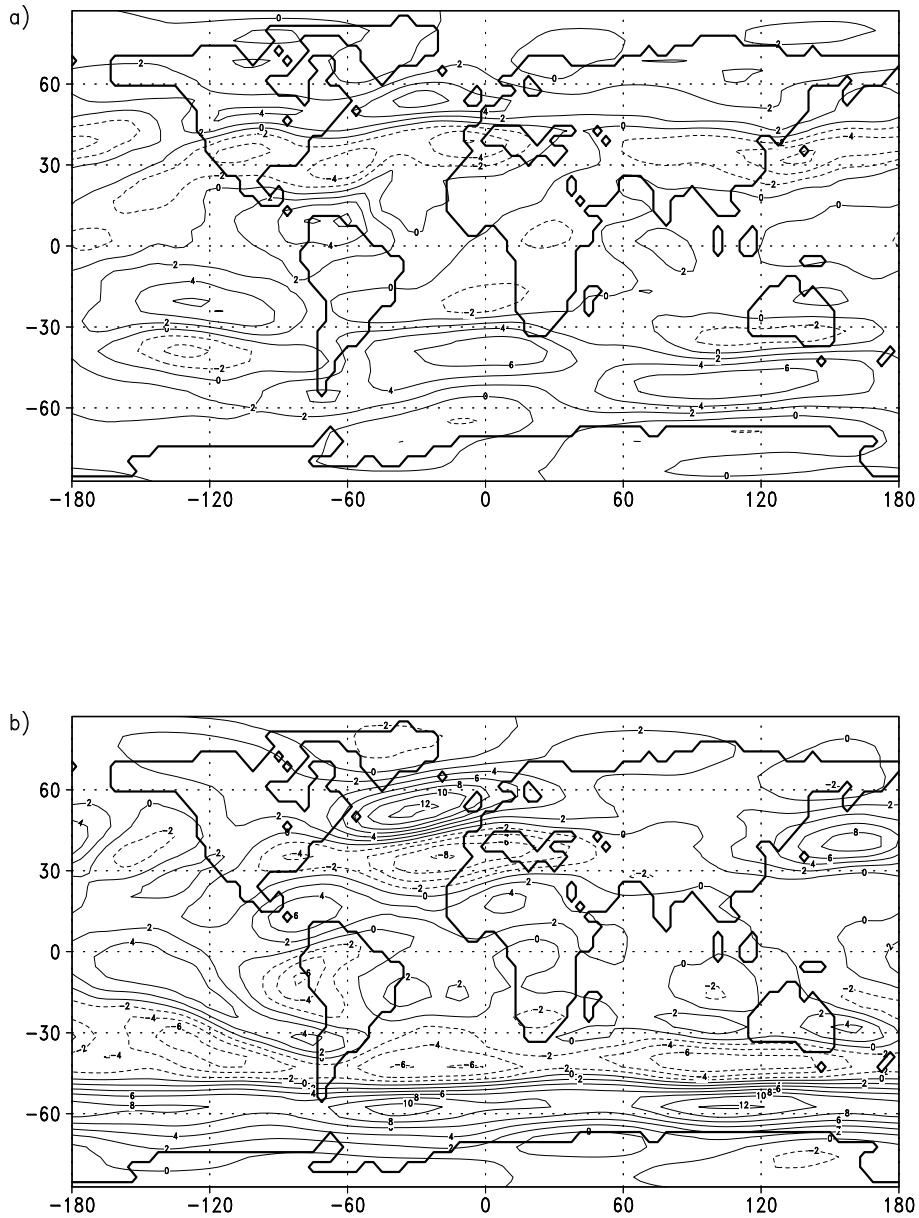

Figure 2.29: *Zonal wind anomalies in 200 hPa height Tortonian and single CO_2 Tortonian run a) JJA, b) DJF. Contour interval is 2 m/s.*

of the continents. While the snow cover diminishes, the albedo becomes smaller. In addition, land is further warmed because it is getting drier as there is less moisture available in the soil. Since there is no dynamic description of vegetation cover in the model, a potential spreading of vegetation cover into northern parts cannot be represented. And potential evaporation processes which would be induced by a different vegetation cover cannot be considered. However, a change in vegetation from ice-covered bare soil to taiga would change the albedo to lower values which would lead to a further warming. Thence, a possible warming or cooling at high latitudes due to vegetation-temperature interactions cannot by assessed without a dynamic vegetation module or a Tortonian prescribed

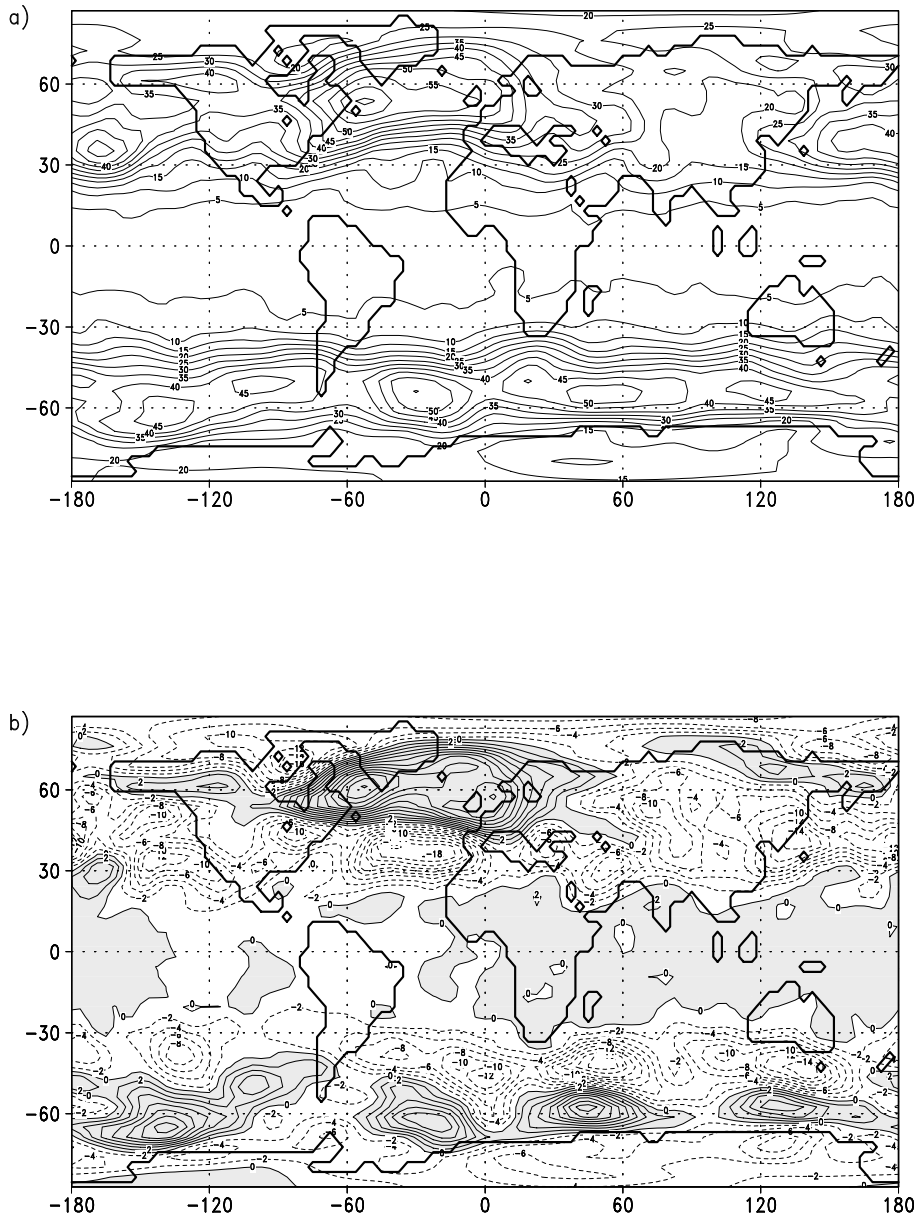

Figure 2.30: *Standard deviation of the geopotential in 500 hPa height. The geopotential is band-pass filtered. Shaded area represent positive values. a) Double Tortonian run with contour interval of 5 gpm b) Differences between Double CO_2 Tortonian run and single CO_2 Tortonian run with contour interval of 2 gpm.*

vegetation cover. Furthermore, temperature increases are more intense on the Northern Hemisphere due to the imbalance in global land distribution. The additional "greenhouse effect" attributed to carbon dioxide doubling leads to a less distinct seasonal cycle which can be seen in a stronger warming during DJF in comparison to JJA. The contribution of long-wave radiation makes high latitudes less sensitive to the seasonal solar cycle. A study from Berger et al. (1998) also establishes a great sensitivity of ice volume to carbon dioxide forcings. With their simple and not yet fully accomplished 2-dimensional model they suggest a weakened response to astronomical forcings - these studies were performed

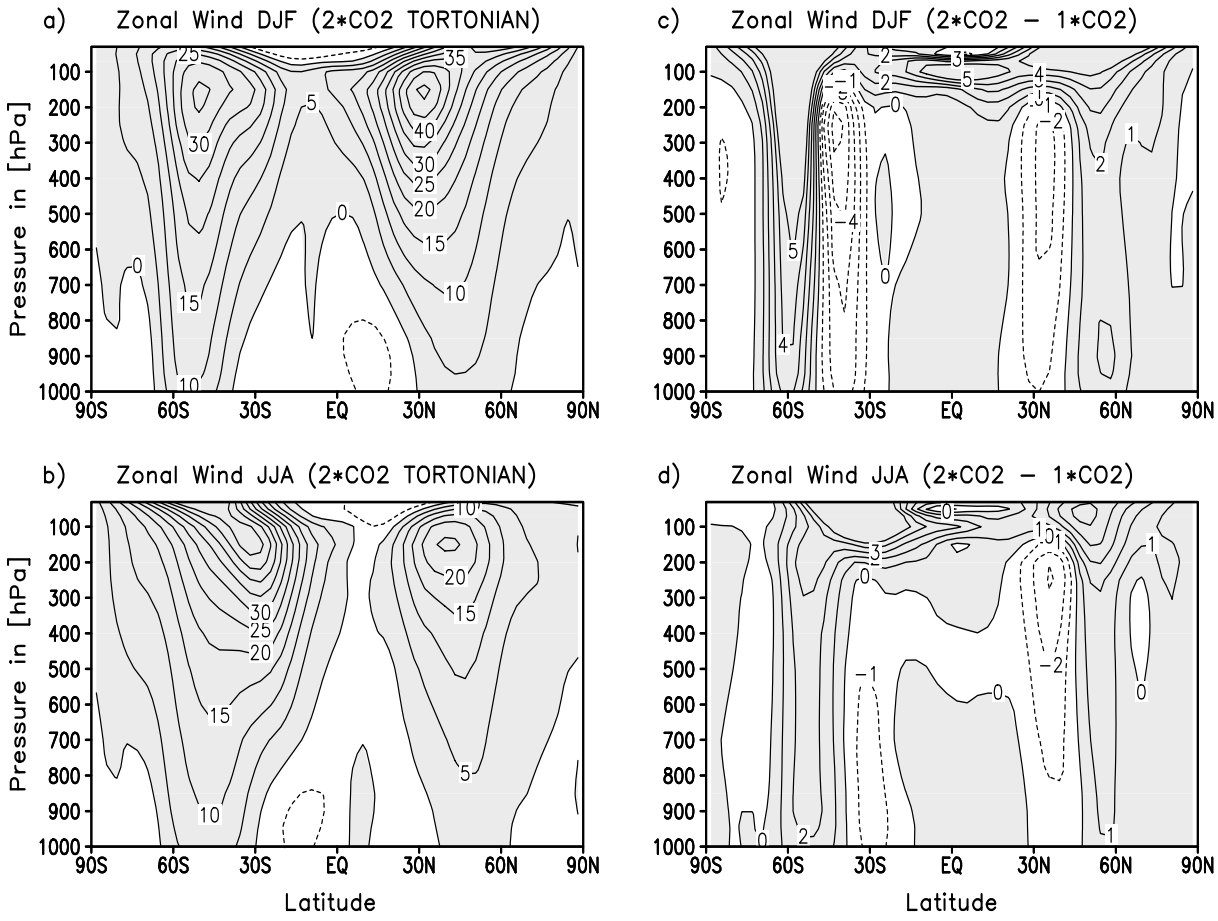

Figure 2.31: *Zonal averaged zonal wind and zonal wind anomalies. a) DJF with a contour interval of 5 m/s b) JJA with a contour interval of 5 m/s, c) anomalies between double and single CO_2 Tortonian runs for DJF, contour interval is 1 m/s, d) anomalies double and single CO_2 Tortonian runs for JJA, contour interval is 1 m/s. Shaded area represent positive values.*

for the Holocene - with an increase in carbon dioxide. As a consequence climate conditions with high CO_2 values show a smoothed annual latitudinal temperature curve resp. a reduced seasonal temperature cycle. A similar result representing a less intense variation between summer and winter season was obtained by Raymo et al. (1990). They initialized their model using a reduced sea ice cover in order to reproduce sea ice albedo-temperature feedbacks.

With a global temperature increase the hydrological cycle is intensified because a warmer atmosphere can store more water vapor in form of latent heat (cf. tab. 2.1). Due to warming evaporation is increased in the subtropical oceans (fig. 2.26) and moist air is transported poleward. At higher latitudes (30°N - 70°N) water vapor is released and a

gain of precipitation is noticeable over the North Atlantic and Pacific (fig. 2.25). This additional freshwater input could reduce surface salinities at high latitudes in areas of North-Atlantic Deep Water formation. As a result this could induce a further reduction of the overturning cell in the North Atlantic which is shown for present day scenarios (e.g., Mikolajewicz and Voss 2000, Rahmstorf 1995). On the other hand a further strengthening of the overturning cell is supported by an increase in subtropical evaporation. As a consequence more saline ocean water is transported to higher latitudes and thus the thermohaline circulation is affected. These processes are investigated with a climate model containing a more sophisticated ocean module (Mikolajewicz and Voss 2000). Due to the deficiency of a dynamic ocean model our ECHAM4/ML cannot represent a further weakening of the overturning cell. Nevertheless, our ECHAM results represent an aridification over the ocean in the subtropical Atlantic Ocean during DJF (fig. 2.26).

In the doubled CO_2 experiment the reduction of Arctic ice cover during winter is combined with a strong polar warming. The polar heating causes a weakening of the Polar High and a decrease in surface pressure. Simultaneously, the Iceland Low over the North Atlantic region is shifted further northwards (fig. 2.27). An intensification of this low pressure region leads to an amplification in 10 m height wind speed over the North Atlantic (fig. 2.28). Studies by Raymo et al. (1990) also show a relationship between a decrease in Arctic sea ice and stronger winds in mid-latitudes on the Northern Hemisphere. Increases in surface winds can be attributed to an intensification in the westerlies at almost the same latitudinal position. The cause of this intensification can be explained as follows. The more unstable atmosphere in the double CO_2 experimental run results in warmer tropospheric temperatures. The more baroclinic condition leads to an intensification of the jet-stream which is located in about 200 hPa height (fig. 2.29). In comparison to the standard Tortonian run there is a northward shift of the jet-stream. A similar northward shift of the jet-stream is also found in modern climate scenarios with enhanced carbon dioxide studies (Hall et al. 1994). This magnified wind speed at higher levels has an impact on the variability of the 500 hPa geopotential (fig. 2.30). As a consequence the geopotential height variation over the North Atlantic and coastal parts of Europe is intensified. The analysis of the geopotential height variability also shows a widening of the storm track locations to the East and North. Despite this reorganization the increase in geopotential height variation could imply a higher frequency of storm tracks (Schubert et

al. 1998, Lunkeit et al. 1998). This can be traced back to a greater amount of latent heat in a more humid atmosphere or to changes in local baroclinicity (Hall et al. 1994).

With regard to the North Atlantic Oscillation, Recent climate modeling studies with enhanced carbon dioxide show an increase in the latitudinal surface pressure gradient and an enhancement of zonal wind over the Atlantic Ocean (e.g., Paeth et al. 1999, Rogers et al. 1998). Hence for the doubled CO_2 Tortonian sensitivity run stronger westerly winds are expected over Europe. The yearly mean surface pressure (fig. 2.27) over the North Atlantic shows a strengthening of some hPa at the location of the Iceland Low. Anomalies corresponding to the Azores High result in an increase of 2-3 hPa. The enhanced pressure gradient being more pronounced during winter indicates a higher North Atlantic Oscillation implying a more zonal circulation in mid-latitudes (cf. fig. 2.28). The increase in meridional pressure gradient leads to more zonal wind advection supplying the European/Asian continent with higher winter temperatures (fig. 2.24). Shortly this index provides an indicator for northern continental winter conditions. In correspondence with a warmer winter climate over Europe, model results show a decrease in seasonality. The model output of the CO_2 sensitivity experiment shows that the intensified momentum-heat flux mechanism in mid-latitudes plays an important role for the European climate.

Both present day CO_2 scenarios with a carbon dioxide doubling (Douville et al. 2000) and the Tortonian CO_2 experimental run cause a temperature increase of several degrees during summer over the Asian continent (fig. 2.24). Thus the temperature gradient between Asian continent and Indic Ocean is increased. The intensity of this horizontal temperature gradient could be of importance as it is widely assumed that the land-sea contrast in surface temperatures drives the intensity of Asian summer monsoon (e.g., Douville et al. 2000). The temperature anomalies over South Asia in the double CO_2 Tortonian run amount an increase of 3 to 4 °C in the annual mean (fig. 2.24). This increase seems to be comparable with other modern climate studies with an enhanced atmospheric carbon dioxide (Douville et al. 2000). Numerical climate modeling studies referring to nowadays scenarios and which were performed by Douville et al. (2000), however, suggest a general weakening of Asian summer monsoon circulation when carbon dioxide is increased. The authors' analysis show that the increase of precipitation rates over South Asia is caused by the more humid atmosphere under stronger greenhouse conditions. This also means

that a slight change in evaporation e.g., due to the vegetation cover, can affect rainfall over land. In compliance with modern scenarios our double CO_2 Tortonian run shows an increase of precipitation over Southern Asia (fig. 2.25). However, there is an indication of a northward shift of the Asian monsoon system which can be seen in the increased low-level flow of the summer average (fig. 2.28) and an increase in the subtropical easterly jet (fig. 2.31). Thus the monsoonal circulation is enhanced in the double CO_2 Tortonian experiment. One main process which could lead to such discrepancies between present-day experiments and the Tortonian run could be the additional effect of a reduced height of the Tibetean Plateau. Furthermore one should consider that there are still large uncertainties in climate models in representing a modified Asian monsoon system (Douville et al. 2000).

2.5 Summary of ECHAM4/ML studies

Tortonian time slice experiments (8 Ma BP) with the complex model ECHAM4/ML have been performed. Therefore boundary conditions have been changed with regard to orography, glaciers, CO_2 forcing, and a prescribed oceanic heat transport. In order to specify ocean properties for the Tortonian time slice, oxygen isotope data from planktonic foraminifera were used. They provide a data base for sea surface conditions and therefore a tool for reproducing the meridional temperature gradient. These data were used in order to adjust the oceanic heat transport for the Upper Miocene situation. Therefore it is assumed that the meridional temperature gradient is a measure of the heat transport in the ocean. As the latitudinal temperature gradient of the Tortonian time-slice is smaller than the Recent one the oceanic heat transfer is also reduced. Including the above mentioned assumptions the performed model simulations provided the following results:

- The prescribed oceanic heat transport for the Upper Miocene is in qualitative agreement with oceanic proxy data. Model results represent less intense ocean currents - like the Gulf Stream, Kuroshio, Humboldt, and Benguela Current - on the Northern and Southern Hemisphere.

- The results of the standard Tortonian simulation (Recent values of atmospheric carbon dioxide were used) shows hardly any change in the global averaged temperatures in comparison to the Control run. Despite this fact some circulation patterns differ

significantly from the Control run. For example the location of the North Atlantic storm tracks is shifted equatorwards in comparison to today affecting Southern Europe with more rainfall. Furthermore the model results represent a weakening of the Asian monsoon, which is caused by the reduction of the height of the Tibetean Plateau. Additionally, a reduced polar sea ice distribution is represented by model results which is in agreement with several proxy data.

- The simulation of the double CO_2 sensitivity run for the Tortonian represents an increase in the global surface temperature of 3 °C, which is in the same order as predicted by modern climate scenarios with enhanced carbon dioxide. With an increase in greenhouse gases atmospheric circulation pattern vary from the standard Tortonian run. For instance, the CO_2 doubling sensitivity run shows a northward shift of storm tracks combined with a milder winter climate and a reduction in seasonality for Europe. With regard to the Asian monsoonal circulation pattern the results show an intensification, which is controlled by a more humid atmosphere.

Chapter 3

Simulations with CLIMBER-2

The global climate model CLIMBER (CLIMate and BiosphERe) was developed at the Potsdam Institute for Climate Impact Research. This model contains several components describing a simple atmosphere, a 2-dimensional ocean, sea ice, land surface processes, and terrestrial vegetation distribution. This model is of intermediate complexity, so several sensitivity studies can be performed at low computational cost. One constraint, however, is its coarse resolution. Nevertheless, its features qualify CLIMBER for studies with respect to the Tortonian time slice. It enables one to investigate the role of vegetation in climate, especially at high latitudes, and allows one to explore the effect of different boundary conditions such as changed sea-land distribution.

The studies in this chapter utilize these possibilities. Results are discussed corresponding to a doubling of atmospheric carbon dioxide content, the effect of a changed Mediterranean Sea (Paratethys), and a shifted Australian continent.

3.1 The model CLIMBER 2.2

CLIMBER-2 has an atmospheric resolution of 10° in latitude and about 51° in longitude. In order to represent an acceptable land-sea distribution the fraction of land and ocean is considered for each grid point. The atmosphere is represented by a 2.5-dimensional statistical-dynamical model. The model works like most general circulation models except that the synoptic scale is parametrized (Ganopolski et al. 1998 a). Hence, a much longer time step is allowed. The model is described in further detail by Petoukhov et al. (2000).

The zonally averaged ocean is divided into three basins (Atlantic, Pacific and Indian Ocean) based on the model of Stocker et al. (1992). The basins are connected to each other, but with no seaway between Atlantic and Pacific Ocean. As is the case for the atmospheric model, the latitudinal resolution is 10°. A simple thermodynamic sea-ice model predicts sea ice fraction and thickness together with advection and diffusion of ice.

The optional terrestrial vegetation model VECODE (VEgetation COntinous DEscription) is written by Brovkin et al. (1997). Potential vegetation is represented by fraction of trees, grass and bare soil (desert). These fractions are dependent on growing degree days (sum of mean daily temperature for days with temperature above 0 °C) and annual precipitation. Changes in vegetation cover can be interpreted as changes in vegetation zones whereby the vegetation is in equilibrium with climate.

The three modules are connected via the fluxes of momentum, heat and water at the surface interface. There is no flux adjustment necessary, which makes different timeslice experiments more reliable.

A comparison of CLIMBER-2 results with preindustrial climate shows good agreement of seasonal and annual means (Petoukhov et al. 2000). It also does a good job in simulating a large set of characteristics of the climate system, including radiative balance, temperature, precipitation, large-scale circulation patterns, ocean circulation and the cryosphere. For the benefit of a fast turnaround time CLIMBER cannot simulate weather, interdecadal variabilities like El Niño/Southern Oscillation, or regional climates, in contrast to general circulation models that can also resolve weather systems like the North Atlantic Oscillation. Additionally CLIMBER-2 presents reasonable results for enhanced CO_2 experiments (Ganopolski et al. 1998 a, Rahmstorf and Ganopolski 1999). So far time slice experiments have been established for the Last Glacial Maximum (Ganopolski et al. 1998 b), the climatic Optimum during the Holocene (Ganopolski et al. 1998 a), and the Interglacial Eemian (Kubatzki et al. 2000).

3.2 Tortonian run

For the Tortonian, boundary conditions for CLIMBER-2 simulations are set as for ECHAM4 runs. Due to the coarse spatial resolution only the Tibetean Plateau is reduced by half of its present height (e.g., Molnar et al. 1993, Wang et al. 1999). Additionally Greenland glaciers are eliminated. The atmospheric carbon dioxide is set to 353 ppm for both the Control and the Tortonian run. In order to provide a best-guess run for the Tortonian the **A**tmosphere-**O**cean-**V**egetation-model (AOV) was used. This run enables one to interpret responses in the ocean, the atmospheric circulation, and vegetation cover due to Tortonian boundary conditions. Thus different results are expected in comparison to ECHAM simulations.

The time evolution of the globally averaged temperature and sea ice volume (fig. 3.1) shows that the model reaches equilibrium after several hundred years and that only small deviations occur after 1000 years of integration. Therefore integrations of at least 2000 years were performed. A short list of relevant experimental runs with CLIMBER is represented in appendix E. The global mean of near surface temperature for the Control run (fig. 3.1 a) yields a value of 15.7 °C. In contrast to previous ECHAM results (tab. 2.1), there is a difference noticeable of less than 0.1 °C. Thus there is a good agreement between ECHAM4/ML and CLIMBER simulation results with regard to the Control run. In view of the climate reconstruction of the Upper Miocene, it should be noted that the usage of climate models of different complexity and different climate modules - such as ECHAM4/ML and CLIMBER - renders a direct comparison of simulation results more difficult. However, in order to enable a proper classification of our simulation results, general conformities in atmospheric circulation pattern are described. Starting from the same Tortonian boundary conditions, including above mentioned changes for the Tortonian run, CLIMBER leads to a 0.8 ° warmer atmosphere. The temperature rise at high latitudes causes a significant reduction of northern sea ice cover (fig. 3.1 b). This is expected because of the elimination of Greenland ice. Additionally the positive sea ice-albedo feedback strengthens the warming. The comparison of sea ice cover between CLIMBER-2 and ECHAM4/ML (fig. 2.15) is difficult, because the sea ice model in ECHAM represents sea ice changes inadequately due to the non-dynamic description. Nevertheless, both models indicate less sea ice for the Tortonian time slice in the Northern Hemisphere. The

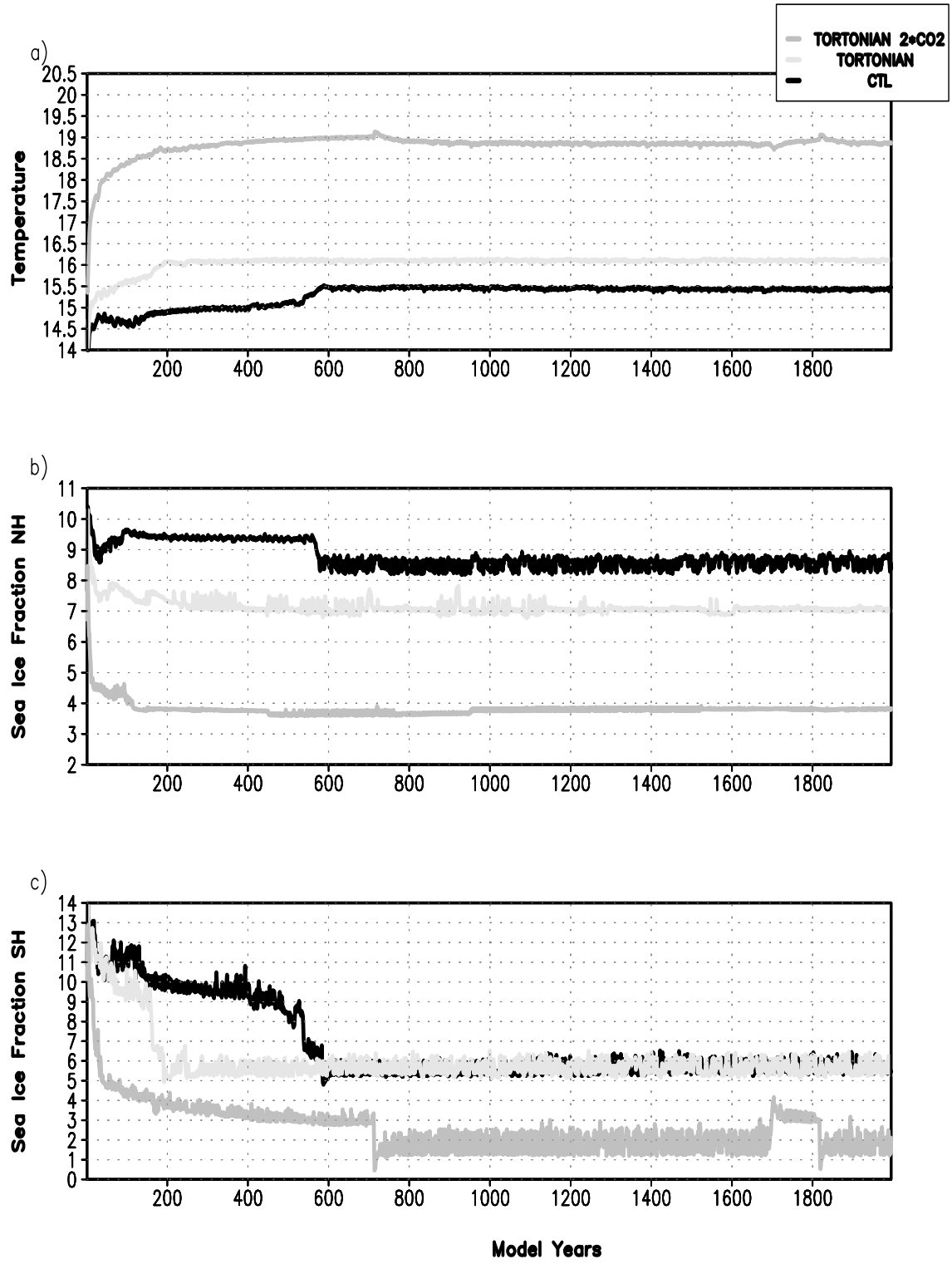

Figure 3.1: *Time evolution of results of Control run, Tortonian run and double carbon dioxide Tortonian run. a) Near surface temperature in °C, b) sea ice fraction on the Northern Hemisphere and c) sea ice fraction on the Southern Hemisphere in 10^6 km^2*

decrease for CLIMBER and ECHAM amounts $1.5 \cdot 10^6$km^2 and $0.2 \cdot 10^6$km^2 respectively. Hence, both models result in a much warmer polar region for the Tortonian even though the quantitative amounts are different.

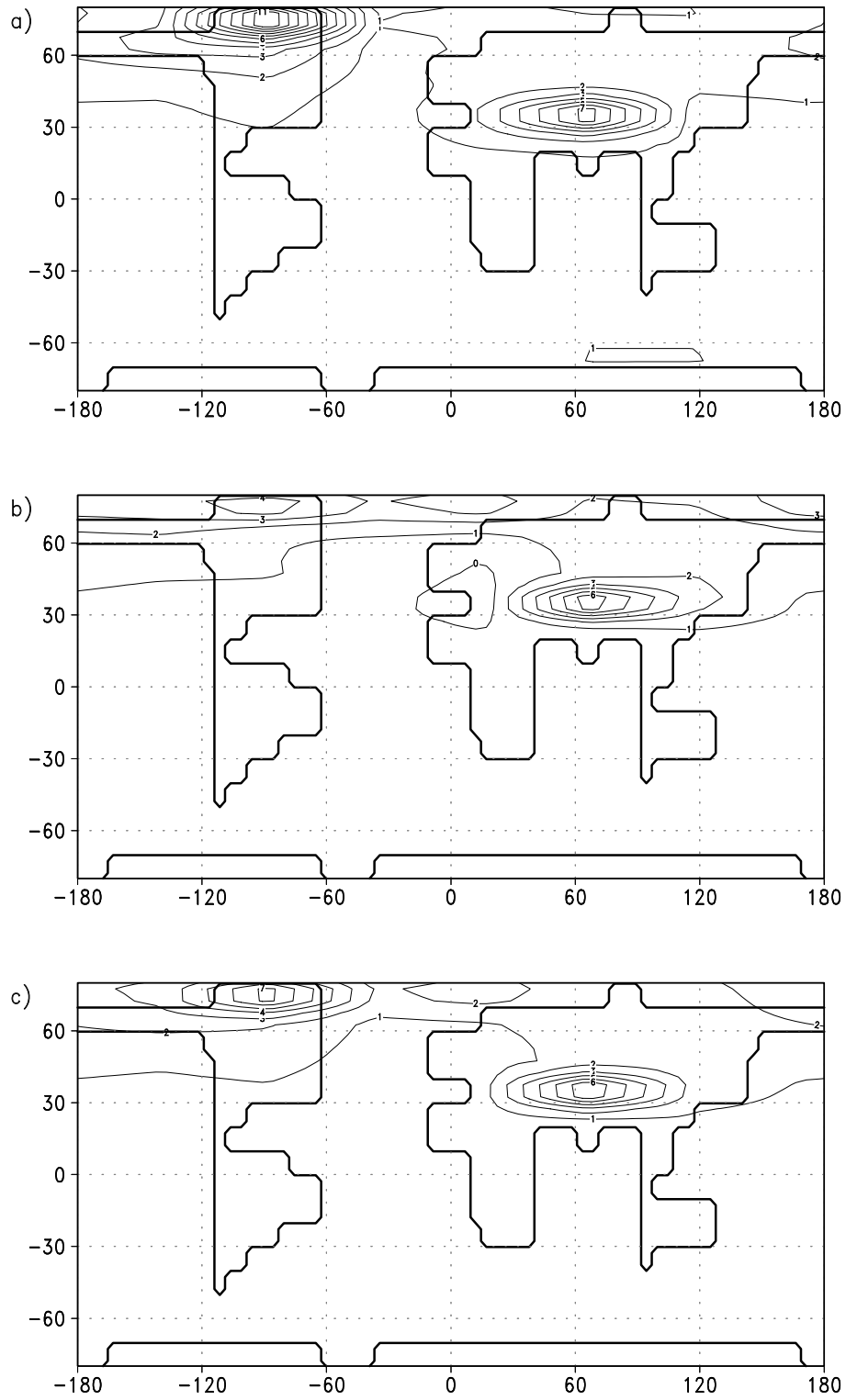

Figure 3.2: *Near surface temperatures of Tortonian run (AOV) minus Control run (AOV). a) JJA, b) DJF and c) annual mean. Contour interval in K.*

On the following pages the comparison of selected variables and their anomalies of Control and Tortonian run will be described. Results of this Tortonian run which are not figured in this chapter can be found in appendix C.

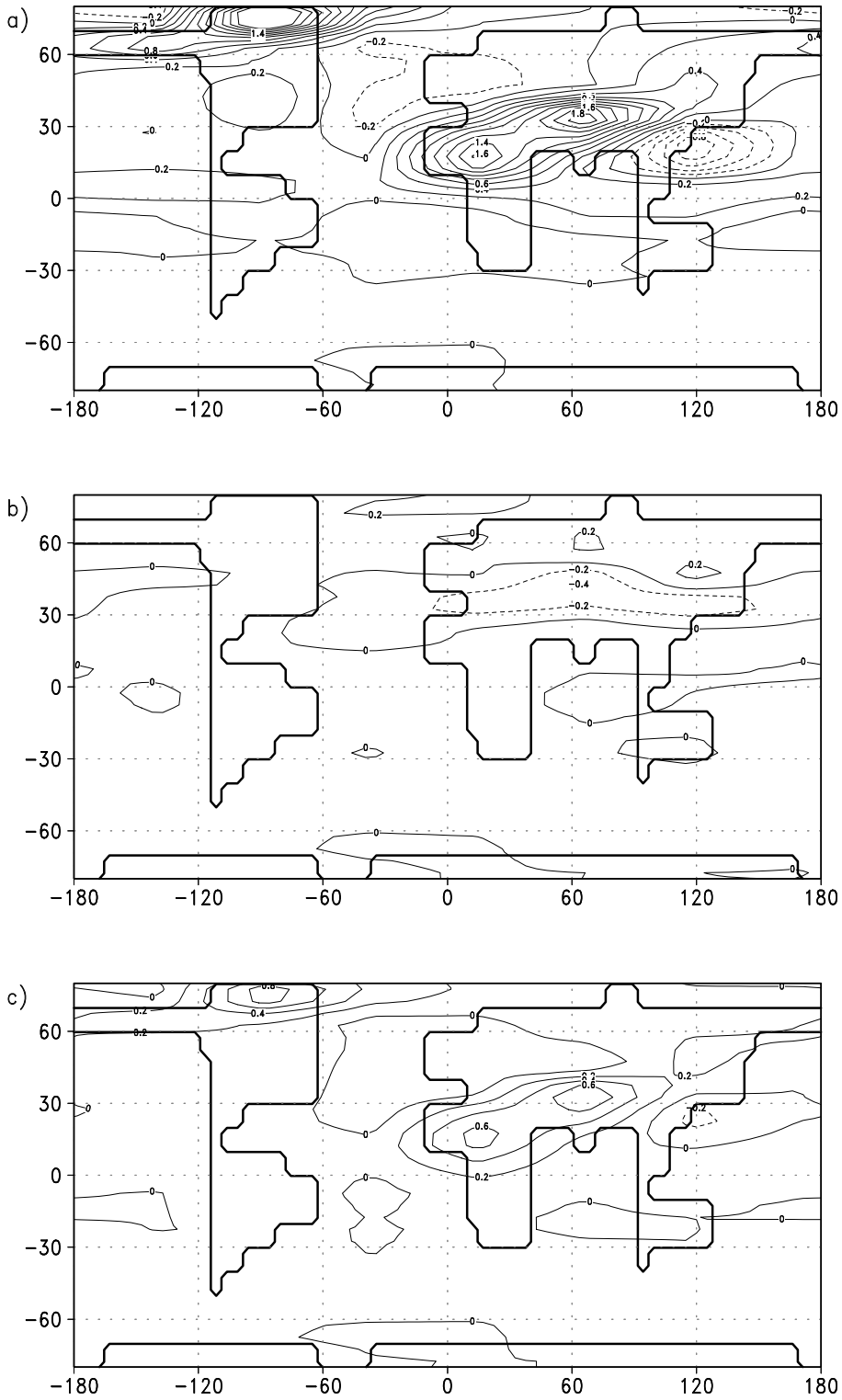

Figure 3.3: *Surface precipitation rates of Tortonian run (AOV)minus Control run (AOV). a) JJA, b) DJF and c) annual mean.*

As is the case for the ECHAM runs (fig. 2.16), CLIMBER run shows a strong temperature increase over Northern Hemisphere (fig. 3.2) due to the reduction of the height of the Tibetean Plateau and the elimination of Greenland ice. Seasonal temperature vari-

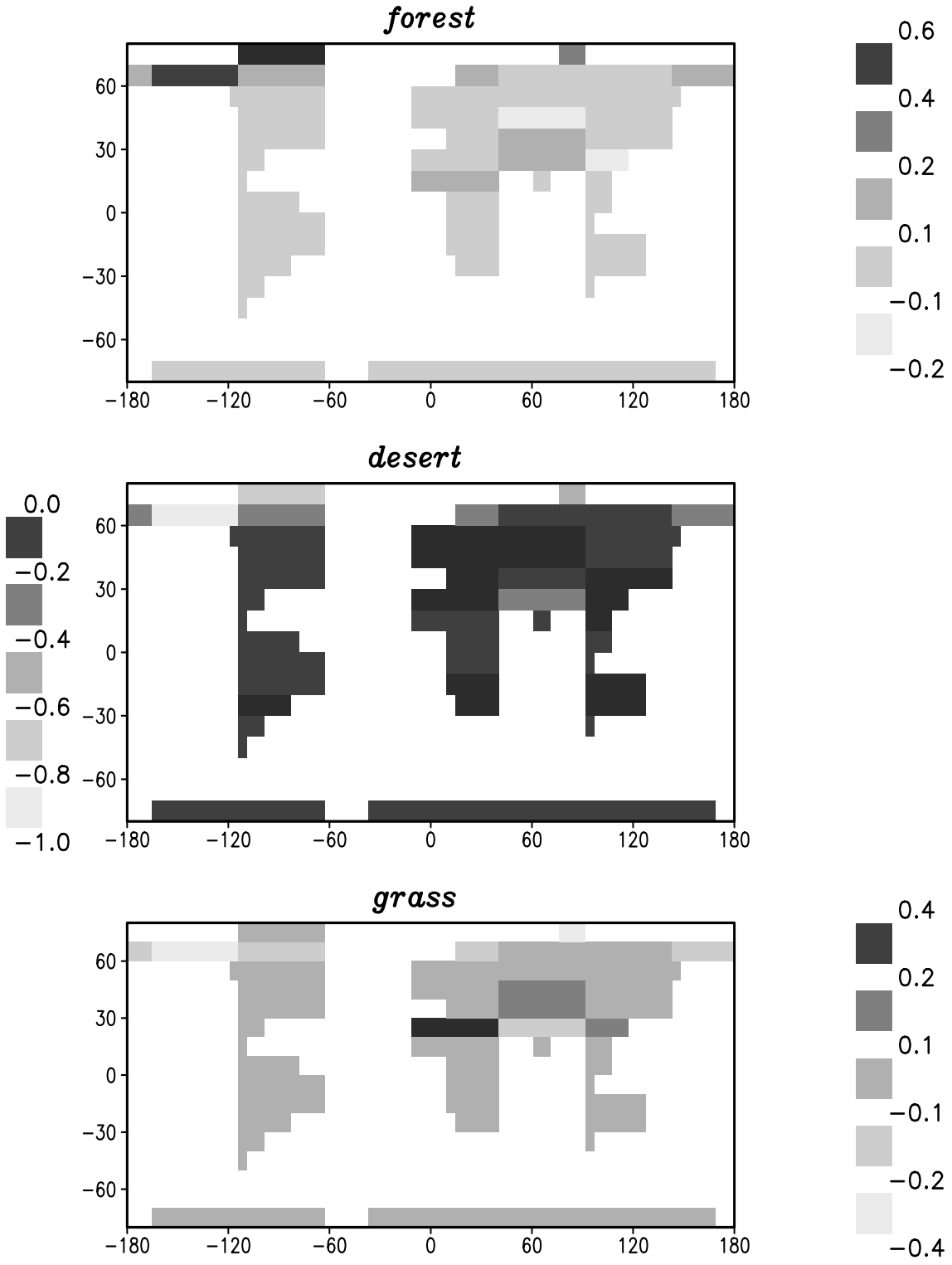

Figure 3.4: *Anomalies in vegetation fraction of Tortonian run (AOV) and Control run for forests, desert and grass.*

ations differ slightly, with a warming over North Polar Sea during winter months. This phenomenon can also be seen in the ECHAM results indicating a lower seasonal change in temperature relative to the Control run. The annual mean in fig. 3.2 c) features a

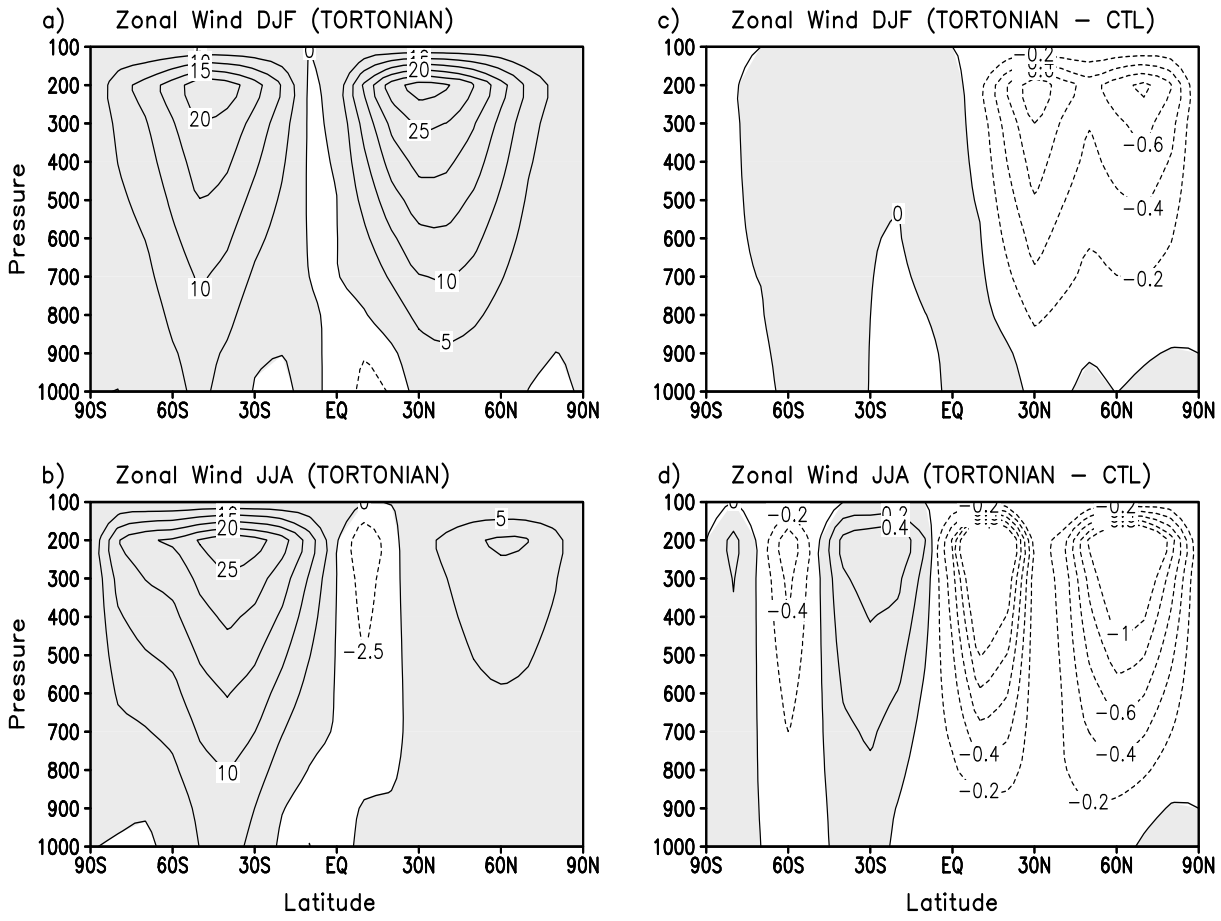

Figure 3.5: *Zonal averaged zonal wind and the anomalies. a) DJF with a contour interval of 5 m/s b) JJA with a contour interval of 5 m/s, c) anomalies between Tortonian and Control run for DJF, contour interval is 0.2 m/s, d) anomalies between Tortonian and Control run for JJA, contour interval is 0.2 m/s. Shaded areas represent positive values.*

reduced temperature gradient between North Pole and Equator, which was initially assumed for the Tortonian on the basis of oceanic proxy data (cf. chapter 2).

With respect to the general precipitation patterns, significant discrepancies exist between ECHAM (fig. 2.17) and CLIMBER (fig. 3.3) results. This is caused by a different atmospheric circulation which drives large-scale precipitation patterns. With regard to the CLIMBER experiment, anomalies in precipitation rates occur mainly during northern summer season (fig. 3.3). These changes can partly be attributed to a warmer Northern Hemisphere caused by an ice-free Greenland shield and a reduced mountain range over Asia. Associated with this process is an establishment of a different vegetation cover with a greater percentage of forests (fig. 3.4). The additional vegetation cover leads to an

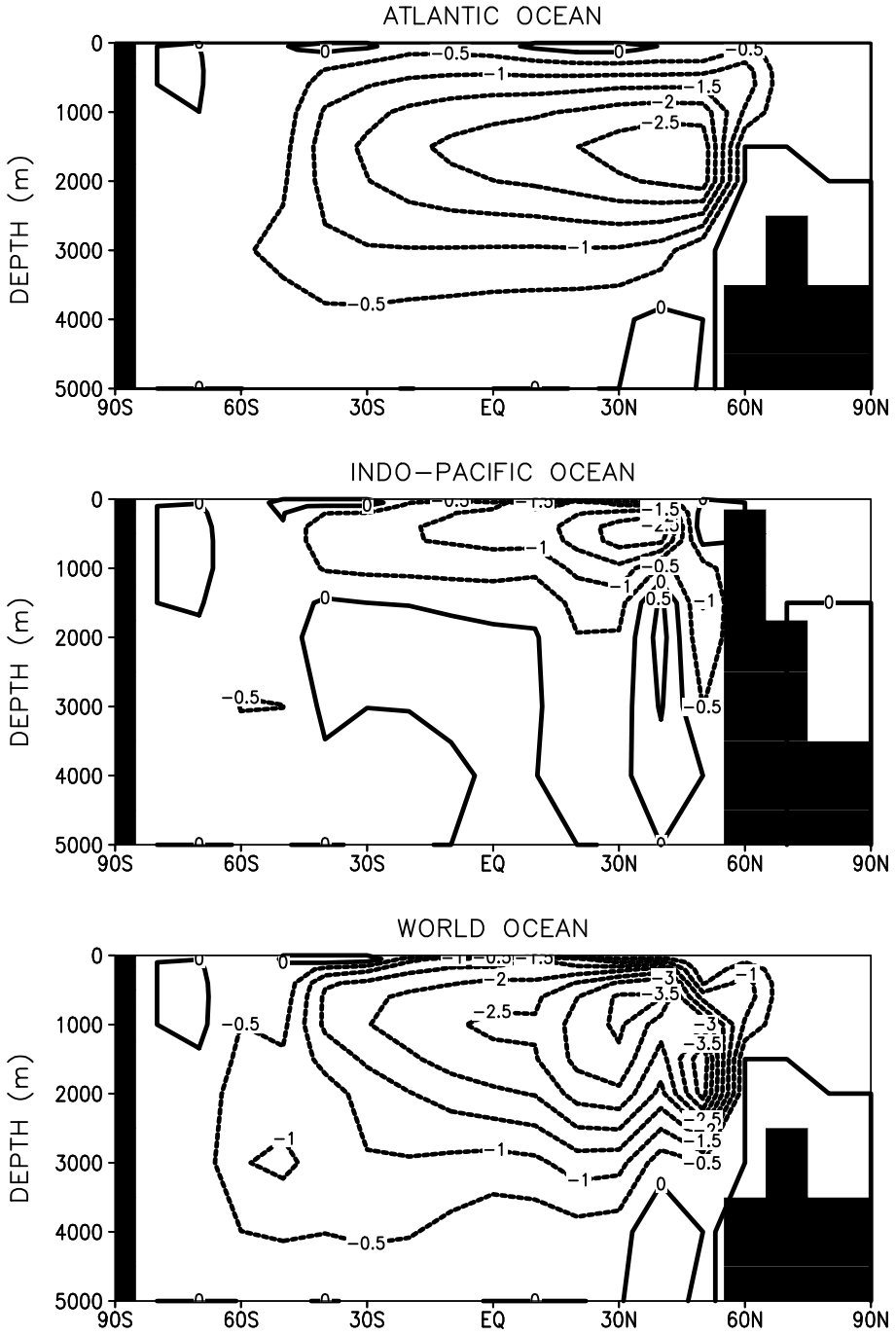

Figure 3.6: *Anomalies of Tortonian and Control run of zonally averaged mass transport streamfunction of the meridional overturning circulation in the Atlantic, Indo-Pacific and World ocean. Contour interval is 0.5 Sv.*

enhanced evaporation and therefore to an increase of precipitation, producing a positive feedback mechanism. Therefore the precipitation rate is increased for both described areas.

With regard to the Asian monsoonal circulation on the Northern Hemisphere, a further westward shift of the wind system can be found. Therefore, over East Asia precipitation rates are decreased, whereas they are magnified further westwards. The reorganization of the Asian monsoon can also be seen in the slightly intensified tropical easterly jet during JJA (fig. 3.5). The reduction of the height of the Tibetean Plateau causes a greater flux of moisture to be transported to Central Asia, causing a wetter climate. This, in turn, causes an increase in the fraction of grass and forests (3.4). The shift of this circulation pattern is in qualitative agreement between ECHAM and CLIMBER; however, a strengthening of the monsoonal regions is not supported by ECHAM results. As in the ECHAM run (fig. 2.17) the African monsoon is intensified, leading to greater precipitation rates over North Africa. In CLIMBER this is connected to a strong positive feedback mechanism between vegetation and precipitation, which involves a further greening of the North African desert belt. This effect was also found in Holocene time slice experiments with CLIMBER (Ganopolski et al. 1998 a).

Over the North Atlantic, higher precipitation rates dilute surface waters and reduce oceanic salinity at higher latitudes. This has a direct effect on the oceanic circulation, because the additional input of freshwater reduces the intensity of the North Atlantic overturning cell (fig. 3.6). This process is also predicted for future climates by different climate modelers (e.g., Rahmstorf and Ganopolski 1999, Stouffer and Manabe 1999). The rate of weakening of North Atlantic Deep Water for future climate scenarios or a possible stagnancy is a matter which is still discussed.

Due to a greater precipitation rate over the northern Atlantic Ocean the overturning cell is reduced, resulting in a reduction of more than 2.5 Sv (fig. 3.6). The weakening of North Atlantic Deep Water formation leads to a less intense oceanic heat transport in the North Atlantic in the order of 0.1 PW (fig. 3.7). The same process also occurs in the Pacific Ocean leading to a less effective oceanic heat transport to the North Pole. It is important to note that the order of the variation complies with the initial changes which were assumed for the changed oceanic heat transport of the ECHAM run.

Quantitatively there are no major changes in the zonal mean wind amount (fig. 3.5); however, a general pattern can be found. In the Northern Hemisphere westerlies are

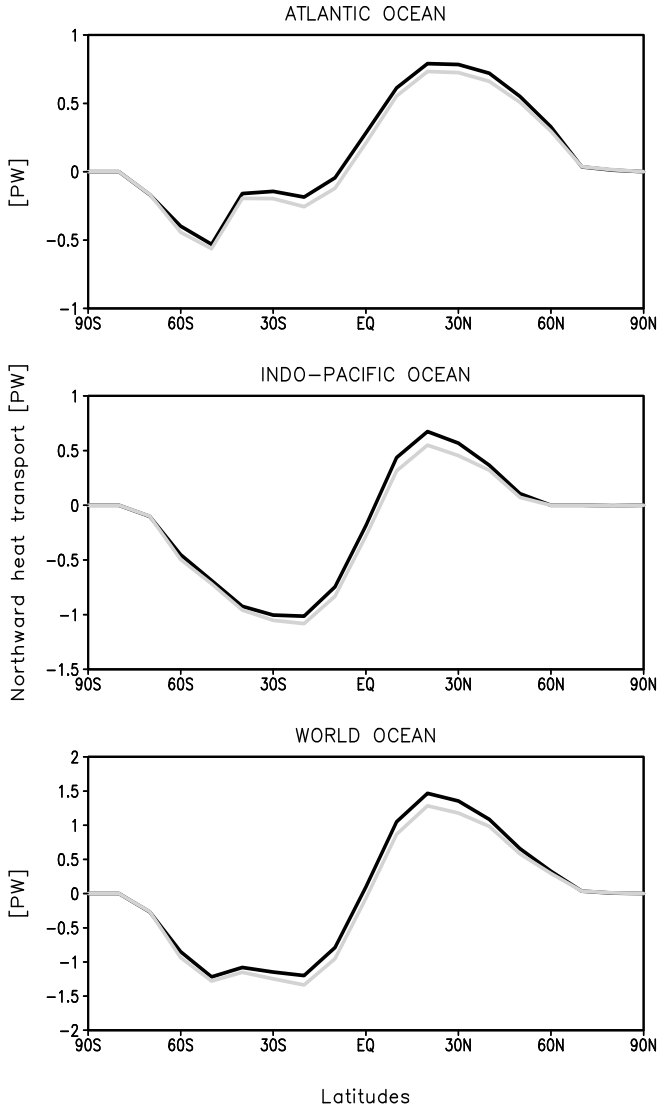

Figure 3.7: *Northward heat transport in Peta Watts for Atlantic, Indo-Pacific and World ocean. Black line: Control run; Grey line: Tortonian run.*

decreased throughout the year due to a smaller meridional temperature gradient. This fact leads to a decreased fresh water flux in mid-latitudes resulting in drier regions in Europe (fig. 3.3). Similar results can be seen in ECHAM simulation, where a drying is located at high mid-latitudes due to the southward shift of storm tracks. Nevertheless, the variations differ significantly with regard to the zonal mean wind (fig. 3.5). Here the CLIMBER simulation represents a reduced momentum transport in contrast to ECHAM results. Hence the warming of the Arctic Ocean and surroundings in the Tortonian run does not depend solely on the oceanic heat transfer. The temperature rise in northern high latitudes is driven by the removal of the Greenland ice shield and the related positive feedback mechanism. For instance the positive snow-albedo-vegetation feedback mechanism leads to warmer climate conditions.

With respect to the Southern Hemisphere the ECHAM and CLIMBER model produce a qualitatively similar pattern. During JJA anomalies of both models indicate a more equatorial shift of the mid-latitudinal frontal zone, in DJF, however, changes are negligible.

3.3 Sensitivity studies

Sensitivity studies are performed to learn how different prescribed boundary conditions affect atmospheric circulation. One sensitivity study doubled atmospheric carbon dioxide as in the ECHAM runs. A second sensitivity study doubled the size of the Mediterranean Sea to understand the influence of the Paratethys Ocean. A third sensitivity run shifted Australia further southwards as suggested by geological data (e.g., Lee and Lawver 1995, Gahagan et al. 1988).

3.3.1 Carbon dioxide experiment

In parallel with the ECHAM sensitivity study, a CLIMBER run with doubled carbon dioxide is performed. As known from different modern sensitivity studies with CLIMBER (Ganopolski et al. 1998 a, Rahmstorf and Ganopolski 1999) the global averaged temperature increases by 3.0 K (see also fig. 3.1) with a doubling of CO_2. Due to the ice melt at the poles and the increase in forests, high latitudes are warmed the most. A horizontal difference plot of the change in near surface temperature between the Tortonian run with double carbon dioxide and the standard Tortonian run is shown in fig. 3.8. The temperature range between mean summer and mean winter temperatures is reduced northward of 60° N. The anomalies over landmasses are greatest whereas over ocean surface the meridional temperature gradient is lower. The reduction of the seasonal temperature cycle is more emphasized in this experiment in comparison to the standard Tortonian run. A qualitatively similar pattern can also be seen in ECHAM results (fig. 2.16.)

The global averaged precipitation rate is increased from 2.87 mm/d in the Control run to 3.15 mm/d in the standard Tortonian run, a difference of 0.28 mm/d. The precipitation rate increases almost everywhere (fig. 3.9). ECHAM results indicate an increase in the water cycle of 0.06 mm/d. The differences between models can be ascribed partly to the

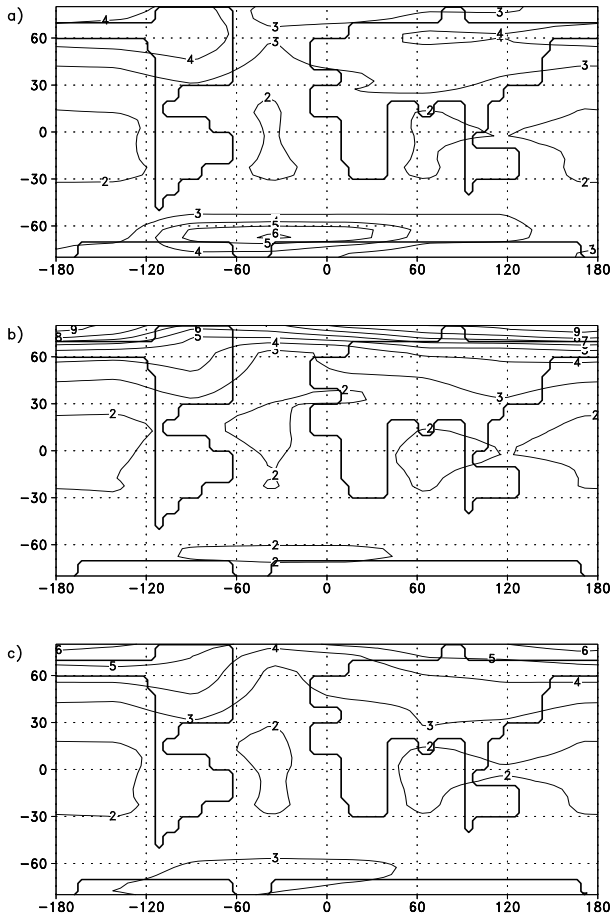

Figure 3.8: *Near surface temperature anomalies between doubling carbon dioxide Tortonian and the standard Tortonian run: a) JJA, b) DJF, and c) the annual mean. Contour interval is 1 K.*

colder polar regions in the ECHAM run. Lower temperatures cause a smaller capability of holding water vapour in the air. In combination with the seasonal shift of the intertropical convergence zone, the precipitation rate increases due to a greater availability of vapour water in the atmosphere. This phenomenon also can be seen in the ECHAM simulation. However, discrepancies occur over areas with extreme climatic conditions like deserts or tundra-like (boreal forests) regions. For these areas CLIMBER results indicate greater precipitation rates. This can be attributed to the implemented vegetation module whereas the ECHAM results are based on Recent vegetation, i.e. potential vegetation feedback mechanism are not represented.

In contrast to the ECHAM model, CLIMBER produces no intensification of Northern Hemisphere zonal circulation (not shown) and in fact shows a slight decrease in the zonal wind component. This effect can be attributed to the lower meridional temperature gra-

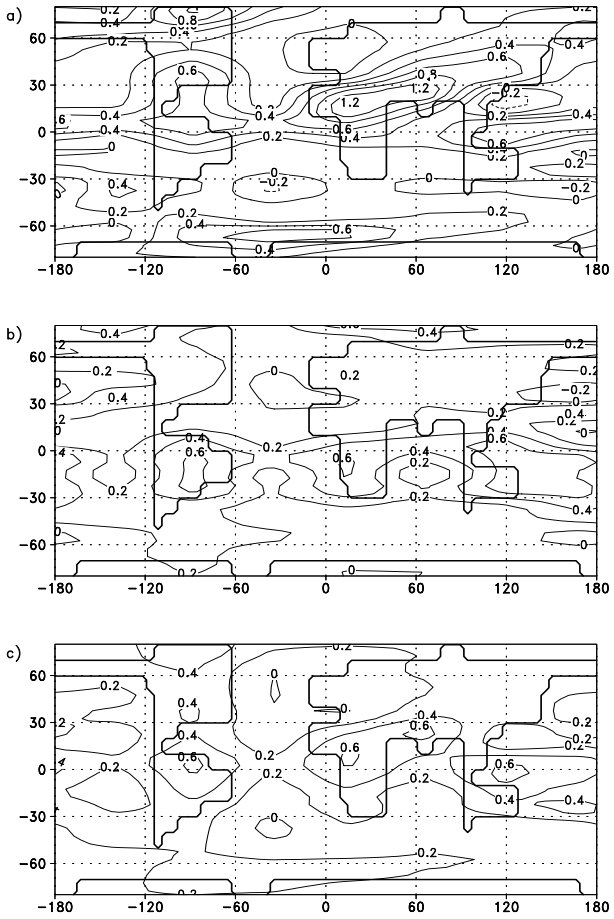

Figure 3.9: *Precipitation rate anomalies between doubling carbon dioxide Tortonian and the standard Tortonian run: a) JJA, b) DJF, and c) the annual mean. Contour interval is 0,2 mm/d.*

dient. Additionally, due to the coarse resolution of CLIMBER, a slight northward or southward shift of westerlies cannot be detected.

3.3.2 Paratethys experiment

The exact size of the Paratethys Ocean and its influence on palaeoclimate are still intensely discussed. During middle Miocene the size of the Eastern Paratethys shrinks drastically in combination with a closure of the Paratethys-Indic. Subsequently during the Late Miocene (Tortonian/Pannonian) European continentalisation continued and the Central Paratethys was confined to the Pannonian Basin and its satellite basins (e.g., Dercourt et al. 1993, Rögl 1998, Steininger and Rögl 1984). The existence of a residual lake in the Pannonian Basin is also supported by palaeoclimatic proxy data (e.g., Bruch 1998). Proxy data show a damping effect on seasonal temperatures that depends on the size of the Paratethys (Bruch 1998). Therefore, the size of the Mediterranean Sea can play a major role for the regional and European climate (Fluteau et al. 1999). In order

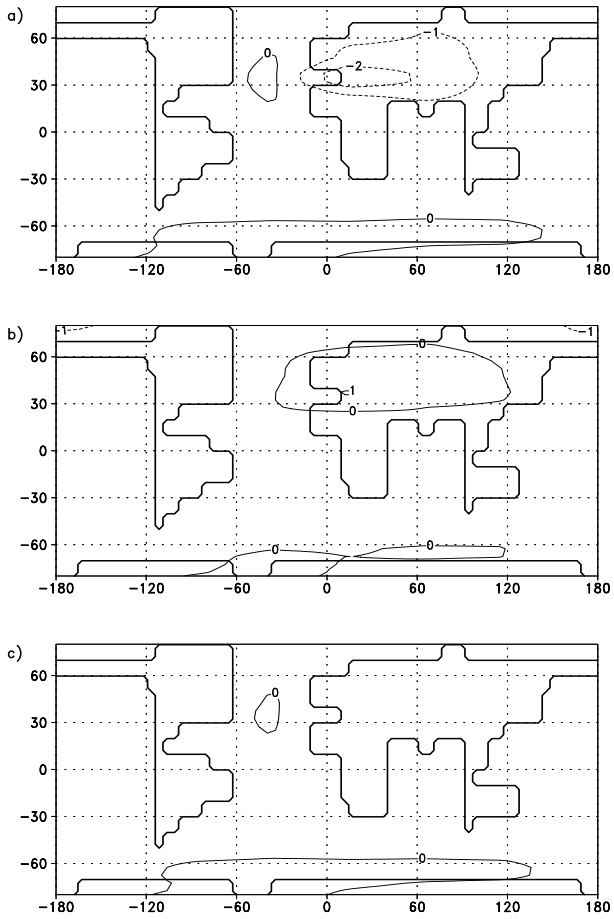

Figure 3.10: *Near surface temperature anomalies between a Tortonian run with a Mediterranean Sea of double size and the Tortonian run: a) JJA, b) DJF, and c) annual mean. Contour interval is 1 K.*

to represent the effect of a larger Mediterranean Sea the size of the ocean, i.e. the sea fraction, is doubled in this experimental run.

As expected, the temperature anomalies show a dampening effect on the seasonal temperature cycle over the Mediterranean Sea and surroundings (fig. 3.10). During summer additional evaporation takes place due to the larger water reservoir and leads to a cooling. Conversely, during winter months warmer water masses release heat into the atmosphere. The contour shape is asymmetrical and spread further eastwards due to the predominantly west winds in mid-latitudes. The above described effect is known as the "Paratethys effect", which is also indicated by palaeobotanical proxy data (e.g., Bruch 1998, Fluteau et al. 1999, Ramstein et al. 1997).

Atmospheric circulation is significantly affected by the doubling of the size of the Mediterranean Sea. During northern summer a stabilization and an eastward shift of the Azores

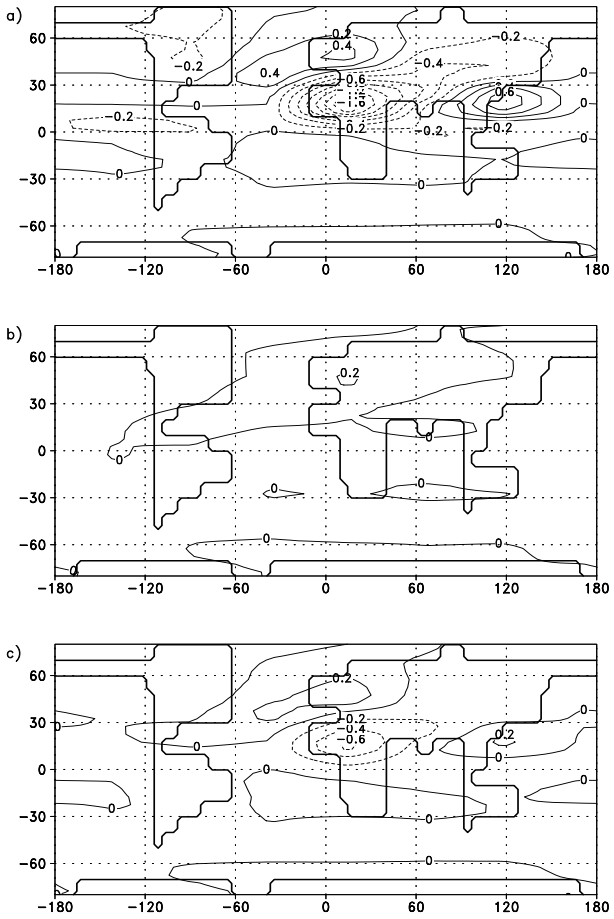

Figure 3.11: *Anomalies in precipitation rate between a Tortonian run with a Mediterranean Sea of double size and the Tortonian run: a) JJA, b) DJF, and c) annual mean. Contour interval is 0.2 mm/d.*

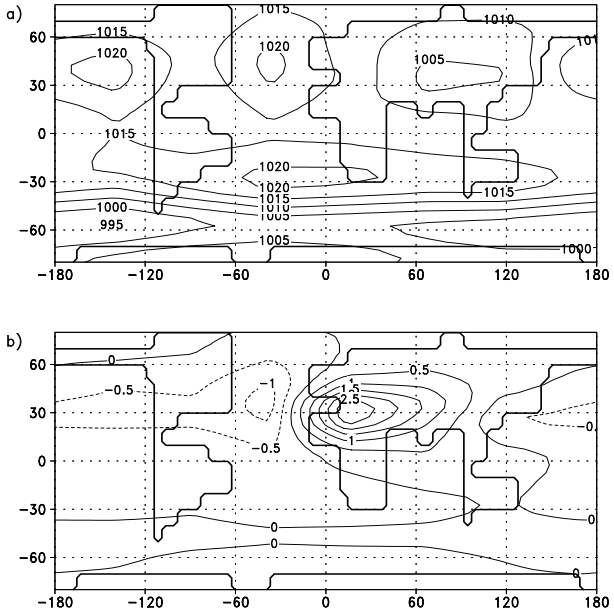

Figure 3.12: *Surface pressure for JJA: a) Tortonian run, b) anomalies between Tortonian run with a Mediterranean Sea of double size and the Tortonian run. Contour interval is 5 and 0.5 hPa correspondingly.*

High can be found (fig. 3.12). This reorganization over Southern Europe has also an effect on the North African monsoonal system. Due to the high pressure system the Mediterranean region experiences a more continental climate. Therefore a weakening in North African monsoonal system is observed. This leads to a smaller precipitation rate close to the North African coast (3.11). Because of its latitudinal position North African region is sensitive to small differences in precipitation rates. Hence the vegetation cover is predominantly affected. Due to the different atmospheric circulation system this region becomes drier. Additionally, the intensified high pressure cell over the Mediterranean Sea affects Asian monsoonal circulation. In combination with the further eastward shift of the summer High the Asian Low is slightly reduced. This involves a reduction of low level flow and therefore the rate of precipitation, which weakens the summer monsoon system for the Indian region and causes an aridification north of Tibetean Plateau. In correspondence with the decreased circulation the subtropical easterly jet is reduced by nearly half (not shown).

The precipitation anomalies are characterized by a seesaw pattern between Europe and Africa (fig. 3.11 c), with a more humid climate for Northern Europe and a more arid climate for North Africa. This pattern is supported by the reorganization of the atmospheric circulation. The subtropics are more influenced by dry continental air masses from Asia, while the mid-latitudes are more influenced by the westerlies.

Changes in Mediterranean outflow cannot be resolved by CLIMBER. However, there is a noticeable process for the North Atlantic Ocean. Due to the smaller freshwater input into the North Atlantic (fig. 3.11) an anomalous higher salinity is noticeable at 30 °N. Finally this more saline water amplifies the thermohaline circulation and leads to an increase of 1 Sv for the North Atlantic.

3.3.3 Australian landmass experiment

Plate tectonic reconstructions indicate a more southerly location of Australia during the Late Miocene than today (e.g., Lee and Lawver 1995, Gahagan et al. 1988). Therefore an experiment was conducted with a southwardly shifted Australian continent. This is

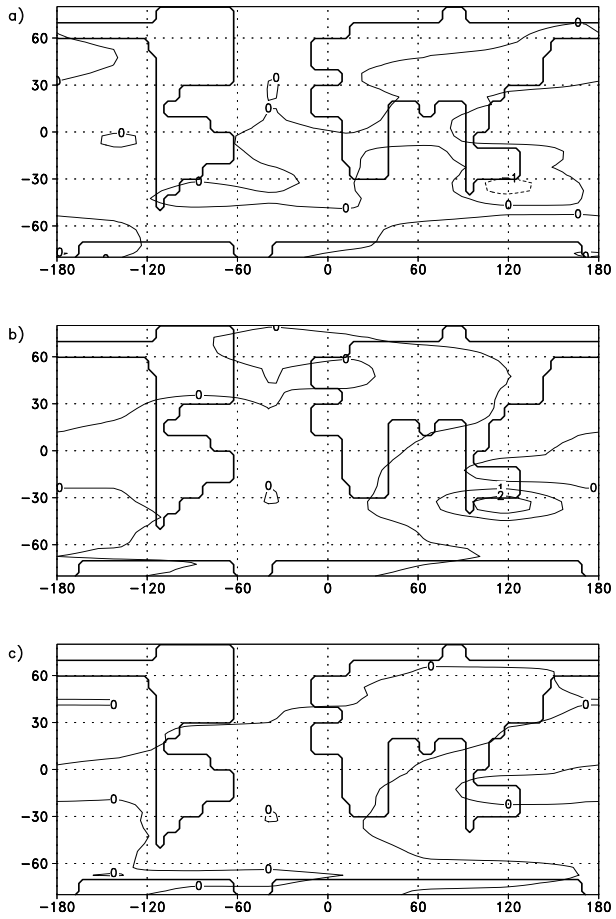

Figure 3.13: *Anomalies in near surface temperature between a Tortonian run where Australia is placed further south and the Tortonian run: a) JJA, b) DJF, and c) annual mean. Contour interval is 1 K.*

performed by displacing Australia continent one grid point in CLIMBER resolution (10 °) farther to the South. In correspondence with this shift, a more humid climate is expected for Australia as its simulated position is closer to the southern Polar Frontal Zone and farther displaced from the subtropical anticyclone belt (Beard 1977). Proxy data indicate greater precipitation rates for Southern Australian coastal areas during the Miocene. Sluiter et al. (1995) and Martin (1998) suggest at least a doubling of present-day rainfall values to an annual mean of about 1500 mm for Southern Australia, based on palaeobotanic data.

The southward shift of Australia amplifies the seasonal temperature cycle. During the summer temperatures increase, while during the winter temperatures decrease slightly (fig. 3.13). The southward shift induces a higher sensitivity of land masses to the seasonal solar cycle. The annual mean, however, shows no essential differences. These results are not in correspondence with the palaeobotanic studies of Sluiter et al. (1995) which

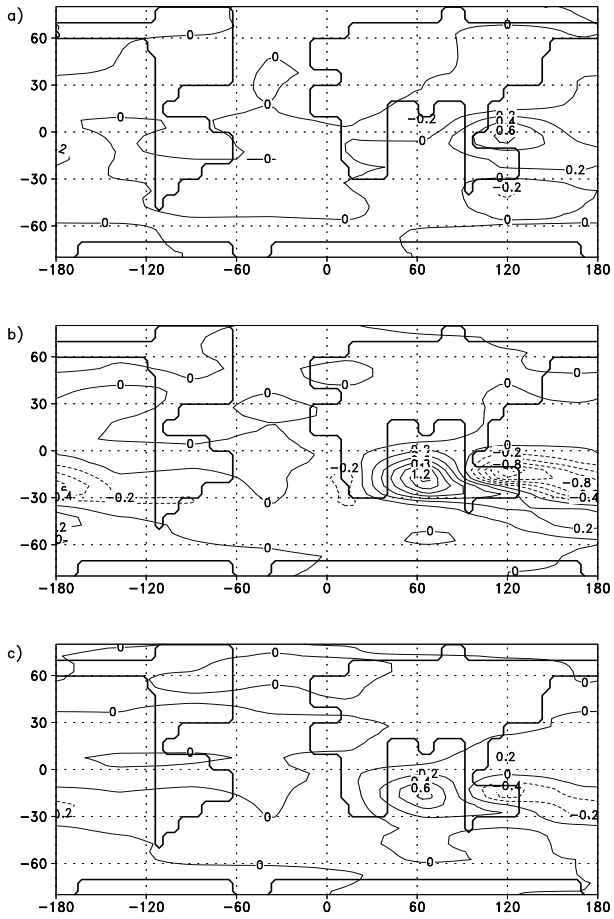

Figure 3.14: *Anomalies in precipitation rate between a Tortonian run where Australia is placed further southward and the Tortonian run: a) JJA, b) DJF, and c) annual mean. Contour interval is 0.2 mm/d*

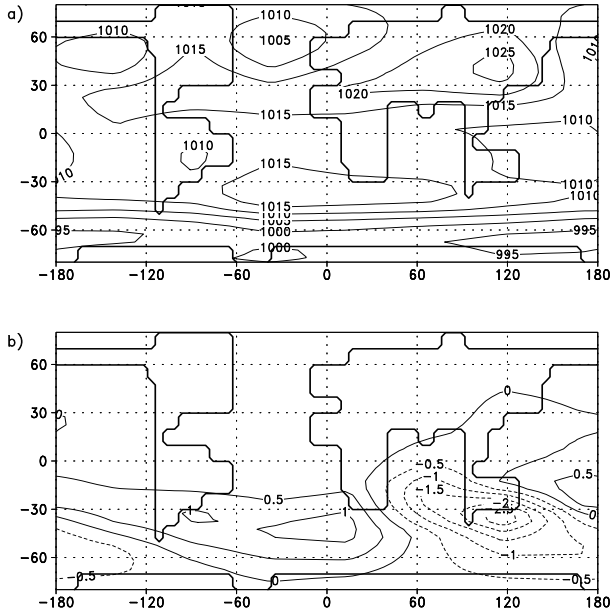

Figure 3.15: *Surface pressure for DJF: a) Tortonian run, b) anomalies between Tortonian run where Australia is placed further southward and the Tortonian run. Contour interval is 5 and 0.5 hPa correspondingly.*

infer a temperature increase of several degrees. Because Sluiter et al. (1995) derive their data from the Early and Middle Miocene, discrepancies between model simulation results and palaeo-data may result from the comparison of different time-slices.

A slight increase in precipitation is noticeable (fig. 3.14). Changes in surface pressure anomalies (fig. 3.15) lead to a reorganization of the subtropical High over the Indian Ocean. A slight reduction of its intensity leads to an increase in zonal wind southward of 30 °S, which causes the southern Australian coast to be more influenced by strong westerlies. Hence an annual increase of close to 100 mm/a is noticeable. These model results, however, obviously underestimate precipitation values derived from palaeobotanical proxies (Sluiter et al. 1995, Martin 1998). However, the tendency of a wetter climate is represented in the model. With regard to ECHAM results and available proxies the lack of precipitation increase in ECHAM simulations for Southern Australia can be partly attributed to the neglected southward shift of Australian continent during the Upper Miocene.

3.4 Summary of CLIMBER studies

With the model CLIMBER-2 of intermediate complexity a run for the time slice Tortonian was performed. Due to the available ocean and vegetation module the experiments allow one to investigate specific feedback mechanisms. Model output, however, is constrained by the low resolution and the confined ocean basins. In comparison to a complex general circulation model like ECHAM this model enables to investigate several sensitivity runs with a fast turnaround time.

A summary of conclusions from the CLIMBER experimental runs is listed below:

- For the standard Tortonian run CLIMBER and ECHAM show agreements in the tendency of variations with regard to the Northern Hemisphere sea ice fraction, the decrease in seasonality at high latitudes, an intensification of North African summer monsoon, and a reduced heat transport in the oceans.

- However, the absolute differences (e.g., sea ice volume and temperature increase) between Control and Tortonian run of both climate models are different.

- These discrepancies between CLIMBER and ECHAM with respect to the standard Tortonian runs can be attributed to the different types of implemented modules. Hence vegetation-temperature feedbacks are only resolved by CLIMBER. This effect can be seen in vegetation changes over Asia. Here, CLIMBER shows in contrast to ECHAM a slight intensification of the monsoonal system.

- A CLIMBER sensitivity experiment with CO_2 doubling is similar to ECHAM with regards to an intensified hydrological cycle and a global temperature increase of about 3 °C. Additionally, the double CO_2 sensitivity runs of both models represent warmer climate at mid and high-latitudes with a decrease in seasonality. There is, however, no intensification of westerlies noticeable in contrast to ECHAM results.

- An experimental run including a simulated Paratethys largely fits palaeoclimatic reconstructions from proxy data. The changed boundary conditions result in a reduction of the annual temperature cycle and an increase in rainfall over Europe.

- CLIMBER model results show that the precipitation rate over South Australia is sensitive to the continent's latitudinal position which varied during the last 8 million years. An experimental run was performed which considers a southward shift of Australian continent. Even though the corresponding model output represents precipitation rates quite lower than comparable proxy data, simulation results show the tendency of a wetter climate.

Chapter 4

Validation with proxy data

The limited number of Tortonian terrestrial sediments on a global scale provide relatively sparse proxy data for comparison with model data. A further restriction for a widespread analysis of the available data is the lack of precise stratigraphy. Consequently for the following comparison terrestrial proxy data of the time span from 11 to 7 Ma BP were taken into account. This corresponds to the full time span of the Tortonian (Upper Miocene). For the following investigation the comparison is divided into a quantitative and a qualitative analysis. Quantitative proxy data are yielded from palaeobotanical or palynological techniques. These data provide amongst others temperature and precipitation values of yearly, summer, and winter means. As the resolution of a climate model is quite small a direct comparison of proxy data and climate model output is difficult (von Storch 1995, Sloan et al. 2001). Nevertheless the constitutive climate changes supplied by the model and the proxy data can be compared. In global circulation models the general temperature pattern can be used as a good guideline for the regional climate as the temperature field itself is smoothed. Thus a comparison with proxy data is justifiable. The precipitation field, however, is a more demanding task in climate prediction. This is not only true for palaeo-reconstructions but also for Recent climate modeling and observations. Uncertainties in the order of about $\pm 0.5\,\mathrm{mm/d}$ ($\pm 180\,\mathrm{mm/a}$) in mid-latitudes are controlled by the global and regional temperature pattern, humidity, wind dynamics and the simplistic parametrization of rain processes (Chahine 1992, von Storch et al. 1993). Therefore discrepancies in precipitation values should not be overestimated. For example orographical rain pattern is not resolved correctly by circulation models due to the coarse resolution. For the following comparison these restrictions of model data should be taken into ac-

count. First of all, a comparison between quantitative proxy data and model output is presented with concentration on Europe and North America because of the distribution of available climatic proxy data. Hence the evaluation of the results are confined to regional climates. In order to test the influence of CO_2 forcing, model results of the sensitivity experiments are also considered. Subsequently qualitative specifications of climate conditions from proxy data are compared with ECHAM and CLIMBER results. In the second section there is a comparison of CLIMBER vegetation results with a potential Tortonian vegetation map reconstructed from proxies. In accordance with the ECHAM comparison the fraction of trees, grass, and deserts are discussed for the standard Tortonian and the run with CO_2 doubling.

4.1 Comparison of model results with temperature and precipitation proxies

Terrestrial palaeoclimatic proxy data used for the comparison with our model output are based, on the one hand on published specifications on fossil plant communities all over the world related of Tortonian age. By means of the coexistence approach (Mosbrugger and Uterscher 1997) the yearly mean temperature and precipitation rate was computed from these fossil plants communities. On the other hand, previously analysed and published climatic specifications were compiled and added to the above ones. The resultant data base (Bruch and Uhl pers. comm.) covers studies by Bruch 1998, Gregor and Unger 1988, Mai 1995, Sachse and Mohr 1996, Utescher et al. 2000, Wolfe 1994a, Wolfe 1994b and others including climatic specifications from micro (pollen) and macro botanical (leaves) fossils dated between 7 and 11 Ma BP.

The computation of yearly mean temperature values and precipitation rates from the compiled Tortonian botanical data base was performed by Bruch and Uhl (pers. comm.). Their analysis is based on the ansatz of the Nearest Living Relatives in order to determine the palaeoclimatic environment of a fossil flora. For this, fossils are investigated on possible relationships with Recent taxa. If it is possible to affiliate a relationship between a Recent and fossil taxons, climatic conditions of the nearest living relative are transferable to the fossil taxon. However, some uncertainties can occur when applying this method.

For instance, there could be a false assignment of the fossil relative to the Recent one. Furthermore, errors could occur, if the Recent and palaeo-taxa reflect different climatic conditions. These palaeoclimatic reconstructions are represented by specific temperature and precipitation intervals corresponding to a particular taxon. In order to define more specific climatic conditions the coexistence method (Mosbrugger and Utescher 1997) was applied on the Tortonian plant communities at each location of a fossil flora. Instead of using the temperature and precipitation intervals of each particular taxon, this approach considers a temperature and precipitation interval which equals the joint intersection of all intervals of the taxa. Hence this so called coexistence interval equals or is smaller than the intervals of all taxa. This idea corresponds to the assumption that all taxa of one sample do coexist, and, therefore, reflect the same climatic conditions. Consequently the application of this method results in a reduced temperature and precipitation interval for the corresponding plant community. For a comparison of climate model results with proxy data, mean annual temperature and precipitation intervals were taken into account.

For climate model results, yearly mean temperature and precipitation values were calculated of each year from the last 10 years of integration. From these values the minima and maxima were considered for defining a corresponding temperature and precipitation interval. Hence the comparison of proxy data with climate model results shows a good agreement when the corresponding climate intervals overlap. Then the difference between the climate intervals is zero. However, if these intervals do not coincide there is a gap of some °C or mm/a. In order to specify this gap between both intervals the smallest distance between both interval limits is determined.

The results of the inter-comparison between quantitative proxy data and climate model results of the standard Tortonian run are shown in fig. 4.1 and 4.3 for temperature and precipitation values respectively. In order to evaluate climatic distinctions the differences between the temperature and precipitation intervals were determined. Subsequently the differences between the quantitative proxy data intervals and climate model intervals from the double CO_2 sensitivity run are represented (fig. 4.2 and fig. 4.4).

The comparison of the temperature results of the standard Tortonian run with proxy data shows partly good agreements with regard to mid- and low-latitudes (fig. 4.1 b)

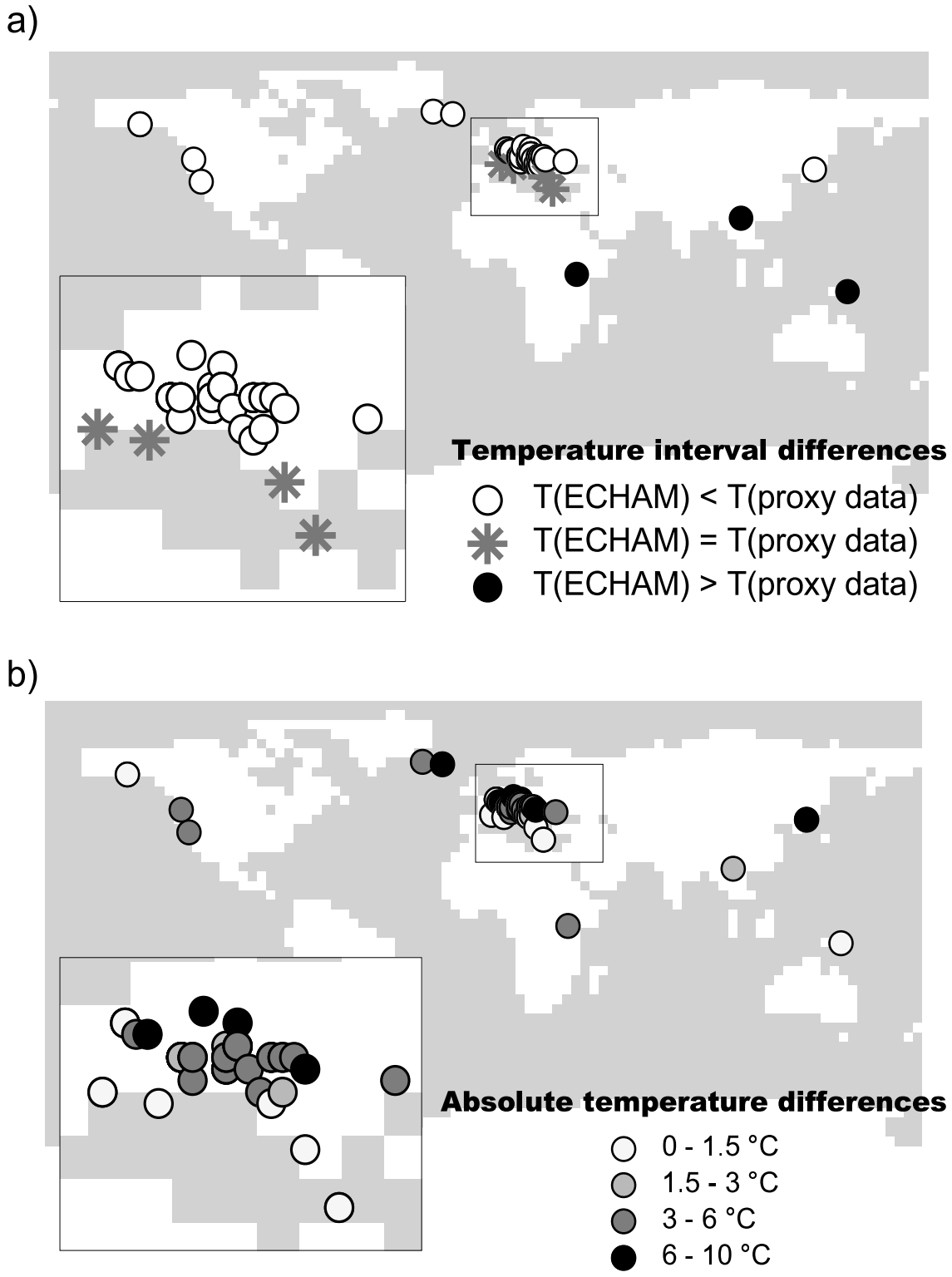

Figure 4.1: *Differences in yearly mean temperature intervals between ECHAM results (standard Tortonian run) and botanical proxy data. a) white circles: simulated temperature maximum is smaller than minimum temperature specified by proxy data, grey stars: temperature intervals overlap, black circles: simulated temperature minimum is greater than maximum temperature specified by proxy data. b) Temperature difference in absolute values between temperature interval from simulated data and proxy data.*

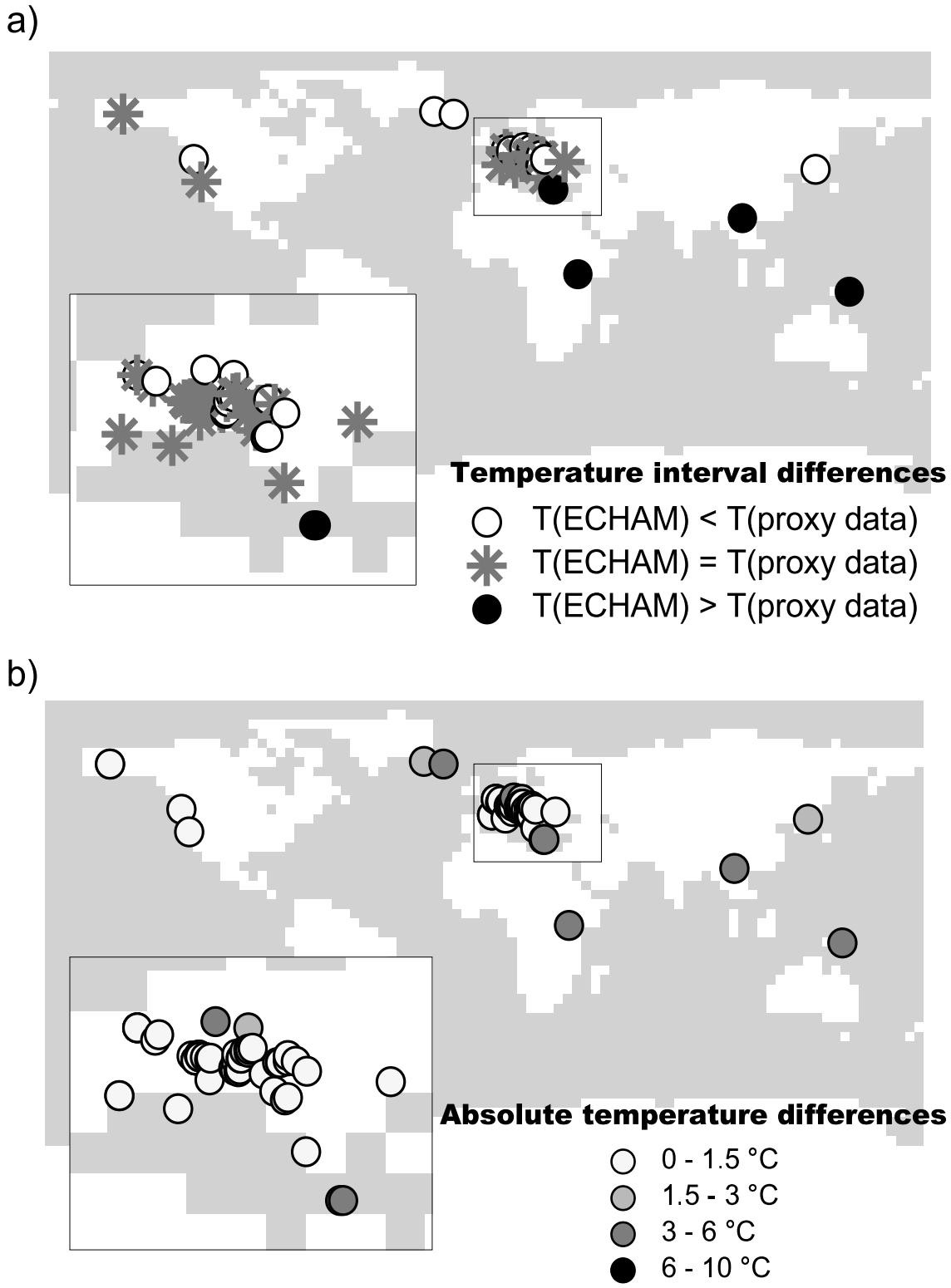

Figure 4.2: *Differences in yearly mean temperature intervals between ECHAM results (Tortonian double CO_2 content) and botanical proxy data. a) white circles: simulated temperature maximum is smaller than minimum temperature specified by proxy data, grey stars: temperature intervals overlap, black circles: simulated temperature minimum is greater than maximum temperature specified by proxy data. b) Temperature difference in absolute values between temperature interval from simulated data and proxy data.*

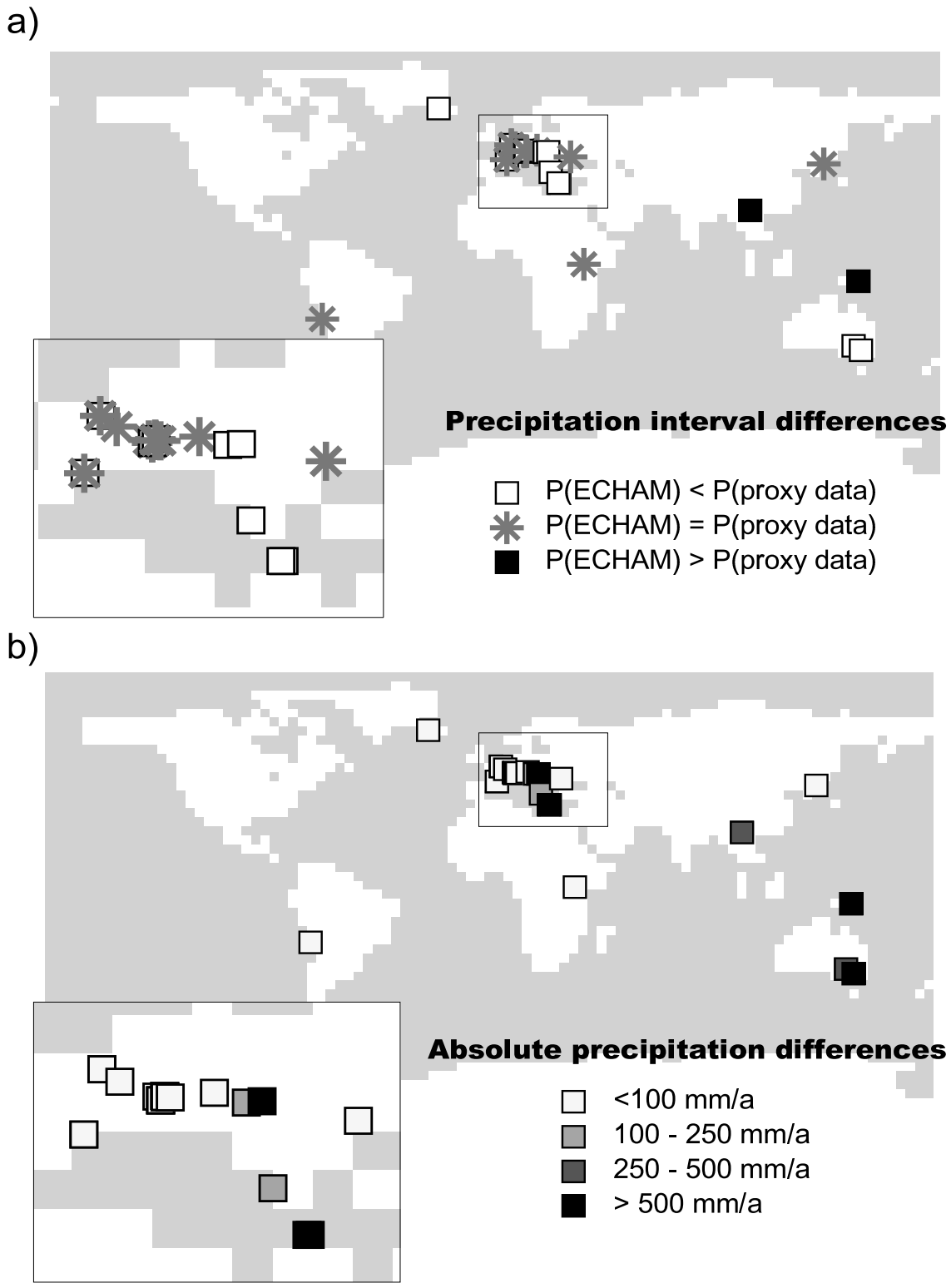

Figure 4.3: *Differences in yearly mean precipitation intervals between ECHAM results (standard Tortonian run) and botanical proxy data. a) white circles: simulated precipitation maximum is smaller than minimum precipitation specified by proxy data, grey stars: temperature intervals overlap, black circles: simulated precipitation minimum is greater than maximum precipitation specified by proxy data. b) Precipitation difference in absolute values between temperature interval from simulated data and proxy data.*

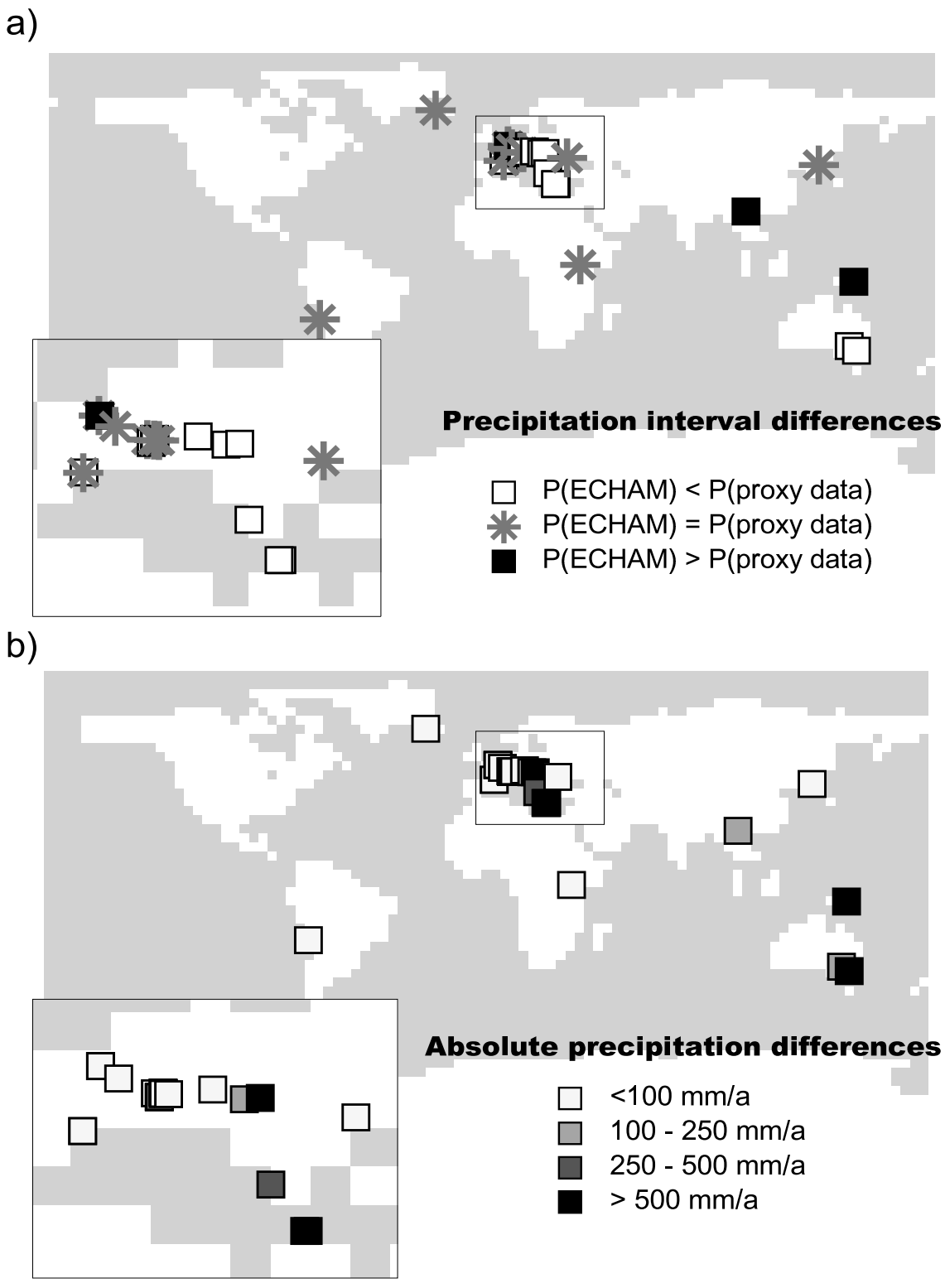

Figure 4.4: *Differences in yearly mean precipitation intervals between ECHAM results (Tortonian double CO_2 content) and botanical proxy data. a) white circles: simulated precipitation maximum is smaller than minimum precipitation specified by proxy data, grey stars: temperature intervals overlap, black circles: simulated precipitation minimum is greater than maximum precipitation specified by proxy data. b) Precipitation difference in absolute values between temperature interval from simulated data and proxy data.*

because the temperature intervals are separated from each other by less than 3 °C. Concentrating on Europe, discrepancies between both data sets vary with latitude. In the zoomed window in fig. 4.1 b) the circles represent a significant meridional gradient in temperature differences. For the area around the Mediterranean Sea model results are in good agreement with proxies (fig. 4.1 a). For the mid-European area, however, model results tend to represent cooler conditions than proxy data (fig. 4.1 a). The differences range from 1.5 to 6 °C whereas the coexistence approach yields temperature values of up to 5 °C higher than nowadays (Gebka et al. 1999, Utescher et al. 1997). This warming is in contrast to our simulation results as there is no positive temperature anomaly noticeable over European area (fig. 2.16).

Another method of obtaining palaeo-temperatures is based on Recent and fossil macro botanical data, which is performed by Wolfe (1994a). For the time range 12MA to 10Ma BP Wolfe (1994a) collected leaves in mid-latitudes of North-America. The author found out that the mean annual temperatures were in the range from 9.8 to 12.3 °C. These given mid-latitudinal palaeo-temperatures are nearly 3°C higher than the values represented by numerical model results referring to the standard Tortonian run (see also fig. 4.1). Regarding high latitude regions such as Beringia and Alaska the discrepancies between proxy data and model results are smaller. For example, Wolfe (1994b) found out that in the Upper Miocene mean annual temperatures were about 2 to 4 °C higher than today. He proposes that these higher temperatures were caused by an anomalously warmer climate during winter months. This process is also supported by a pollen analysis from White et al. (1997). The corresponding temperature differences between simulation data of the standard Tortonian run and proxy data can also be seen in fig. 4.1. For Alaska differences in simulation data of the standard Tortonian run and Control run represent an increase in temperatures of about 1 °C in the yearly mean (fig. 2.16). Proxy data, however, indicate a warmer palaeoclimate with temperatures up to 1.5 °C higher. A tendency to a warmer high-latitudinal climate is also represented by the simple model CLIMBER (fig. 3.2). CLIMBER results of the standard Tortonian run show increases in annual mean temperature of about 2 °C in comparison to the Control results. Additionally the above mentioned high-latitudinal reduction in seasonality indicated by proxy data is supported by CLIMBER results of the standard Tortonian run whereas numerical results of ECHAM only represent this reduction over the polar ocean.

For high latitudes the standard Tortonian simulation produces mean annual temperatures that are too low in comparison to proxy data. However, for low latitudes this pattern is reversed, as model output yields higher temperatures than suggested by proxy data. These temperature discrepancies, which can be nearly 6 °C for Africa could be due to different reasons. First, during the Neogene the tropics may have been significant colder than today. In contrast to this there is the assumption that there was no greater temperature increase in the tropics of more than 2 °C between the Palaeogene and today (Greenwood and Wing 1995). Nevertheless, there is no significant temperature decrease in the tropics represented by our model results which could explain the discrepancies between proxy data and simulation results. On the other hand it could be possible that the nearest living relative is nonexistent for the coexistence approach. This could result in a palaeoclimate reconstruction which is not matching the fossils' climate conditions. Finally climate model results of the standard Tortonian run could also differ from palaeoclimatic conditions. This could be caused by a different representation of the tropical atmospheric circulation (e.g., down branch of the Hadley cell could be shifted poleward or equatorward during the Tortonian). Thus temperature and precipitation pattern could not be represented accurately. Due to these sources of errors an interpretation of temperature discrepancies and also the precipitation discrepancies in the tropics should be done carefully.

In contrast to the results for the standard Tortonian run, the double CO_2 scenario shows a better agreement with proxy data in general on the global scale (fig. 4.2). There are only small discrepancies for Europe and America with maximum deviations of 4.3 °C and 1.2 °C respectively. Despite some outliers there is widespreaded agreement between temperature intervals of proxy data and model output overlap, which means that there are no significant differences in climatic specifications. Like the standard Tortonian run, though, discrepancies are significant in the tropics. These differences can be ascribed to the additional greenhouse effect in the double CO_2 run, which also warms the atmosphere in the tropics. Thus, temperature discrepancies between proxy data and climate results are increased (fig. 4.2).

Precipitation rates show a slightly different pattern when comparing model results of the standard Tortonian run and proxy data (fig. 4.3). Over Southern Europe precipita-

tion rates are up to 180 mm/a higher when comparing ECHAM results for the standard Tortonian run and the Control run (cf. fig. 2.17). European proxy data also suggest an increase in precipitation relative to modern values. Both data sets show a good agreement for absolute values in western Europe. This region is strongly controlled by a maritime climate, i.e. it is provided with high precipitation rates. However, proxies for the East-Mediterranean show greater discrepancies, which can be attributed to the fact that the actual size of the Paratethys during the Upper Miocene is not represented in the ECHAM model. Due to the lack of a larger ocean there are no additional evaporation processes to supply surrounding areas with a more humid climate. This could explain drier regions in model results as compared to proxy data.

For the locality corresponding to Papua New-Guinea a precipitation rate of 1096 to 1864 mm/a is suggested by proxy data. This value is more than 2000 mm/a lower than simulated by the model for the standard Tortonian run. In this case proxy data values can also be controlled by local effects which could also lead to this great discrepancy. Additionally, Southern Australian proxies suggest a much more humid climate which is not represented by climate model results of the standard Tortonian run. Such differences in rainfall specification might also be related to the geographical position of Australian continent. It is assumed that the Australian continent was located further southwards during the Upper Miocene than today (Beard 1977). Naturally, the latitudinal position of a landmass can have a significant influence on the annual precipitation rate.

Precipitation rates of the double CO_2 sensitivity run and the standard Tortonian run differ only slightly (fig. 2.17 and fig. 2.25). Thus the difference between model results and proxy data is also small (fig. 4.4). The double CO_2 sensitivity run, however, shows better agreements with proxy data in the regions of Iceland, Southern Asia, and Southern Australia, which show greater rainfall. For these regions regions higher rainfall result from the northward shift of the Polar Frontal Zone, a reorganization of Asian monsoonal circulation, and a moister atmosphere due to a regional enhanced hydrological cycle.

Regarding European climate a major role plays the change of climatic conditions around Mediterranean Sea. van Dam and Weltje (1999) reconstructed the climate on the Iberian peninsula for the Late Miocene using rodent palaeocommunities. Their investigation

which is related to the time-span 10.5 to 8.5 Ma BP provides cooler and more humid climate conditions in contrast to the precedent time-slice. van Dam and Weltje (1999) suggest that the time-span from 10.5 to 8.5 MA BP is a temperature determined episode as there is no shortcoming of rain. The time-span between 10.5 and 8.5 Ma BP is separated from the succeeding time-span which has a precipitation controlled character. These changed climate conditions are characterized by warmer and more arid conditions. This arid climate condition in direct vicinity to the Mediterranean Sea is assumed to be the first indication of the starting point of the Messinian Crises. Likewise proxy data results from Alonso-Zarza and Calvo (2000) and Bertini (1994) show same climatic conditions for the corresponding Upper Miocene time spans whereas their studies are based on sedimentary records in Spain and palynological investigations in Italy respectively. Furthermore it is assumed by Alonso-Zarza and Calvo (2000) that their investigation region in Spain represents a boundary between a humid and subtropical-dry climatic belt . This corroborates that some Mediterranean surroundings like Spain are sensitive regions to slight changes in circulation patterns. With regard to climate modeling the ECHAM results corresponding to Spain of the standard and double CO_2 Tortonian run represent consistently a slight increase in precipitation rate in comparison to the Control run (cf. fig. 2.17 and fig. 2.25). Thus our numerical results of the Tortonian represent a more humid climate condition for the Mediterranean area which is comparable with above described results from proxy data.

Fox (2000) suggests a correlation between climatic change and habitat change of North American mammals. The author's investigation concentrates on fossil records for the Late Miocene. Fox (2000) found out that the incremental growth of *Gomphotherium* tusks reflect climate changes. The results show that in contrast to the Miocene Climate Optimum, the Upper Miocene was more arid and had a distinct wet season. These results for the interior of North-America (Oklahoma and Nebraska) are consistent with ECHAM results. Simulation data from both Tortonian scenarios represent dry conditions with a high seasonal temperature range for the area corresponding to Oklahoma and Nebraska. Climate conditions in the standard Tortonian run are slightly colder than today representing a cool temperate climate. Yet a validation of absolute temperatures is not possible as the climate conditions derived from proxy data are compared with Mid-Miocene climate conditions. In contrast to the Control run, the CO_2 sensitivity run provides higher temperatures in the North American interior, which is more in agreement with above-freezing cold month

means as suggested by e.g. Markwick (1998) on the basis of fossil crocodilians. Likewise palynological studies by Pazzaglia et al. (1997) concentrated on the east coast of North America suggest a change from a Mid-Miocene warm-temperate or subtropical climate to cool temperate conditions during Pliocene with an enhanced seasonality in mid-latitudes.

Model results from regional palaeontological and meteorological climate reconstructions (Utescher et al. 1997, Gebka et al. 1999) indicate temperatures for the lower Rhine embayment that are several degrees higher than today (cf. fig. 4.1). Both the proxy data and the mesoscale model results of Utescher et al. (1997) and Gebka et al. (1999) give higher temperatures than the standard Tortonian run. However, one main aspect which should be considered is the different resolution between a mesoscale model and a global climate model. The coarse resolution in a global climate model like ECHAM restricts the possibility representing regional temperature anomalies. Despite the discrepancies of proxy data and the standard Tortonian run, the CO_2 sensitivity experiment gives temperatures nearly as high as those suggested by Utescher et al. (1997). In general the differences are smaller than 1.5 °C (fig. 4.2). Nevertheless, for the standard Tortonian run CLIMBER and ECHAM agree in a lower intensity of west winds over Northern Europe. This fact coincides with the assumption for the Tortonian mesoscale model performed by Gebka et al. (1999). In contrary to the work of Gebka et al. (1999), westerlies are intensified in the CO_2 experiment. In contradiction to the regional climate modeling results of Gebka et al. (1999), our study shows that a warmer European climate is associated with a stronger west wind in high mid-latitudes. In the work of Gebka et al. (1999) it is assumed that less intense westerlies maintain a warm climate over Europe. In contrast to this assumption, ECHAM results with double CO_2 support a higher intensity of westerlies. One possibility for explaining these discrepancies could be the propagation of polar ice sheets. As the polar regions are still covered by great ice sheets in our ECHAM results the meridional temperature gradient is still high. As a consequence strong westerlies are maintained which are shifted further north. Due to this shift Europe is affected by warmer and wetter climate conditions. Hence, a precise determination of the expansion of polar ice volume is necessary for climate reconstruction as this could affect the general atmospheric circulation pattern. Moreover, an accurate description of ice modules in numerical models is an important matter for palaeoclimate studies.

In comparison to the Northern Hemisphere only sparse data are available for the Southern Hemisphere with respect to the Tortonian time-slice. Thus the model set-up is much more reliable for the Northern Hemisphere,which means that discrepancies between model and proxy data are more likely to occur on the Southern Hemisphere. An example for northeast Australia indicates such differences between proxy data and model results. Investigations of tropical reef growth rates for northeast Australia indicate significant cooler water for the Late Miocene (7-11 Ma BP) with temperatures close to 20 °C (Isern et al. 1996, Betzler 1997). These low temperatures are not reproduced by model results, which could be attributed to an insufficient data base for the initial boundary conditions in the Southern Hemisphere. However, there could also be another explanation for these low temperatures. The geographical position of Australian continent was farther south than today. This different condition could induce an ocean circulation which transports colder water masses to North East of Australia.

4.2 Comparison of model results with vegetation distribution

CLIMBER model calculates a fraction of trees, grass, and bare soil that is in equilibrium with climate and is based on changes in temperature and precipitation values (Brovkin et al. 1997). The corresponding results are shown in fig. 4.5 and fig. 4.6 for the standard Tortonian run and the CO_2 doubling experimental run, respectively. These values are compared with a vegetation map suggested by Uhl and Micheels (pers. comm.) which is based on plant communities and divided into biomes after Claussen (1993). Unfortunately for the global scale there is not sufficient information available. Thus for the regions with deficiencies in Tertiary sediments and plant fossils a best-guess interpolation of vegetation zones is used. The reconstructed vegetation zones are transformed into fraction of trees and grass using the classifications after Brovkin et al. (1997). The results are represented in fig. 4.7.

There are some remarkable differences between Tortonian vegetation cover and that of todays. At high latitudes a complete lack of tundra vegetation is assumed based on proxies. The tundra is replaced by taiga and there is a noticeable northward shift of vegetational

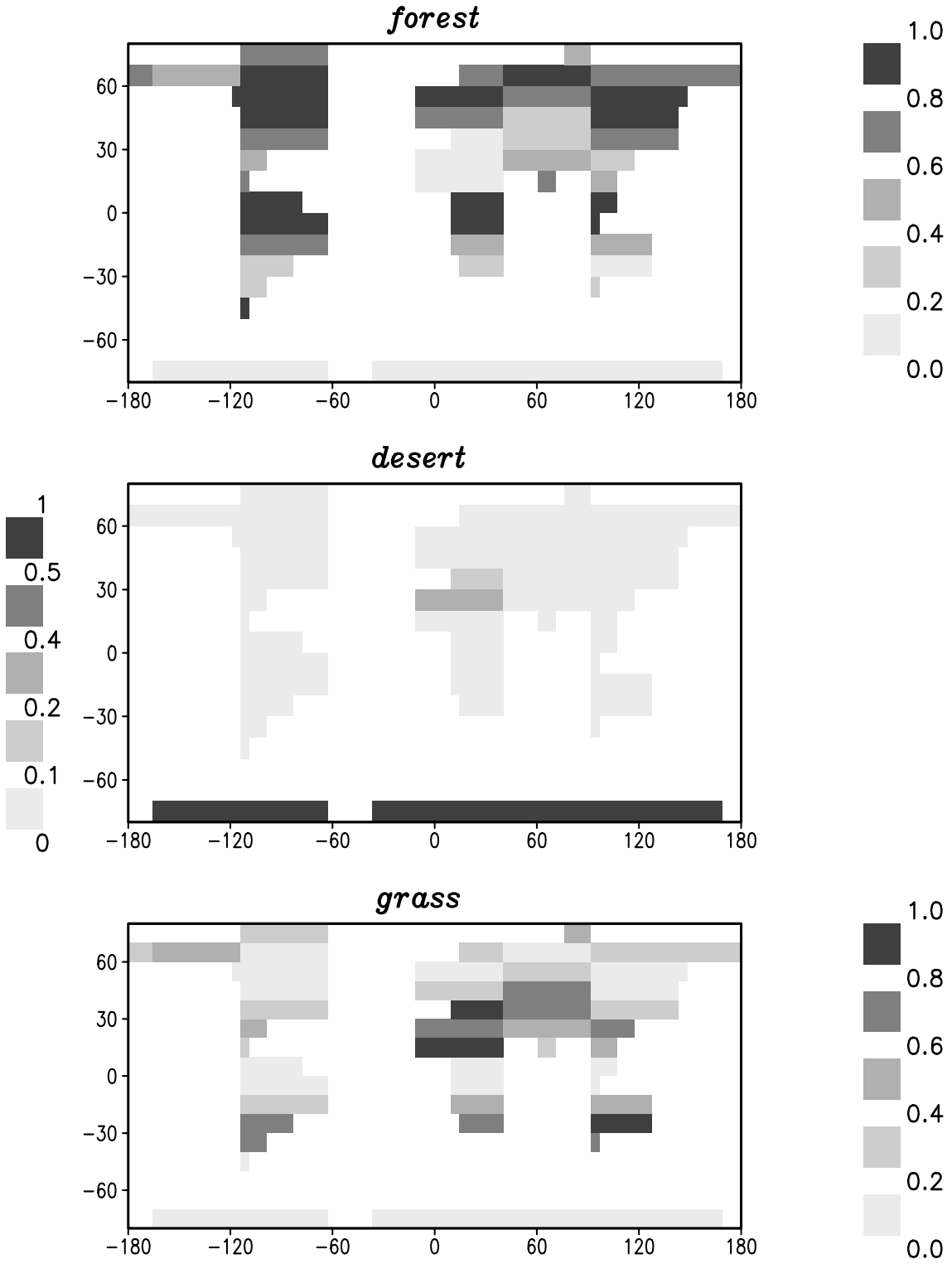

Figure 4.5: *Vegetation fraction of Tortonian run (AOV) for forests, deserts, and grassland.*

zones. In contrast to the present-day, the potential vegetation zones are widened, indicating a smoothed transition from equatorial to polar regions. Another distinct change is the replacement of subtropical deserts by grassland and shrubs.

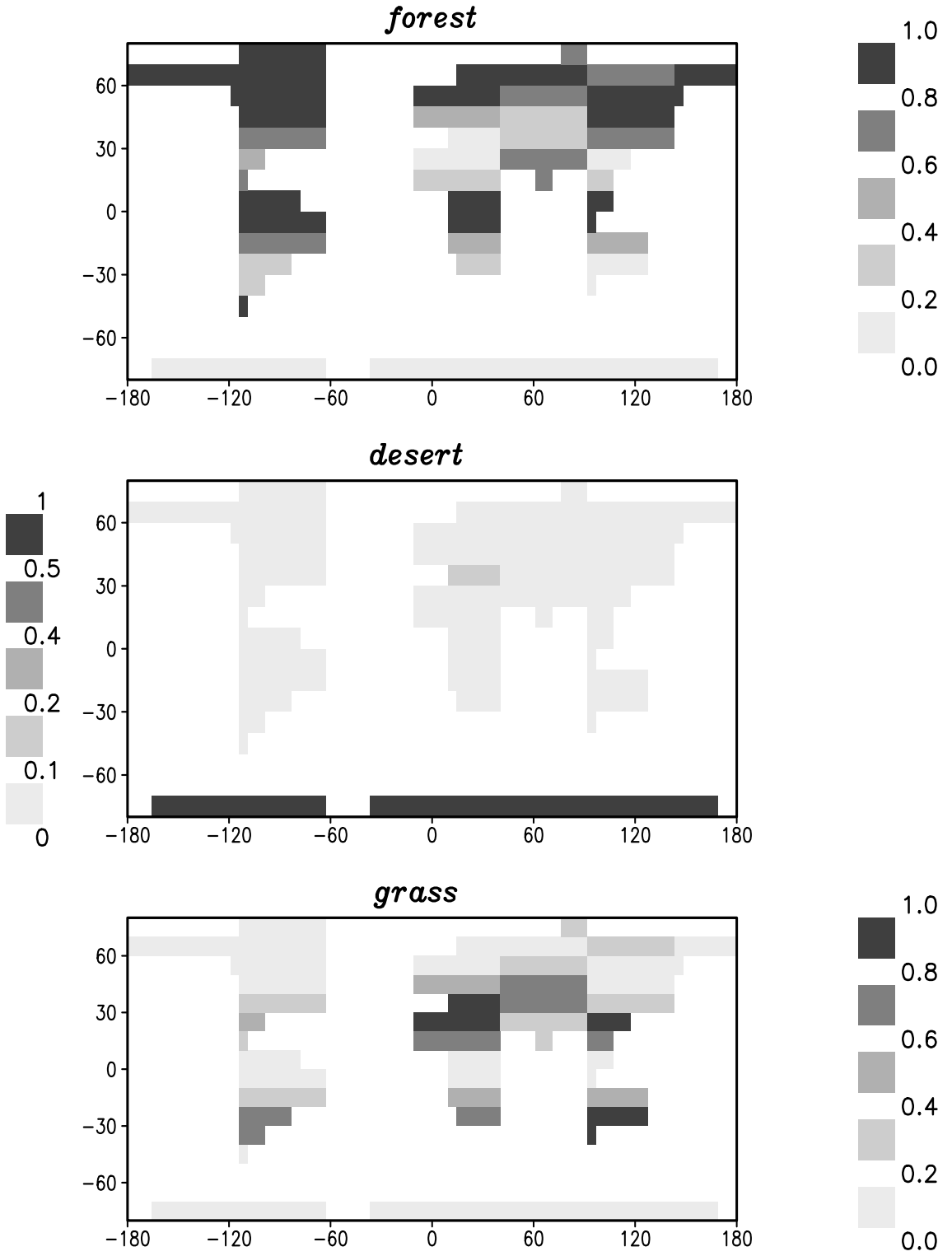

Figure 4.6: *Vegetation fraction of Tortonian run (AOV) with double CO_2 for forests, deserts, and grassland.*

Dutton and Barron (1997) demonstrate that a boreal forest induces positive feedbacks that lead to warmer climates in northern areas. There are several studies with regard to changes in vegetation distribution at high latitudes. Forested areas existed at the Arctic fringes far north of the present-day forest-tundra boundary until about 2 Ma BP

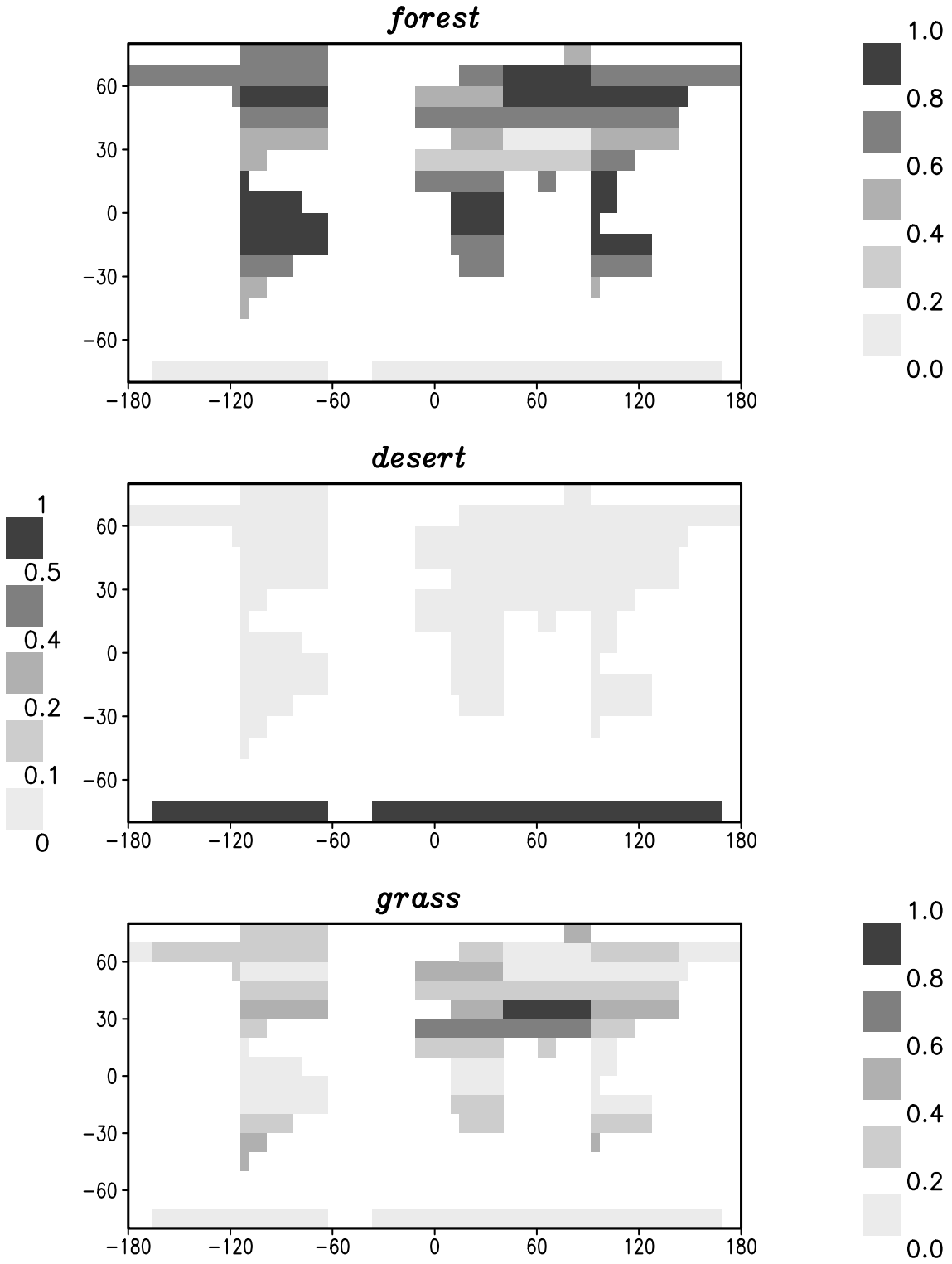

Figure 4.7: *Best-guess vegetation fraction of forests, deserts, and grassland based on plant distributions (see text).*

(e.g., Carter et al. 1986, Nelson and Carter 1985). Carter et al. (1986) and Nelson and Carter (1986) show a decrease in forest vegetation for the Quaternary. White et al. (1997) found, on the basis of pollen and spores, a trend from a dense to a more open forest canopy during the last 10 Ma. Furthermore they suggest a significantly warmer

climate for 8 Ma BP than today. This change in climate conditions during the last 8 Ma years could be a response to global orographical changes causing global climatic changes and variations in vegetation cover. The tendency of a warmer high latitudinal climate is only slightly represented in the standard Tortonian ECHAM simulation. An evaluation of quantitative values is difficult as there is a non-dynamic vegetation formulation in the ECHAM model which lacks in representing vegetation-temperature feedbacks. With the model CLIMBER, however, it is feasible to compare the reconstructed vegetation cover with model results (see below). In general the standard Tortonian run and the CO_2 doubling scenario show an increase in forest vegetation at high latitudes (fig. 3.4, fig. 4.5, and 4.6). In the double CO_2 experimental run of CLIMBER the areal extent of forests is slightly increased for North America and Greenland. These changes are caused by the increase in temperature which also amplifies the high latitudinal precipitation rate and the vegetation cover leading to a positive feedback mechanism. The reconstructed vegetation map for the Tortonian time slice (fig. 4.7) agrees with CLIMBER results in that way that there is a greater vegetation cover at high-latitudes. However, small differences indicate that numerical results do not represent the widened vegetation zones as reconstructed by proxy data. In order to yield such results higher high-latitudinal temperatures are needed to maintain a taiga vegetation. Nevertheless, CLIMBER model results generate a tendency to a much warmer climate for northern Eurasia and North American continent.

As proxy data suggest (Wang et al. 1999) a drying in Central Asia is caused by the rise of the Tibetean Plateau. Therefore a widespreaded region with low plants is assumed for Asian interior. CLIMBER results also represent a higher fraction of grass than forests. This shows that this area is affected by the presence of the high mountain range. In correspondence with the reconstructed vegetation, the North African desert belt vanishes in the CLIMBER run and is replaced mainly by grass. For this change the increase in North African monsoonal circulation plays an important role providing subtropics with more precipitation.

Because boundary conditions are changed only for the Northern Hemisphere, CLIMBER produces few climate changes for the Southern Hemisphere (cf. fig. 3.1). As a result the fraction of trees and grass on the Southern Hemisphere does not differ from that of the Control run. The proxy vegetation map (fig. 4.7), however, shows a spreading of tropical

forests that is nearly symmetrical with respect to the equator. Likewise the Australian continent is more covered by tropical rain and seasonal forests as indicated by Martin (1998). The more southerly location of this landmass, which is suggested by e.g., Lee and Lawver (1995), Gahagan et al. (1988) can partly explain the greater vegetation cover of this continent. With regard to Neogene climate change of Australia, Kennett (1993) considers that the continental shift alone is too slow to account for the climatic changes. Thus it is likely that other processes e.g., an additional greenhouse warming or a different ocean conveyer belt could play an important role for Southern Australia climate.

4.3 Summary of the comparison of proxy data with simulation results of ECHAM and CLIMBER

In this chapter quantitative and qualitative proxy data are compared with numerical results of ECHAM and CLIMBER simulations. This juxtaposition of reconstructed temperature and precipitation proxies with simulated data are in partial agreement with the standard Tortonian and double CO_2 experimental run. The analysis with ECHAM results shows that quantitative proxies coincide best with the CO_2 doubling scenario.

The main consequences with regard to the ECHAM simulation derived from the comparison above is listed in the following:

- A validation of rainfall is difficult as such coarse climate models like ECHAM in T30 resolution lack in representing precipitation pattern accurately. However, there are conformities between simulated precipitation rates and proxy data indicating an increase in rainfall in mid-latitudes. This increase occurs in both the standard Tortonian run and the double CO_2 experimental run.

- A decrease in seasonality at high latitudes is indicated by proxy data and indicated by the results of the standard Tortonian run and the CO_2 sensitivity experiment.

- The validation between model results and proxy data for tropical regions shows great discrepancies. These inconsistencies may be due to the coarse climate model resolution, regional orographical effects, or deficiencies in assigning the next living relative of the corresponding fossil.

- An exact validation of Mediterranean Sea climate and its surroundings is difficult as these regions are sensitive to a change in climate zones (subtropical to warm temperate during the Tortonian). Nevertheless, model results can represent well the anomalous temperature and precipitation fields for the Tortonian time-slice for Southern Europe.

- The double CO_2 scenario with ECHAM is in very good agreement with the temperature pattern of the proxies. This experiment enables to explain a warmer and wetter climate in mid-latitudes. Simultaneously there is also a good conformity with high-latitudinal temperatures at the corresponding proxy locations.

- Deficiencies in the standard Tortonian run can be explained by the positive vegetation-temperature feedbacks not represented in ECHAM. This mechanism plays an important role in controlling high-latitudinal temperatures.

A validation of temperature and precipitation proxy data with CLIMBER simulation results is more difficult because of the coarse resolution. With an intermediate model variables are smoothed so that no direct comparison is feasible on the horizontal plane with proxy data from borehole locations. In order to circumvent this difficulty and take advantage of the model's possibilities a comparison of vegetation cover between proxy data suggestions and simulated values is performed. Therefore a vegetational map is reconstructed based on qualitative proxy data and is downscaled on CLIMBER resolution. The main results of this comparison are summarized below:

- A tendency in temperature increase and an increase in boreal forests is noticeable. Thus CLIMBER results and the reconstructed vegetation map show especially good agreement at high-latitudes.

- For the numerical and reconstructed palaeo-information a decrease of subtropical deserts is noticeable up to a complete disappearance. As for the ECHAM runs, CLIMBER model results for the double CO_2 experiment are even closer to the suggested vegetational map.

- Due to the vegetation-temperature feedback mechanism a widespread greening with regard to Northern Africa and central Asia can be seen from the results. These data are in good agreement with vegetation distributions derived from Miocene botanical data.

Both models show similarities in their tendency to a warmer climate and to an intensified precipitation cycle affecting Europe with more rain fall. The CO_2 doubling experiment, however, shows in general a better agreement with proxy data. This is valid for temperature and precipitation fields as well as for the distribution of vegetation.

Chapter 5

Discussion

Generally speaking, models are simplified pictures of reality. Although the models used in this study differ in their complexity, none is able to represent Tertiary conditions comprehensively. They are not able to correctly represent all parts of climate system, namely the atmosphere, hydrosphere, biosphere, geosphere, pedosphere, and cryosphere. This is due to the fact that the time for computing such a complexity would exceed a reasonable amount. Naturally a higher resolution would give more specific results about regional climates but this would also raise computational costs. However, proxies also confine climate modeling resolution because they are sparse on the global scale and limit an accurate setting of boundary conditions. Moreover, for this time slice experiment time-homogeneous boundary conditions are assumed corresponding to at least one million years. Proxy data, however, cannot represent such a long time period which would assume constant sedimentation, an exact dating, and a precise process for proxy data probing.

Apart from these constraints, however, an accurate choice of models enables one to reconstruct climate and climate processes for the Upper Miocene quite well. In the following basic results of the models ECHAM and CLIMBER and the validation with proxy data will be presented. Furthermore, the outcomes will be discussed with studies from different authors. With regard to palaeoclimate modeling, the significance of our results will be debated. And there will be several alternative suggestions for further investigations on Tortonian climate.

Oceanic Heat Transport

To adjust the model ECHAM to Tortonian boundary conditions, oceanic properties such as the heat flux (and thus the momentum flux) were changed. Because proxy data cannot provide sufficient information on reconstructing the whole palaeo-ocean circulation or oceanic properties for the world oceans, a method was developed to change heat transport in a slab ocean model.

In general a change in oceanic heat transfer can be attributed to a different continental distribution and to different sea-ways, which change through geological time. Also important is ocean bathymetry. For example, there can be no formation of deep convection zones in a shallow ocean basin. For resolving such complex circulation patterns a three dimensional ocean model is needed but because this type of model needs high computation time a mixed-layer ocean model was used. In order to adjust oceanic heat transport in a slab ocean model one approach must be chosen for this performance. An alternative to our approach would be the application of an iterative method based on interactive variations of the flux correction (oceanic heat transport). At this the flux correction could be adjusted until the simulated sea surface temperatures do best fit the given palaeo-temperatures. When using this method one should consider that few data are available on the horizontal plane for specifying changes in heat transport for the global ocean. Thus such variations are not necessarily more reliable than using a less complex idea such as that used for our studies. In this work the variation of heat transport in the ocean is based on a simple model. In order to represent a changed oceanic heat transport for the Upper Miocene the meridional temperature gradient was chosen as a representative of the general heat transfer in the ocean. The comparison of model results regarding the extention of polar sea ice and descriptive proxy data yield good agreements. Furthermore, the change in vertical and horizontal flow pattern represents a circulation pattern which is similar to characteristic ocean patterns indicated by Tortonian proxy data.

From the simpleness of this method and the qualitative structure it follows that the results cannot be applied to palaeoceanographic predictions. Additionally it is self-evident that this procedure is a rough simplification of oceanic processes. Our approach provides an adjustment to a different ocean forcing which should not be neglected for simulating

a different time-slice. An investigation of the sole effect of a changed heat transport is already in process and will follow this work.

Whether oceanic heat transport in the past differed from that of today is still a controversial topic. One problem is derived from the nature of the ocean. In contrast to heat transport that is prescribed as a latitudinal-dependent variable, the ocean basins are three-dimensional. Rind and Chandler (1991) discuss that a different ocean orography is one possible factor for changing the ocean circulation, i.e. the ocean conveyer-belt. Furthermore, Bice et al. (2000) found out that changes in the ocean geography both on the Northern and Southern Hemisphere play a significant role for the intensification of the heat transport. Another problem with the oceanic heat transport is the interactions at the atmosphere-ocean interface, which are as well still not completely understood. Model experiments show that an increased oceanic heat transport can be partly compensated by decreased atmospheric heat transfer or vice versa (see also Covey and Thompson 1989, Bice et al. 2000, Crowley 1996). Additional experimental runs are needed to explain the contribution of the oceanic and atmospheric heat transport to different palaeoclimates. A third problem with the oceanic heat transport mechanism is the question of whether increased or decreased heat transfer could be responsible for a warmer climate during the Tortonian. Investigations of Pliocene climate by Rind and Chandler (1991) and Chandler et al. (1994) show an increase in oceanic heat transport associated with a warmer global climate. Rind and Chandler (1991) show that there is an increase in oceanic heat transport while the high-latitudinal temperature gradient is reduced. The authors try to explain this fact with feedback mechanisms concerning the thermohaline circulation. Correspondingly Haywood et al. (2000) assume that the Pliocene warming would increase precipitation and most significantly evaporation in the oceans. This has the effect of altering the salinity and density of ocean waters, which could modify the thermohaline circulation. These assumptions seem to contradict ocean set-up, which contains a presumed reduced oceanic heat transport corresponding to a reduced latitudinal temperature gradient (see also fig. 2.5). Our approach, however, is justifiable as it is a plain application of the gradient law and a different ocean circulation is not considered. Despite discrepancies between Pliocene modeling results and our simulation results there are agreements between our results and Late Miocene modeling simulations. The studies by Bice et al. (2000) of the Cenozoic ocean are based on three-dimensional ocean models.

Their simulations show an intensification of oceanic heat transport from the Palaeogene to the Neogene coupled, with an intensification of the Northern Hemisphere overturning cell and a reduction of the latitudinal temperature gradient. On the one hand this study reinforces our approach, which implies a reduction of oceanic heat transport and a reduction of Northern Hemisphere temperature gradient for the Tortonian time-slice. On the other hand this work by Bice et al. (2000) emphasizes the complexity of the palaeo-ocean which should be taken into account for further palaeo-studies.

Results of the standard Tortonian run with the complex model ECHAM show that a change in oceanic heat transport has a main influence on the climate of the mid-latitudes. This is indicated by a temperature reduction of several degrees that is probably associated with the reduction of oceanic heat transfer. With regards to the Neogene, the palaeo-ocean was slightly different from that of today (e.g. an open Panama Strait) and, thus, it is quite likely that the ocean could had a main influence on the atmospheric circulation. Consequently, it is necessary to consider at least the oceanic heat transport for further palaeoclimate studies of the Neogene.

ECHAM model

Two experimental runs were performed with ECHAM4/ML with regard to both a present-day value of atmospheric carbon dioxide and a doubling of CO_2, including a changed oceanic heat transport. To provide an analysis of atmospheric and oceanic circulation patterns, data from both runs are compared with regional proxy data. Consequently, in the case of a good agreement model results can represent the corresponding predominant circulation pattern for that region. On the other hand if the comparison of simulation data and proxy data show disagreements, then either climate model results, proxy data, or both could be inaccurate in representing the Tortonian climate.

With regard to proxy data there are sources of errors in specifying climate conditions due to different methods (e.g., Wolfe 1995, Mosbrugger and Utescher 1997). Different methods could result in different values of climatic proxy data for the same sample (cf. Mosbrugger and Schilling 1992). This fact also causes problems in comparing climatic proxy data with simulation results. Another problem with proxy data is that even though the time-span proxy data refer to is broadened with geological time, proxy data do not

represent constant conditions of one million years which it is also assumed for the Tortonian time-slice. Beyond this climate model results for the Jurassic have been compared with proxy data for an interval of about 10 million years (e.g., Sellwood et al. 2000). Thus, disagreements between proxy data and results of general circulation models should be judged carefully.

The results of the double CO_2 sensitivity run show a good agreement with quantitative and qualitative temperature and precipitation fields from proxy data representing our best-fit Tortonian climate. With regards to mid and high-latitudes, proxy data and the results of the double CO_2 sensitivity run suggest a warmer Tortonian climate than today. The corresponding simulation shows that the elimination of the Greenland ice cap provides a distinctly warmer climate at high latitudes. Additionally, the replacement of glaciers with vegetation amplifies the warming of the Arctic Ocean. Due to a positive vegetation-temperature feedback mechanism the yearly temperature cycle is smoothed and leads to a less distinctive seasonality. Additionally, the enhanced greenhouse effect heats the atmosphere. Thus a conformity regarding sea ice volume between proxies and model results is yielded. Due to the source of proxies there is no quantitative estimation of ice volume available. However, even indirect data derived from studies of ice rafted debris (Wolf and Thiede 1991) indicate an existence of glaciers around 9 Ma BP. Therefore the comparison shows an agreement between calculated and derived data inasmuch that there is a tendency of less ice on the Northern Hemisphere compared to today. As a result of initially changed boundary forcings - mainly referring to the Northern Hemisphere - in comparison to today a significant anomalous climate on the Northern Hemisphere can be observed. With regard to the Southern Hemisphere changes in ice volume are relatively small. An approximately unchanged ice cover (model results represented in this study correspond to a reduced sea ice fraction and not to a reduction of inland ice masses) over Antarctica is also supported by proxy data. Furthermore, a reduction in the latitudinal temperature gradient is evident in both numerical results from other authors corresponding to the Miocene (Dutton and Barron 1996, Dutton and Barron 1997) and in our results. Consequently the assumed boundary conditions and a doubling of atmospheric carbon dioxide for the Tortonian seem to be reasonable with regard to several model and proxy results.

With regard to the Asian atmospheric circulation, both the standard Tortonian run and the double CO_2 sensitivity run result in a change of the Asian monsoonal circulation system. Mainly these variations are caused by the reduction of the height of the Tibetean Plateau. It is widely assumed that the uplift of the Tibetean Plateau during the Late Neogene is the major cause of the intense formation of the Asian summer monsoon (Kutzbach et al. 1989, Prell and Kutzbach 1992, Ding et al. 1999). Combined with the onset of the Asian summer monsoon during the Late Neogene is a significant change in regional and large-scale flow resulting in different surface wind and precipitation patterns. Therefore, several investigations concerning the influence of the height of Tibetean Plateau on the global circulation have been performed. Studies by Rind et al. (1997) and Hay (1996) show that a reduction in mountain heights has an influence on poleward heat and moisture transports. In order to investigate such processes mountain heights were eliminated, which yielded a reduced meridional temperature gradient. In our study the orographical effect on the planetary wave pattern is supposed to be quite small as the global mountain range differences are small in comparison to the above mentioned studies. Nonetheless, the interactions between atmosphere and ocean could be of importance for the Tortonian climate. Therefore further investigations on the sensitivity of mountain heights and a changed ocean conveyer-belt representing Tortonian conditions is needed. Several numerical experiments have been performed in order to investigate regional changes in the Asian summer circulation. In compliance with numerical studies by Prell and Kutzbach (1992) the standard Tortonian results show a weakening of Asian monsoonal circulation in summer relative to today. In contrast to the standard Tortonian run, the double CO_2 experimental run produces a monsoonal circulation that is more intense than in the standard Tortonian run. Thus, in the double CO_2 sensitivity run the precipitation rates are close to present-day rates. Hence the intensification of Asian summer monsoon is not controlled solely by mountain heights (cf. also Douville et al. 2000). The more intense monsoonal circulation is caused by a more moist atmosphere and the capability of advecting moisture. Palaeo-sensitivity studies by Fluteau et al. (1999) also indicate that in comparison to present-day the greater extent of the Paratethys into the Asian interior during the Neogene contributes to a decrease in rainfall over the Himalaya for the Tortonian. The size of the Paratethys is also responsible for the release of latent heat, which strengthens the moisture advection in comparison to today (Fluteau et al. 1999, Ramstein et al. 1997). Even though a greater size of Paratethys is not considered

in our standard Tortonian run, there is an increase in moisture flux North of the Asian mountain range in our model results. This feature is in compliance with investigations on proxy data (e.g., Ding et al. 1999). In conclusion, it can be seen from several numerical simulations that since the onset of the Asian summer monsoon this circulation pattern is at least influenced by both boundary conditions such as palaeogeography and the level of greenhouse gases which should be considered for reconstructing Tortonian climate.

One problem in global palaeoclimate modeling is the coarse resolution of such models. In contrast to climatic proxy data, modeled temperature and precipitation specifications represent a greater horizontal space. Additionally the temperature and precipitation fields are smoothed whereby local climate effects in comparison to proxy data become indistinct. Thus in order to represent Tortonian climate conditions more accurately on the regional scale an adjustment of both the palaeontological data base and meteorological features would be of advantage. For minimizing errors between those different data bases a geological-palaeontological and mesoscale modeling approach was used by Gebka et al. (1999) and Utescher et al. (1997) to reconstruct Tortonian climate for Northern Germany. Contrary to regional climate modeling based on nesting methods (a mesoscale model is "nested" in a global general circulation model), this approach has the benefit of representing a self-contained climate system which coincides with proxy data. Nevertheless, due to gaps in boundary conditions on the global scale for the Tortonian time-slice, inconsistencies in climate predictions - see also our results - could occur when comparing global climate modeling results with such mesoscale modeling results as performed by Gebka et al. (1999). In contrast to this, disagreements in climate model results do not exist when applying nesting techniques. However, when using a nested mesoscale model, discrepancies between proxy data and climate model results are likely to occur and probably tend to be greater.

One deficiency in the complex model ECHAM is the description of the vegetation. There have been a variety of numerical studies concerning the past vegetation cover and their feedbacks with climate regarding selected time-slice experiments (e.g., Upchurch et al. 1998, Dutton and Barron 1996). A vegetation cover different from that of today could cause enhanced evapotranspiration, which affects such factors as the strength of the African summer monsoon (Fluteau et al. 1999, Kutzbach et al. 1996). Thus, a greening

of North Africa leads to an intensification of the North African monsoon. Investigations on vegetational effects of boreal forests during the Late Miocene represent positive feedback mechanism (Dutton and Barron 1996) that is assumed to be one main factor for providing high-latitudes with greater warming. In order to calculate the sole effect of the Tortonian vegetation cover a sensitivity run has been performed in correspondence to our former runs (Micheels pers. comm.). In general, the results of this standard Tortonian run including a Tortonian vegetation cover yields considerably agreements with proxies. Thus the question has to be answered if the consideration of the Tortonian vegetation map alone could explain Tortonian climate and climate processes or if the amount of atmospheric carbon dioxide plays a major role in the Tortonian climate system. According to above mentioned initial results of this numerical experiment with a reconstructed vegetation cover (Micheels pers. comm.), the setting-up of vegetation maps should be one main interest in pre-Quaternary time-slice experiments.

CLIMBER model

Experimental runs with CLIMBER-2 investigate sensitivity studies regarding CO_2 forcing and changes in land-sea distributions. These runs were performed analogous to the ECHAM model; however, due to the model's possibilities the ocean and vegetation modules were included. In realizing such runs the question is traced if the model reproduces an adequate imprint of Tortonian climate comparable with ECHAM results. If so, a much more simple model like CLIMBER could be sufficient for pre-Quaternary sensitivity studies. This would be of advantage because of the low costs, the possibility of investigating small changes in boundary conditions, and in analysing specific feedback mechanisms for understanding past-climate changes (cf. also Kubatzki et al. 2000).

CLIMBER results of the standard Tortonian run are in partial agreement with the results of the ECHAM standard Tortonian run and proxy data. Consistent patterns include a warming at high latitudes, an increase in high-latitudinal forests, and a greening in central Asia. Furthermore, with a doubling of CO_2 the fraction of boreal forests increases further still reproducing palaeo-data fairly well. Admittedly, CLIMBER cannot resolve a mass transfer of ocean water through the supposed Panama Strait. Therefore information on possible Tortonian oceanic properties get lost. Nevertheless, a reduced oceanic heat transport is yielded by CLIMBER which is in the same order as in the initialized heat

transport for ECHAM. Due to quite similar changes in oceanic properties there is a possibility in comparing CLIMBER results with ECHAM results. Therefore model results are opposed even though models of different complexity were used.

However, there are also discrepancies between both models with regard to Asian summer monsoon. Here CLIMBER represents a strengthening of Asian monsoonal circulation in contrast to ECHAM results. This is assumed to be caused by the additional vegetation cover enhancing evaporation and therefore the vertical motion. Thus the biosphere contributes additionally to the intensification of Asian monsoonal flow. There is also a change in circulation pattern combined with a greening of North Africa. Thus CLIMBER model results seem to be sufficient for a comparison with ECHAM even though there are disagreements between both models. A further sensitivity experiment with CLIMBER with exact the same boundary conditions used for ECHAM would be of advantage. This would mean that the same oceanic heat transport should be used as it was set-up for the ECHAM model.

Combination of ECHAM and CLIMBER results

Even though ECHAM results of the double CO_2 sensitivity run are in good agreement with proxy data there are still some deficiencies which can be revealed by using CLIMBER. These discrepancies were investigated by changing the palaeogeography in CLIMBER performing further sensitivity runs. These variations are based on further geological proxy data which are dated for the Late Miocene. In changing the boundary forcings in the CLIMBER model it is assumed that this variation might have an influence on the large-scale atmospheric circulation. Therefore for evaluating changes in atmospheric circulation, the size of the Paratethys and Australia were matched to Tortonian situation.

The simulation results yield a better agreement with proxies at least in the tendency of a further shift from control data to Tortonian climate conditions. Hence a consideration of the size of the Paratethys extension and the latitudinal position of Australian continent are important for leastwise the corresponding regional climate. CLIMBER results represent an increase in moisture flux over Europe/Asia due to a greater Paratethys. This feature is also found in numerical results represented by Fluteau et al. (1999) and Ramstein et al. (1997). Beyond this an investigation with a combination of several changed

boundary conditions could also lead to a different amplification factor which would be of special interest. With regard to temperature and precipitation fields, these above mentioned boundary conditions could be applied to ECHAM and could possibly result in a better agreement with proxies.

To conclude, the performed studies demonstrate several feedback mechanisms and interactions between ocean, atmosphere and biosphere that significantly influenced Tortonian climate. Related to the mentioned hypotheses exposed in the introduction both the ocean-atmosphere interactions and the description of the ocean conveyer-belt are important factors which should not be neglected for palaeoclimate studies as these changes remarkably influence atmospheric circulation. This is shown with a reduced oceanic heat transport applied for the complex model ECHAM. By means of our numerical approach several agreements between proxy data and model results are demonstrated, which are best for the double CO_2 experiment. These include a reduced latitudinal temperature gradient, a reduced sea ice cover, a slight reduction of Asian monsoon, an intensification of African monsoon and warmer climates in mid-latitudes. Beyond this, further CLIMBER studies show deficiencies of the ECHAM model which are mainly the numerical description of the sea ice and vegetation code. Furthermore, these studies can explain climate processes, e.g. positive vegetation-temperature feedback mechanisms, leading to a warmer Tortonian climate as indicated by proxy data. Thus the conformities between proxy data and numerical results validate the combined usage of a complex and a simple model. This approach of using models of different complexity as used for our results is also applicable to different Neogene studies. Despite good agreement, there still are some discrepancies between numerical results and Tortonian proxy data. Apart from the physical constraints of our used numerical models these deviations can also be caused by the terrestrial proxy data base which is mainly confined to the Northern Hemisphere and poorly dated. In order to eliminate such deviations the implementation of a Tortonian vegetation cover, or the usage of a complex model containing an atmosphere, three-dimensional palaeo-ocean, and/or a vegetation module would be of advantage.

Chapter 6

Summary

In this work the climate of the Upper Miocene (Tortonian dated with $\approx$ 8 Ma BP) was simulated with general circulation models. For this purpose two models of different complexity were used to provide a climate reconstruction with regard to different forcings. Simulation runs were performed with the complex model ECHAM4 coupled to a slab ocean and with the more simple model CLIMBER-2 which contains out of an atmosphere, ocean, and vegetation module.

For the Tortonian simulations the orography and glaciers were changed on information from available proxy data. For the slab ocean a reduction of oceanic heat transport was applied. The corresponding approach is based on δ^{18}O values of planktonic foraminifera. The qualitative comparison of the results show that there are good agreements between models results and marine proxy data. Furthermore, less intense ocean currents on the Northern Hemisphere (e.g., Gulf Stream, Kuroshio) as represented by the model are also indicated by proxy data.

ECHAM model output of the standard Tortonian run reproduces partly the climate conditions specified by proxy data. There are agreements with regard to a reduced latitudinal temperature gradient and a wetter climate for Europe. The double CO_2 sensitivity run, however, shows great agreements with quantitative temperature and precipitation proxies related to the Tortonian time-slice. The corresponding results indicate a reduction in sea ice extent, a reorganization of the Asian summer monsoon, an intensification of the African monsoon, a warmer climate at high-latitudes and a warmer and wetter climate

over Europe. Additional, numerical results represent a stronger influence of westerlies for the Tortonian affecting the European region with greater precipitation rates and higher temperatures.

The comparison of numerical results of the model with intermediate complexity (CLIMBER) and of the general circulation model (ECHAM) show agreements corresponding to a reduction of the Northern Hemisphere sea ice fraction, a decrease in high-latitudinal seasonality and a reduced oceanic heat transport. These agreements enable us to compare both models of different complexity. Thus the simple model CLIMBER with a fast turnaround time enables to investigate changes in palaeogeography and their effect on regional climates. Further experimental runs with CLIMBER result in a noticeable sensitivity of atmospheric circulation to the size of the Paratethys and to the latitudinal location of Australian continent. Additionally CLIMBER enables to reconstruct a palaeo vegetation which agrees quite well with our reconstruction of a vegetation distribution based on macro and micro fossils.

Finally, our numerical investigations on Tortonian climate show that the two climate models can be used to reconstruct Late Miocene climate. There are, however, still deficiencies which can be attributed to feedback mechanisms associated with the palaeovegetation as well as with the palaeoocean feedback mechanisms. Nevertheless, several studies have already been started in order to solve these problems.

Chapter 7

Acknowledgements

This work was financially supported by the Deutsche Forschungsgesellschaft with the project SFB 275, Universität Tübingen, named "Klimagekoppelte Prozesse in meso- und känozoischen Geoökosystemen (Climatically Coupled Processes in Mesozoic and Cenozoic Geo-Ecosystems) " for the time span 1998 until 2001. This work is connected to the sub-project B5 called "Modellierung des Klimas für ausgewählte Zeitscheiben des Tertiärs unter besonderer Berücksichtigung des alpinen und circumalpinen Raumes" and was hosted by Prof. V. Mosbrugger and his research team (amongst others Dr. M. Gebka, Dr. D. Uhl, Dr. A.A. Bruch, and Dipl.-Met. A. Micheels). Furthermore, the evaluation of this work by Prof. Dr. C. Hemleben is gratefully acknowledged. Additionally, the cooperation with PD Dr. G. Schmiedl, PD Dr. A. Kuhlemann, and other members from the SFB was fruitfully and contributed essentially to this work. A special thank-you to Dr. G.R.Jr. Upchurch who revised the English grammar and spelling of this work.

Simulations with ECHAM4/ML were kindly granted by the Max-Planck Institute of Meteorology, Hamburg, with a special support by Dr. E. Roeckner and Dipl.-Met. U. Schlese.

The work with CLIMBER-2 was kindly granted by the Potsdam Institute of Climate Impact, Potsdam. The performance of simulation runs were especially assisted by the team group of Prof. Dr. M. Claussen and his colleagues Dr. A. Ganopolski and Dr. C. Kubatzki.

Chapter 8

References

Attendorn, H. G., R.N.C. Bowen, 1997: Radioactive and stable isotope Geology. Chapman & Hall, London, 522 pp.

Alonso-Zarza, A.M., J.P. Calvo, 2000: Palustrine sedimentation in an episodically subsiding basin: the Miocene of the northern Teruel Graben (Spain). Palaeogeography, Palaeoclimatology, Palaeoecology, *160*, 1-21.

Beard, J.S., 1977: Tertiary evolution of the Australian flora in the light of latitudinal movements of the continent. Journal of Biogeography, *4*, 111-118.

Barker, P.F., P.J. Barrett, A.K. Cooper, P. Huybrechts, 1999: Palaeogeography, Palaeoclimatology, Palaeoecology, *150*, 247-267.

Barron, E.J., W.H. Peterson, 1991: The Cenozoic ocean circulation based on ocean general circulation model results. Palaeogeography, Palaeoclimatology, Palaeoecology, *83*, 1-28.

Barry, R.G., R.J. Chorley, 1992: Atmosphere, weather and climate. Routledge, 6th ed., London, 392 pp.

Berberich, D., 1996: Die planktische Foraminifere Neogloboquadrina pachyderma (Ehrenberg) im Weddelmeer, Antarktis. Berichte zur Polarforschung, *196*, 193 pp.

Berger, A., M.F. Loutre, C. Tricot, 1993: Insolation and Earth's orbital periods. Journal of Geophysical Research, *98*, 10341-10362.

Berger, A., M.F. Loutre, H. Galeé, 1998: Sensitivity of the LLN climate model to the astronomical and CO_2 forcings over the last 200ky. Climate Dynamics. *14*, 615-629.

Berner, R.A., 1991: A model for atmospheric CO_2 over phanerozoic time. American Journal of Science. *291*, 339-376

Berner, R.A., 1998: The carbon cycle and CO_2 over Phanerozoic time: the role of land plants. Philosophical transactions of the Royal Society of London/B., *252*, 75-82.

Bertini, A., 1994: Palynological investigations on Upper Neogene and Lower Pleistocene sections in central and northern Italy. Memorie della Societa Geologica Italiana, *48*, 431-443.

Betzler, C., 1997: Ecological controls on geometries of carbonate platforms: Miocene/Pliocene shallow-water microfaunas and carbonate biofacies from the Queensland Plateau (NE Australia). Facies, *37*, 147-166.

Bice, K.L., C.R. Scotese, D. Seidov, E.J. Barron, 2000: Quantifying the role of geographic change in Cenozoic ocean heat transport using uncoupled atmosphere and ocean models. Palaeogeography, Palaeoclimatology, Palaeoecology, *161*, 295-310.

Bigg, G.R.,1999: The oceans and climate. Cambridge University Press, Cambridge, 266 pp.

Blackmon, M.L., 1976: A climatological spectral study of the 500 mb geopotential height of the Northern Hemisphere. Journal of Atmospheric Sciences. *40*, 1410-1425.

Broccoli, A.J., S. Manabe, 1997: Mountains and midlatitude aridity. In: Ruddiman W.F. (Ed.): Tectonic uplift and climate change. Plenum Press, London, 89-121.

Broecker, W.S., 1989: The salinity contrast between the Atlantic and Pacific Ocean during glacial time. Paleoceanography, *4*, 207-212.

Brovkin, V., A. Ganopolski, Y. Svirezhev, 1997: A continuous climate-vegetation classification for use in climate-biosphere studies. Ecological modeling, *101*, 251-261.

Bruch, A.A., 1998: Palynologische Untersuchungen im Oligozän Sloweniens - Paläo-Umwelt und Paläoklima im Ostalpenraum. Tübinger Mirkopaläntologische Mitteilungen, *18*, 193 pp.

Carissimo, B.C., A.H. Oort, T.H. VonderHaar, 1985: Estimating the meridional energy transports in the atmosphere and ocean. Journal of Physical Oceanography, *15*, 82-91.

Carter, L.D., G.J. Brigham, L.Jr. Marincovich, V.L. Pease, J.W. Hillhouse, 1986: Late Cenozoic Arctic Ocean sea ice and terrestrial paleoclimate. Geology. *14 (8)*, 675-678.

Cerling, T.E., 1991: Carbon dioxide in the atmosphere: evidence from Cenozoic and Mesozoic paleosoils. American Journal of Science, *291*, 377-400.

Cerling, T.E. J.M. Harris, B.J. MacFadden, M.G. Leakey, J.Quade, V. Eisenmannm J.R. Ehleringer, 1997: Global vegetation change through the Miocene/Pliocene boundary. Nature, *389*, 153-159.

Chahine, M.T., 1992: The hydrological cycle and its influence on climate. Nature. *359*, 373-380.

Chandler, M., D. Rind, R. Thompson, 1994: Joint investigations of the middle Pliocene climate II: GISS GCM Northern Hemisphere results. Global and Planetary Change, *9*, 197-219.

Charnock, H., 1994: Air-sea exchanges and meridional fluxes. Malanotte-Rizzoli, P., A.R. Robinson (Eds.): Ocean processes in climate dynamics: Global and Mediterranean Examples. Nato ASI series, Series C. Mathematical and Physical Sciences, *Vol. 419*, Kluwer Academic Publishers, Dordrecht, 437 pp.

Claussen, M., 1993: Shift of biome patterns due to simulated climate variability and climate change. Technical Report *115*, Max-Planck-Institut für Meteorologie, Hamburg.

Collins, L.S., A.G. Coates, A.G. Berggren, M. P. Aubry, J. Zhang, 1996: The late Miocene Panama isthmian strait. Geology, *24*, 687-690.

Cohen-Solal, E., H. Le Treut, 1997: Role of the oceanic heat transport in climate dynamics. A sensitivity with an atmospheric general circulation model ocean heat transport GCM sensitivity studies. Tellus, *49A*, 371-387.

Cohen-Solal, E., H.Le Treut, 1999: Unstable behaviour of an upper ocean-atmosphere coupled model: role of atmospheric radiative processes and oceanic heat transport. Climate Dynamics, *15*, 895-908.

Covey, C., S.L. Thompson, 1989: Testing the effects of ocean heat transport on climate. Palaeogeography, Palaeoclimatology, Palaeoecology, *75*, 331-341.

Craig, H., L. I. Gordon, 1965: Deuterium and oxygen-18 variations in the ocean and the marine atmosphere. In: Stable isotopes in oceanographic studies and paleotemperatures, Spoleto: 1-122, Pisa, Consiglio Nazionale delle Richerche, Laboratorio di Geologica Nucleare.

Crowley, T.J, 1996: Pliocene climates: the nature of the problem. Marine Micropaleontology, *27*, 3-12.

Danabasoglu, G., 1998: On the wind-driven circulation of the uncoupled and coupled NCAR climate system ocean model. Journal of Climate, *11*, 1442-1454.

Dercourt, J., L.E. Ricou, B. Vrielynck, 1993: Atlas Tethys Paleoenvironmental Maps. Gauthier-Villars, Paris.

Ding, Z.L., S.F., Xiong, J.M. Sun, S.L. Yang, Z.Y. Gu, T.S. Liu, 1999: Pedostratigraphy and paleomagnetism of ca. 7.0 Ma eolian loess-red clay sequence at Lingtai, Loess Plateau, north-central China and the implications for paleomonsoon evolution. Palaeogeography, Palaeoclimatology, Palaeoecology, *152*, 49-66.

DKRZ Modellbetreuungsgruppe, 1994: The ECHAM3 Atmospheric General Circulation Model. Technical Report *6*, Deutsches Klimarechenzentrum, Hamburg, 182 pp.

DKRZ Modellbetreuungsgruppe, 1997: ECHAM4 - Workshop Hamburg, November 25th 1996. Deutsches Klimarechenzentrum, Hamburg,

Douville, H., J-F. Royer, J. Polcher, P. Cox, N. Gedney, D.B. Stephenson, P.J. Valdes, 2000: Impact of CO_2 doubling on the Asian summer monsoon: Robust versus model-dependent responses. Journal of the Meteorological Society of Japan, *78(4)*, 421-439.

Dutton, J.F., E.J. Barron, 1997: Miocene to present vegetation changes: A possible piece of the Cenozoic puzzle. Geology, *25(1)*, 39-41.

Dutton, J.F., E.J. Barron, 1996: Genesis sensitivity to changes in past vegetation. Palaeoclimates, *1*, 325-354.

Epstein, S., R. Buchsbaum, H.A. Lowenstam, H.C. Urey, 1953: Revised carbonate-water isotopic temperature scale. Geological Society of America Bulletin, *64*, 1315-1325.

Erez, J., B. Luz, 1983: Temperature control of oxygen-isotope fractionation of cultured planktonic foraminifera. Nature, *297*, 220-222.

Faure, G., 1986: Principles of isotope geology, 2nd ed., John Wiley & Sons, New York, 589 S.

Filippelli, G., 1997: Intensification of the Asian monsoon and a chemical weathering event in the late Miocene-early Pliocene: Implications for late Neogene climate change. Geology, *25(1)*, 27-30.

Flower, B. P., J. P. Kennett, 1994: The middle Miocene climatic transition: East Antarctic ice sheet development, deep ocean circulation, and global carbon cycling. Palaeogeography, Palaeoclimatology, Palaeoecology, *108*, 537-555.

Fluteau, F., G. Ramstein, J. Besse, 1999: Simulating the evolution of the Asian and African monsoons during the past 30 Myr using an atmospheric general circulation model. Journal of Geophysical Research. *104*, 11995-12018.

Fox, D.L., 2000: Growth increments in Gomphotherium tusks and implications for late Miocene climate change in North America. Palaeogeography, Palaeoclimatology, Palaeoecology, *156*, 327-348.

Gahagan, L.M., Scotese, C.R., Royer, J.-Y., Sandwell, D.T., Winn, J.K., Tomlins, R. L., Ross, M.I., Newman, J.S., Mueller, R.D., Mayes, C.L., Lawver, L.A., and Heubeck, C.E., 1988: Tectonic fabric map of the ocean basins from satellite altimetry data. Tectonophysics, *155*, 1-26.

Ganachaud, A., C. Wunsch, 2000: Improved estimates of global ocean circulation, heat transport and mixing from hydrographic data. Nature, *408*, 453-457.

Ganopolski, A., C. Kubatzki, M. Claussen, V. Brovkin, V. Petoukhov, 1998 a: The influence of vegetation-atmosphere-ocean interaction on climate during the Mid-Holocene. Science, *280*, 1916-1919.

Ganopolski, A. S. Rahmstorf, V. Petoukhov, M. Claussen, 1998 b: Simulation of modern and glacial climates with a coupled global model of intermediate complexity. Nature, *391*, 351-356.

Gebka, M., V. Mosbrugger, H.-D. Schilling, T. Utescher, 1999: Regional-scale palaeoclimate modelling on soft proxy-data basis–an example from the Upper Miocene of the Lower Rhine Embayment. Palaeogeography, Palaeoclimatology, Palaeoecology, *152*, 225-258.

Gleckler, P.J., D.A. Randall, G. Boer, R. Colman, M. Dix, V. Galin, M. Hefand, J. Kiehl, A. Kitoh, W. Lau, X.Y. Liang, V.Lykossov, B. McAvancey, K. Miyakoda, S. Planton, W. Stern, 1995: Cloud-radiative effects on implied oceanic energy transports as simulated by atmospheric general circulation models oceanic heat transport climate modelling GCM. Geophysical Research Letters, *22, no. 7*, 791-794.

Greenwood,D.R., S.L. Wing, 1995: Eocene continental climates and latitudinal temperature gradients. Geology, *23(11)*, 1044-1048.

Gregor H.-J., Unger H.J., 1988: Bemerkungen zur Geologie und Palontologie der Pflanzenfundstelle Aubenham bei Ampfing. Documenta naturae, *42*, 37-39 .

Gordon, C., C.Cooper, C.A.Senior, H.Banks, J.M.Gregory, T.C.Johns, FJ.F.B. Mitchell, R.A.Wood, 2000: The simulation of SST, sea ice extents and ocean heat transports in a version of the Hadley Center coupled model without flux adjustments climate modelling HadCM evaluation CGCM. Climate Dynamics,*16*, 147-168.

Hall, N.M.J., B.J. Hoskins, P.J. Valdes, C.A. Senior, 1994: Storm tracks in a high resolution GCM with doubled carbon dioxide. Quarterly Journal of the Royal Meteorological Society, *120*, 1209-1230.

Harrison, D.E., 1989: On climatological monthly mean wind stress and wind stress curl fields over the world ocean. Journal of Climate, *2*, 57-70.

Hartmann, D.L., 1994: Global physical climatology. Academic Press, San Diego, 411 pp.

Hastenrath, S., 1982: On Meridional Heat Transports in the World Ocean. Journal of Physical Oceanography, *12*, 922-927.

Haug, G. H., R. Tiedemann, 1998: Effect of the formation of the Isthmus of Panama on Atlantic Ocean thermohaline circulation. Nature, *393*, 673-676.

Hay, W.W., 1996: Tectonics and climate. Geologische Rundschau, *85*, 409-437.

Haywood, A.M., P.J. Valdes, B.W. Sellwood, 2000: Global scale palaeoclimate reconstruction of the middle Pliocene climate using the UKMO GCM: initial results. Global and Planetary Change, *25*, 239-256.

Hellermann, S., M. Rosenstein, 1983: Normal monthly wind stress over the world ocean with error estimates. Journal of Physical Oceanography, 13, 1093-1104.

Hemleben, C., M. Spindler, and O.R. Anderson,, 1989: Modern Planktonic Foraminifera. Springer-Verlag, New York, 363 pp.

Herterich, K., A. Berger, 1993: Modelling the last ice-age cycle with 2-D climate models. Palaeogeography, Palaeoclimatology, Palaeoecology, *103*, 107-116.

Holton, J.R., 1992: An introduction to dynamic meteorology. Academic Press, 3rd ed., San Diego, 511 pp.

Houghton, J.T., L.G. Meira Filho, B.A. Callander, N. Harris, A. Kattenberg, K. Maskell, 1995: Climate Change 1995. Cambridge University Press, Cambridge, 572 pp.

Hsiung, J., 1985: Estimates of global oceanic meridional heat transport. Journal of Physical Oceanography, *15*, 1405 - 1413.

Isern, A.R., J.A., McKenzie, D.A. Feary, 1996: The role of sea-surface temperature as a control on carbonate platform development in the western Coral Sea. Palaeogeography, Palaeoclimatology, Palaeoecology, *124*, 247-272.

Kennett, J, 1993: Neogene climatic evolution of the Antarctic. Conference on palaeoclimate and evolution with emphasis on human origins, May 1993, Airlie Conference Centre, Virginia, Abstract.

Kennett, J.P., 1995: A review of polar climatic evolution during the Neogene, based on the marine sediment record. In: Vrba, E.S., G.H. Denton, T.C. Partridge, L.H. Burckle (Eds.): Paleoclimate and evolution, with emphasis on human origins, Yale University Press, London, 547 pp.

Kubatzki, C., M. Montoya, S. Rahmstorf, A. Ganopolski, M. Claussen, 2000: Comparison of the last interglacial climate simulated by a coupled global model of intermediate complexity and AOGCM. Climate Dynamics, *16*, 799-814.

Kutzbach, J.E., G. Bonan, J. Foley, S.P. Harrison, 1996: Vegetation and soil feedbacks on the response of the African monsoon to orbital forcing in the early to middle Holocene. Nature, *384*, 623-626.

Kutzbach, J., R. Gallimore, S., Harrison, P. Behling, R. Selin, F., Laarif, 1998: Climate and biome simulations for the past 21000 years climate modelling palaeo Holocene biome LGM. Quarternary Science Reviews, *17*,473-506.

Kutzbach, J.R., P.J. Guetter, W.F. Ruddiman, W.L. Prell, 1989: Sensitivity of climate to late Cenozoic uplift in southern Asia and the American West. Journal of Geophysical Research, *94*, 18393-18407

Latif, M., J.D. Neelin, 1994: El Niño/Southern Oscillation. Technical Report *129*, Max-Planck-Institut für Meteorologie, Hamburg, 24 pp.

Lee and Lawver 1995, 1995: Cenozoic plate reconstruction of Southeast Asia. Tectonophysics, *251*, 85-138.

Leetmaa, A., A. Bunker, 1978: Updated charts of the mean annual wind stress, convergences in the Ekman layers, and Sverdrup transports in the North Atlantic. Journal of Marine Research, *36(2)*, 311-322.

Lorenz, S., B. Grieger, P. Helbig, K. Herterich, 1996: Investigating the sensitivity of the atmospheric general circulation model ECHAM3 to paleoclimatic boundary conditions. Geologische Rundschau, *85*, no. 3, 513-524.

Lunkeit, F., K. Fraedrich, S.E. Bauer, 1998: Storm tracks in a warmer climate: sensitivity studies with an amplified global circulation model. Climate Dynamics, *14*, 813-826.

Markwick, P.J., 1998: Fossil crocodilians as indicators of late Cretaceous and Cenozoic climates: implications for using palaeontological data in reconstructing palaeoclimate. Palaeogeography, Palaeoclimatology, Palaeoecology, *137*, 205-271.

Mächel, H., A. Kapala, H. Flohn, 1998: Behaviour of the centers of action above the Atlantic since 1881. Part I: Characteristics of seasonal and interannual variability. International Journal of Climatology, *18*, 1-22.

Mai, H.D., 1995: Tertiäre Vegetationsgeschichte Europas: Methoden und Ergebnisse. Jena, G. Fischer, 691 pp.

Maier-Raimer, E., U. Mikolajewicz, T. Crowley, 1990: Ocean general circulation model sensitivity experiment with an open central American isthmus. Paleoceanopgraphy, *5, no. 3*, 349-366.

Martin, H.A. 1998: Tertiary climatic evolution and the development of aridity in Australia. Proceedings of the Linnean Society of New South Wales, *119*, 115-136.

McGuffie, K., A. Henderson-Sellers, N. Holbrook, Z., Kothavala, O. Balchova, J., Hoekstra, 1999: Assessing simulations of daily temperature and precipitation variability with global climate models for present and enhanced greenhouse climates. International Journal of Climatology, *19*, 1-26.

Matthews, R.K., R.Z. Poore, 1980: Tertiary δ^{18}O record and glacio-eustatic sea-level fluctuations. Geology, *8(10)*, 501-504.

Mikolajewicz, U. , T.J. Crowley, 1997:Response of a coupled ocean/energy balance model to restricted flow through the central American isthmus. Paleoceanography, *12, no. 3*, 429-441.

Mikolajewizc, U., R. Voss, 2000: The role of the individual air-sea flux components. Climate Dynamics, *16*, 627-642.

Mikolajewicz, U., E. Maier-Reimer,T.J. Crowley, K.J. Kim 1993: Effect of Drake and Panamanian gateways on the circulation of an ocean model. Paleoceanography, *8, no. 4*, 409-426.

Miller, K.G., J.D., Wright, R.G. Fairbanks, 1991: Unlocking the ice house: Oligocene-Miocene oxygen isotopes, eustasy, and margin erosion. Journal of Geophysical Research. *96*, 6829-6848.

Molnar, P., P. England, J. Martinod, 1993: Mantle Dynamics, uplift of the Tibetean Plateau and the Indian monsoon. Reviews of Geophysics, *31, 4*, 357-396.

Montoya, M.L., 1999: Climate simulations for the last interglacial period by means of climate models of different complexity. Dissertation, Fachbereich Geowissenschaften, Universität Hamburg, 126 pp.

Mosbrugger, V., H.-D. Schilling, 1992: Terrestrial palaeoclimatology in the Tertiary: a methodological critique. Palaeogeography, Palaeoclimatology, Palaeoecology, *99*, 17-29.

Mosbrugger, V., T. Utescher, 1997: The coexistence approach - a method for quantitative reconstructions of Tertiary terrestrial palaeoclimate data using plant fossils. Palaeogeography, Palaeoclimatology, Palaeoecology, *134*, 61-86.

Mote, P., A. O'Neill, (Eds.) 2000: Numerical modeling of the global atmosphere in the climate system. NATO Science Series, Series C: Mathematical and Physical Sciences, London, 550, 517 pp.

Nelson, R.E., L.D. Carter, 1985: Pollen analysis of a late Pliocene and early Pleistocene section from the Gubik Formation of Arctic Alaska. Quarternary Research, *24(3)*, 295-306.

Niebler, H.S., 1995: Rekonstruktion von Palo-Umweltparametern anhand von stabilen Isotopen und Faunen-Vergesellschaftungen planktischer Foraminiferen im Südatlantik. Berichte zur Polarforschung, *167*, 198 pp.

Nikolaev, S. D., N. S. Oskina, N.,S. Blyum, N. V. Bubenshchikova, 1998: Neogene-Quarternary variations of the 'Pole-Equator' temperature gradient of the surface oceanic waters in the North Atlantic and North Pacific. Global and Planetary Change, *8*, 85-111.

Norris, R.D., R.M. Corfield, J.E. Cartlidge, 1994: Evolutionary ecology of Globorotalia (Globoconella) (planktic foraminifera). Marine Micropaleontology, *23*, 121-145.

Osborn, T.J., K.R. Briffa, S.F.B. Tett, P.D. Jones, R.M. Trigo, 1999: Evaluation of the North Atlantic Oscillation as simulated by a coupled climate model. Climate Dynamics, *15*, 685-702.

Paeth, H., A., Hense, R. Glowienka-Hense, R. Voss, 1999: The North Atlantic Oscillation as an indicator for greenhouse-gas induced regional climate change. Climate Dynamics, *15*, 953-960.

Pagani, M., M.A. Arthur, K.H. Freeman, 1999: Miocene evolution of atmospheric carbon dioxide. Paleoceanography, *14 (3)*, 273-292.

Partridge, T.C., G.C. Bond, C.J.H. Hartnady, P.B. deMenocal, W.F. Ruddiman 1995: Climatic effects of the Late Neogene tectonism and volcanism. In: Vrba, E.S., G.H. Denton, T.C. Partridge, L.H. Burckle (Eds.): Paleoclimate and evolution with emphasis on human origins. Yale University Press, London, 547 pp.

Pazzaglia, F.J., R.A.J. Robinson, A. Traverse, 1997: Palynology of the Bryn Mawr Formation (Miocene): insights on the age and genesis of Middle Atlantic margin fluvial deposits. Sedimentary Geology, *108*, 19-44.

Petoukhov, V., A. Ganopolski, V. Brovkin, M. Claussen, A. Eliseev, C. Kubatzki, S. Rahmstorf, 2000: CLIMBER-2: a climate system model of intermediate complexity. Part I: model description and performance for present climate CLIMBER climate modelling GCM biosphere validation. Climate Dynamics, *16*,1-17.

Prentice, M.L., R.K. Matthews, 1991: Tertiary ice sheet dynamics: The snow gun hypothesis. Journal of geophysical Research, *95*, 6811-6827.

Prell, W.L., J.E. Kutzbach, 1992: Sensitivity of the Indian monsoon to forcing parameters and implications for its evolution. Nature, *360*, 647-652.

Rahmstorf, S., 1995: Bifurcation of the Atlantic thermohaline circulation in response to changes in the hydrological cycle. Nature, *378*, 145-149.

Rahmstorf, S., A. Ganopolski, 1999: Long-term warming scenarios computed with an efficient coupled climate model. Climatic Change, *43*, 353-367.

Ramstein, G., F. Fluteau, J. Besse, S. Joussaume, 1997: Effect of orogeny, plate motion and land-sea distribution on Eurasian climate change over past 30 million years. Nature, *386*, 788-795.

Raymo, M.E., D. Rind, W.F. Ruddiman, 1990: Climatic effects of reduced arctic sea ice limits in GISS II general circulation model. Paleoceanography, *5 no. 3*, 367-382.

Reynold, R.W., 1993: Impact of Mount Pinatubo aerosols on satellite-derived Sea Surface Temperatures. Journal of Climate, *6*, 768-774.

Reynolds, R.W. amd D.C. Marsico, 1993: An improved real-time global sea surface temperature analysis. Journal of Climate, *6*, 114-119.

Reynold, R.W. and T.M. Smith, 1994: Improved global sea surface temperature analysis using optimum interpolation. Journal of Climate, *7*, 929.948.

Rind, D., M., Chandler, 1991: Increased ocean heat transports and warmer climates. Journal of Geophysical Research, *96*, 7437-7461.

Rind, D., G. Russel, W.F. Ruddiman, 1997: The effects of uplift on ocean-atmosphere circulation. In: Ruddiman, W.F. (Ed.): Tectonic Uplift and climate change. London, Plenum Press, 124-147.

Roeckner, E., K. Arpe, L. Bengtsson, M. Christoph, M. Claussen, L. Dümenil, M. Esch, M. Giorgetta, U. Schlese, U. Schulzweida 1996: The atmospheric general circulation model ECHAM-4: Model description and simulation of present-day climate. Report *218*, Max-Planck-Institut für Meteorologie, Hamburg, 90 pp.

Roeckner, E., J.M. Oberhuber, A. Bacher, M. Christoph, I. Kirchner, 1993: ENSO variability and atmospheric response in a global coupled atmosphere-ocean GCM, Climate Dynamics, *12*, 737-754.

Roeckner, E., K. Arpe, L. Bengtsson, S. Brinkop, L. Dümenil, M. Esch, E. Kirk, F. Lunkeit, M. Ponater, B. Rockel, R. Sausen, U. Schlese, S. Schubert, M. Windelband, 1992: Simulation of the present-day climate with the ECHAM model: impact of model physics and resolution. Report *93*, Max-Planck-Institut für Meteorologie, Hamburg, 171 pp.

Roemmich, D., Wunsch, C., 1985: Two transatlantic sections: meridional circulation and heat flux in the subtropical North Atlatnic Ocean. Deep Sea Research, *32*, 629-664.

Rögl, F., 1998: Palaeogeographic considerations for Mediterranean and Paratethys seaways (Oligocene to Miocene). Annalen des Naturhistorischen Museums von Wien, *99A*, 279-310.

Rohling,E.J., S.Cooke, 1999: Stable oxygen and carbon isotopes in foraminiferal carbonate shells. In: Barun, K., S. Gupta (Eds.): Modern foraminifera. Kluwer Academic Publishers, 351 pp.

Rogers, J.C., 1997: North Atlantic storm track variability and its association to the North Atlantic oscillation and climate variability of northern Europe. Journal of Climate, *10*, 1635-1647.

Ruddiman,W.F., J.E. Kutzbach, 1989: Forcing of late Cenozoic northern hemisphere climate by uplift in southern Asia and the American West. Journal of Geophysical Research, *94*, 18409-18427.

Rye D. M., M.A. Sommer, 1980: Reconstructing Paleotemperature and paleosalinity regimes with oxygen isotopes, In: Rhoads, D., R. Lutz (Eds.): Skeletal growth of aquatic organisms: Plenum Press, New York, 750 S.

Savin, S., M., L. Abel, E. Barrera, D. Hodell, G. Keller, J. P. Kennett, J. Killingley, M. Murphy, E. Vincent, 1985: The evolution of Miocene surface and near-surface marine temperatures: oxygen isotopic evidence. Geological Society of America, Memoir *163*, 49-73.

Sachse, M., B.A.R. Mohr, 1996. Eine obermiozäne Makro- und Mikroflora aus Südkreta (Griechenland), und deren paloklimatische Interpretation. - Vorläufige Betrachtungen Neues Jahrbuch Geologischer und Paläontologischer Abhandlungen, *200, 1/2*, 149-182.

Schoell, M, S. Schouten, J.S. Sinninghe-Damste, J.W. de-Leeuw, R.E. Summons, 1994: A molecular organic carbon isotope record of Miocene climate changes. Science, *263*, 1122-1125.

Schubert, M., J. Perlwitz, R. Blender, K. Fraedrich, F. Lunkeit, 1998: North Atlantic cyclones in CO_2-induced warm climate simulations: frequency, intensity, and tracks. Climate Dynamics, *14*, 827-837.

Sellwood, B.W., P.J. Valdes, G.D. Price, 2000: Geological evaluation of multiple general circulation model simulations of Late Jurassic palaeoclimate. Palaeogeography, Palaeoclimatology, Palaeoecology, *156*, 147-160.

Sellwood, B.W., G.D. Price, P.J. Valdes, 1994: Cooler estimates of Cretaceous temperature. Nature,*370*, 453-455.

Sloan, L.C., M. Huber, T.J. Crowley, J.O. Sewall, S. Baum, 2001: Effect of sea surface temperature configuration on model simulations of "equable" climate in the Early Eocene. Palaeogeography, Palaeoclimatology, Palaeoecology, *167*, 321-335.

Sluiter, I.R.K., A.P. Kershaw, G.R. Holdgate, D. Bulman, 1995: Biogeography, ecological and stratigraphic relationships of the Miocene brown coal floras, Latrobe Valley, Victoria, Australia. International Journal of Coal Geology, *28*, 277-302.

Slutz, R.J., S. J. Lubker, J. D. Hiscox, S. D. Woodruff, R. L. Jenne, D. H. Joseph, P. M. Steuer, J. D. Elms, 1985: Comprehensive ocean-atmosphere data set: Release 1. NOAA Environmental Research Laboratory, Boulder, CO, 268 pp.

Steininger, F.F., F. Rögl, 1984: Paleogeography and palinspastic reconstruction of the Neogene of the Mediterranean and Paratethys. In: Dixon, J.E., A.H.F. Robertson (Eds.): The geological evolution of the Eastern Mediterranean. Geological Society, Blackwell Scientific Publications, Oxford.

Stocker, T.F., D.G. Wright, L.A. Mysak, 1992: A zonally averaged, coupled ocean-atmosphere model for paleoclimate studies. Journal of Climate, *5*, 773-797.

Stocker, T.F., 1999: Abrupt climate changes: from the past to the future - a review. International Journal of Earth Sciences, *88*, 365-374.

Stommel, H., P.P. Niiler, D. Anati, 1978: Dynamic topography and recirculation of the North Atlantic. Journal of Marine Research, *36*, 449-468.

Stouffer, R.J., S. Manabe, 1999: Response of a coupled ocean-atmosphere model to increasing atmospheric carbon dioxide: sensitivity to the rate of increase. Journal of Climate, *12*, 2224-2237.

Thiede, J., A. Winkler, T. Wolf-Welling, O. Eldholm, A. M. Myhre, K.-H. Baumann, R. Henrich, R. Stein, 1998: Late Cenozoic history of the Polar North Atlantic: results from ocean drilling. Quarternary Science, *17*, 185-208.

Timmermann, A., M. Latif, A. Grötzner, R. Voss, 1999: Modes of climate variability as simulated by a coupled general circulation model. Part I: ENSO-like climate variability and its low-frequency modulation. Climate Dynamics, *15*, 605-618.

Townsend, T., H.E. Hurlburt, P.J. Hogan, 2000: Modeled sverdrup flow in the North Atlantic from 11 different wind stress climatologies. Dynamics of Atmospheres and Oceans, *32*, 373-417.

Trenberth, K.E., A. Solomon, 1994: The global heat balance: heat transports in the atmosphere and ocean. Climate Dynamics, *10*, 107-143.

Trenberth, K.E., W.G. Large, J.G. Olson, 1990: The mean annual cycle on global ocean wind stress. Journal of Physical Oceanography, *20*, 1742-1760.

Tsuchi, R., 1997: Marine climatic responses to Neogene tectonics of the pacific ocean seaways. Tectonophysics, *281*, 113.124.

Upchurch, G.R. Jr., B.L. Otto-Bliesner, C.R. Scotese, 1999: Terrestrial vegetation and its effect on climate during the latest Cretaceous. Geological Society of America, Special Paper *332*, 407-426.

Upchurch, G.R. Jr., B.L. Otto-Bliesner, C. Scotese, 1998: Vegetation-atmosphere interactions and their role in global warming during the latest Cretaceous. Philosophical transactions of the Royal Society of London/B., *353*, 97-112.

Utescher, T., M. Gebka, V. Mosbrugger, H.-D. Schilling, A.R. Ashraf, 1997: Regional palaeontological-meteorological palaeoclimate reconstruction of the Neogene Lower Rhine Embayment. Proceedings 4th, EPPC, *58*, 263-271.

Utescher, T., Mosbrugger, V., Ashraf, A.R., 2000: Terrestrial climate evolution in northwest Germany over the last 25 Million years. Palaios, *15(5)*, 430-449.

van Dam, J.A., G.J. Weltje, 1999: Reconstruction of the Late Miocene climate of Spain using rodent palaeocommunity successions: an application of end-member modelling. Palaeogeography, Palaeoclimatology, palaeoecology, *151*, 267-305.

Van Der Burgh, J., H. Visscher, D.F. Dilcher, W.M. Kürschner, 1993: Paleoatmospheric signatures in Neogene fossil leaves. Science, *260*, 1788-1790.

von Storch, H., E. Zorita, U. Cubasch, 1993: Downscaling of global climate change estimates to regional scales: An application to Iberian rainfall in wintertime. Journal of Climate, *6*, 1161-1171.

von Storch, H., 1995: Inconsistencies at the interface of climate impact studies and global climate research. Meteorologische Zeitschrift, *4 NF*, 72-80.

von Storch, H., F.W. Zwiers, 1999: Statistical Analysis in Climate Research. Cambridge University Press, Cambridge, 484 pp.

Wang, J., Y.J. Wang, Z.C. Liu, J.Q. Li, P.Xi, 1999: Cenozoic environmental evolution of the Quaidam Basin and its implications for the uplift of the Tibetan Plateau and the drying of central Asia. Palaeogeography, Palaeoclimatology, Palaeoecology, *152*, 37-47.

Weaver, A.F., C.M. Bitz, A.F. Fanning, M.M. Holland, 1999: Thermohaline circulation: High-Latitude phenomena and the difference between the Pacific and Atlantic. Annual Reviews of Earth Planetary Sciences, *27*, 231-285.

Wefer, G., 1985: Die Verteilung stabiler Isotope in Kalkschalen mariner Organismen. Geologisches Jahrbuch Reihe A, *82*.

White, J.M., T.A. Ager, D.P. Adam, E.B. Leopold, G.Liu, H. Jette, C.E. Schweger, 1997: An 18 million year record of vegetation and climate change in northwestern Canada and Alaska: tectonic and global climatic correlates. Palaeogeography, Palaeoclimatology, Palaeoecology, *130*, 293-306.

Wolf, T. C. W., J. Thiede, 1991: History of terrigenous sedimentation during the past 10 m.y. in the North Atlantic (ODP Legs 104 and 105 and DSDP Leg 81). Marine Geology, *101*, 83-102.

Wolfe, J.A., 1994a: Tertiary climatic changes at middle latitudes of wester North America. Palaeogeography, Palaeoclimatology, Palaeoecology, *108*, 196-206.

Wolfe, J.A., 1994b: An analysis of Neocene climates in Beringia. Paleogeography, Paleoclimatology, Paleoecology, *108*, 207-216.

Wolfe, J.A., 1995: Paleoclimatic estimates from tertiary leaf assemblages. Annual Review of Earth Planetary Sciences, *23*, 119-142.

Woodruff, S. D., S. J. Lubker, K. Wolter, S. J. Woley and J. D. Elms, 1993: Comprehensive Ocean-Atmosphere Data Set (COADS) Release 1a: 1980-1992. Earth System Monitor, *4, no. 1*, September 1993, NOAA.

Woodruff, F., S.M. Savin, 1989: Miocene deepwater oceanography. Palaeoceanography. *4*, 87-140.

Woodruff, F., S. M. Savin, R. G. Douglas, 1981: Miocene stable isotope Record: a detailed deep pacific ocean study and its paleoclimatic implications. Science, *212*, 665 - 668.

Working Group I of the IPCC - Intergovernmental Panel on Climate Change, 2001: Summary for Policymakers of the Third Assessment Report "Climate Change 2001: The scientific basis". Shanghai, 20 January 2001, *http://www.meto.gov.uk/sec5/CR_div/ipcc/wg1/.*

Wright, J.D., K.G. Miller, 1996: Control of North Atlantic Deep Water circulation by the Greenland-Scotland ridge. Paleoceanography, *11 (2)*, 157-170.

Zachos, J.C., L.D. Stott, K.C. Lohmann, 1994: Evolution of early Cenozoic marine temperatures. Paleoceanography, *9(2)*, 353-387.

Zahn and Mix, 1991: Benthic foraminiferal δ^{18}O in the ocean's temperature-salinity-density field: constraints on ice age thermohaline circulation. Paleoceanography, *6(1)*, 1-20.

Appendix A

Marine carbon isotope data of the Tortonian

Table A.1: *Short list of averaged planktonic and benthic $\delta^{18}O$ data in per mil compiled by Geiger pers. comm. 1998 plus own complements as represented in fig. 2.2. Corresponding references are listed below.*

borehole	planktonic δ^{18}O	benthic δ^{18}O	references
16	0.92		Kennett 1995.
62.1	-1.24	1.66	Kennett 1995, Woodruff and Savin 1989
77B	-1.19	2.03	Kennett 1995, Woodruff and Savin 1989
116		2.07	Woodruff and Savin 1989
158	-1.54	1.63	Kennett 1995, Woodruff and Savin 1989
167		2.67	Woodruff and Savin 1989
206		2.35	Woodruff and Savin 1989
208	-0.2		Kennett 1995
214	-0.57	2.45	Kennett 1995, Woodruff and Savin 1989
216	-0.333	3.041	Seto 1995
237	-0.56	2.41	Kennett 1995, Woodruff and Savin 1989
238	-0.75	2.55	Kennett 1995, Woodruff and Savin 1989
249		2.46	Woodruff and Savin 1989
253	1.24	3.343	Seto 1995

borehole	planktonic δ^{18}O	benthic δ^{18}O	references
289	-1.26	2.26	Kennett 1995, Woodruff and Savin 1989
292	-1.27	2.56	Kennett 1995, Woodruff and Savin 1989
296	-0.64	2.0	Kennett 1995, Woodruff and Savin 1989
310	-1.13	2.24	Kennett 1995, Woodruff and Savin 1989
317B	-0.62	2.33	Kennett 1995, Woodruff and Savin 1989
319	-0.35	2.82	Kennett 1995, Woodruff and Savin 1989
334		2.11	Woodruff and Savin 1989
357		2.25	Woodruff and Savin 1989
360	-0.34	2.276	Kennett 1995, Wright et al. 1991
362	-0.66		Kennett 1995
366		2.57	Seto 1995
372	-0.72		Grazzini 1978
408		1.89	Woodruff and Savin 1989
502	-1.96	1.72	Keigwin 1982
503	-2.53	1.81	Keigwin 1982
516A	0.62	2.42	Kennett 1995, Woodruff and Savin 1989
519		2.333	Seto 1995
521A		2.39	Woodruff and Savin 1989
525	0.39	2.998	Seto 1995
526A	0.44	2.41	Kennett 1995, Woodruff and Savin 1989
527		3.165	Seto 1995
552A		2.33	Woodruff and Savin 1989
558		2.11	Woodruff and Savin 1989
563		1.956	Wright et al. 1991
574		2.46	Woodruff and Savin 1989
588		2.02	Woodruff and Savin 1989
590B	-0.52	1.71	Kennett 1983, Woodruff and Savin 1989
591B		2.16	Woodruff and Savin 1989
608		2.01	Wright et al. 1991
667		2.34	Woodruff and Savin 1989

borehole/location	planktonic δ^{18}O	benthic δ^{18}O	references
704	1.742	2.829	Mueller et al. 1991, Seto 1995
709		3.17	Seto 1995
714	-1.985	2.64	Seto 1995
744		3.131	Seto 1995
751		3.489	Seto 1995
752		1.84	Seto 1995
754		2.078	Seto 1995
756		2.523	Seto 1995
757		2.825	Seto 1995
758	-1.71	2.535	Seto 1995
811	-0.5	1.73	Isern et al. 1996
Monte del Casino/ Italy	-0.1		Kouwenhoven et al. 1999

References:

Grazzini, C.V., 1978: Miocene and Pliocene oxygen and carbon isotopic changes at DSDP sites 372, 374, and 375; implications for the pre-Messinian history of the Mediterranean. Initial Reports of the Deep Sea Drilling Project, *42*, Part1, 829-836.

Isern, A.R., J.A. McKenzie, D.A. Feary,, 1996: The role of sea-surface temperature as a control on carbonate platform development in the western Coral Sea. Palaeogeography, Palaeoclimatology, Palaeoecology, *124*, 247-272.

Keigwin, L.D. Jr., 1982: Stable isotope stratigraphy and paleoceanography of sites 502 and 503. Initial Reports of the Deep Sea Drilling Project, *68*, 445-453.

Kennett, J.P., 1983: Miocene to early Pliocene oxygen and carbon isotope stratigraphy in the southwest Pacific, Deep Sea Drilling Project Leg 90. Initial Reports of the Deep Sea Drilling Project, *90*, Part 2, 1383-1411.

Kennett, J.P., 1995: The Miocene ocean: paleoceanography and biogeography. Geological Society of America, Boulder, Colorado.

Kouwenhoven, T.J., M.S. Seidenkrantz, G.J. van-der-Zwaan, 1999: Deep-water changes; the near-synchronous disappearance of a group of benthic Foraminifera from the late Miocene Mediterranean. Palaeogeography, Palaeoclimatology, Palaeoecology, *152*, 259-281.

Mueller, P.W., D.A. Hodell, P.F. Ciesielski, 1991: Late Miocene to earliest Pliocene (9.8-4.5 Ma) paleoceanography of the subantarctic southeast Atlantic; stable isotopic, sedimentologic, and microfossil evidence. Proceedings of the Ocean Drilling Program, Scientific Results, *114*, 459-474.

Seto, K., 1995: Carbonate and oxygen isotopic paleoceanography of the Indian and south Atlantic oceans; paleoclimate and paleo-ocean circulation. Journal of Science of the Hiroshima University, Series C: Geology and Mineralogy, *10*, 393-485.

Woodruff, F., S.M. Savin, 1989: Miocene deepwater oceanography. Paleoceanography, *4*, 87-140.

Wright, J.D., K.G. Miller, R.G. Fairbanks, 1991: Evolution of modern deepwater circulation; evidence from the late Miocene southern ocean. Paleoceanography, *6*, 275-290.

Appendix B

ECHAM4/ML - Standard Tortonian run

Figures B.1 to B.6 show the summer, winter, and annual means of the standard Tortonian run with regard to surface temperature, total precipitation, precipitation minus evaporation, surface pressure, 10 m height wind field, and the zonal wind in 200 hPa height.

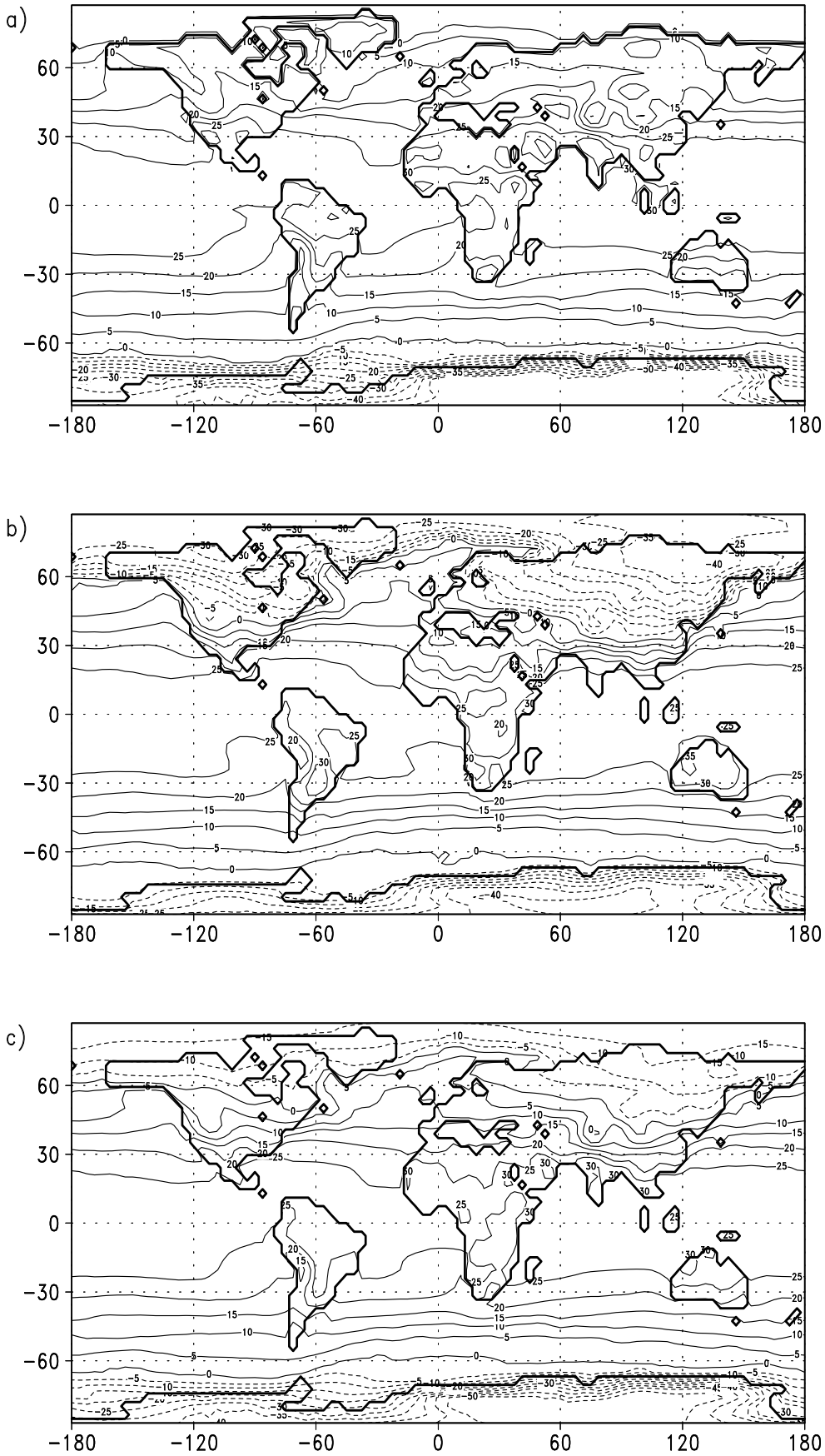

Figure B.1: *Surface temperature of Tortonian run in ° C for a) JJA b) DJF, and c) the year. Contour interval is 5° C*

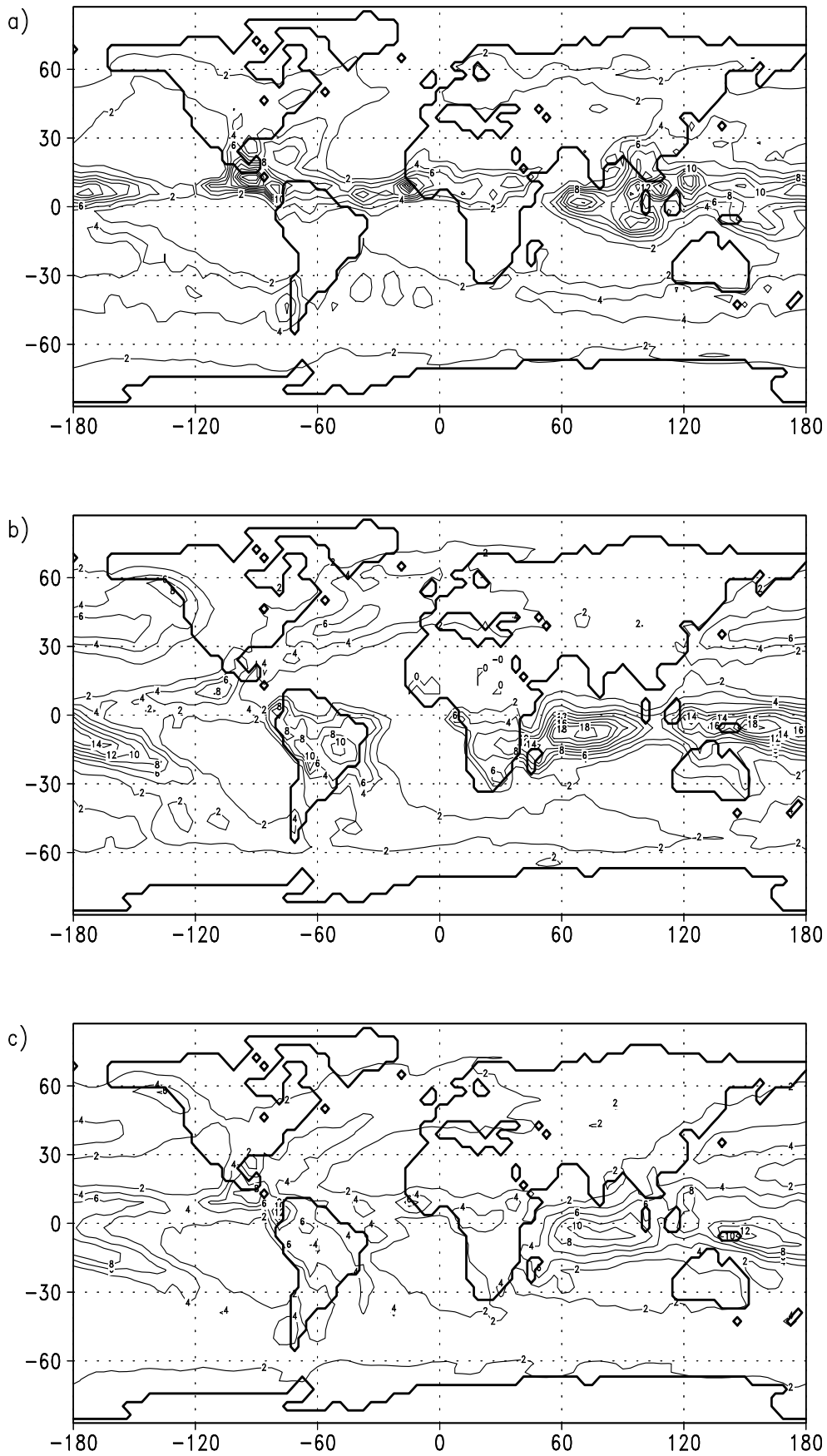

Figure B.2: *Total precipitation for Tortonian run in mm/d. a) JJA b) DJF, and c) the year. Contour interval is 2 mm/d.*

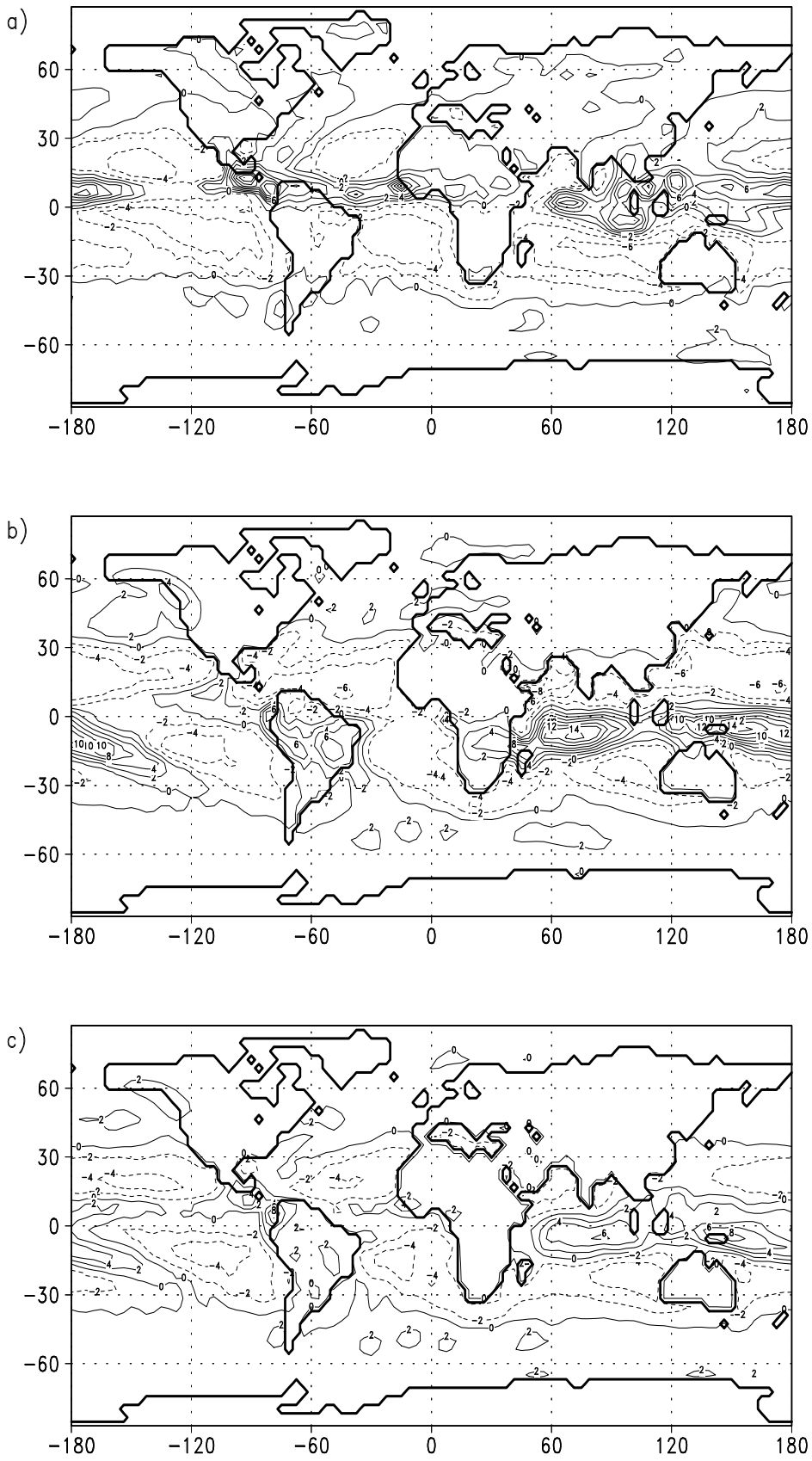

Figure B.3: *Precipitation minus evaporation for Tortonian run in mm/d. a) JJA b) DJF, and c) the year. Contour interval is 2 mm/d.*

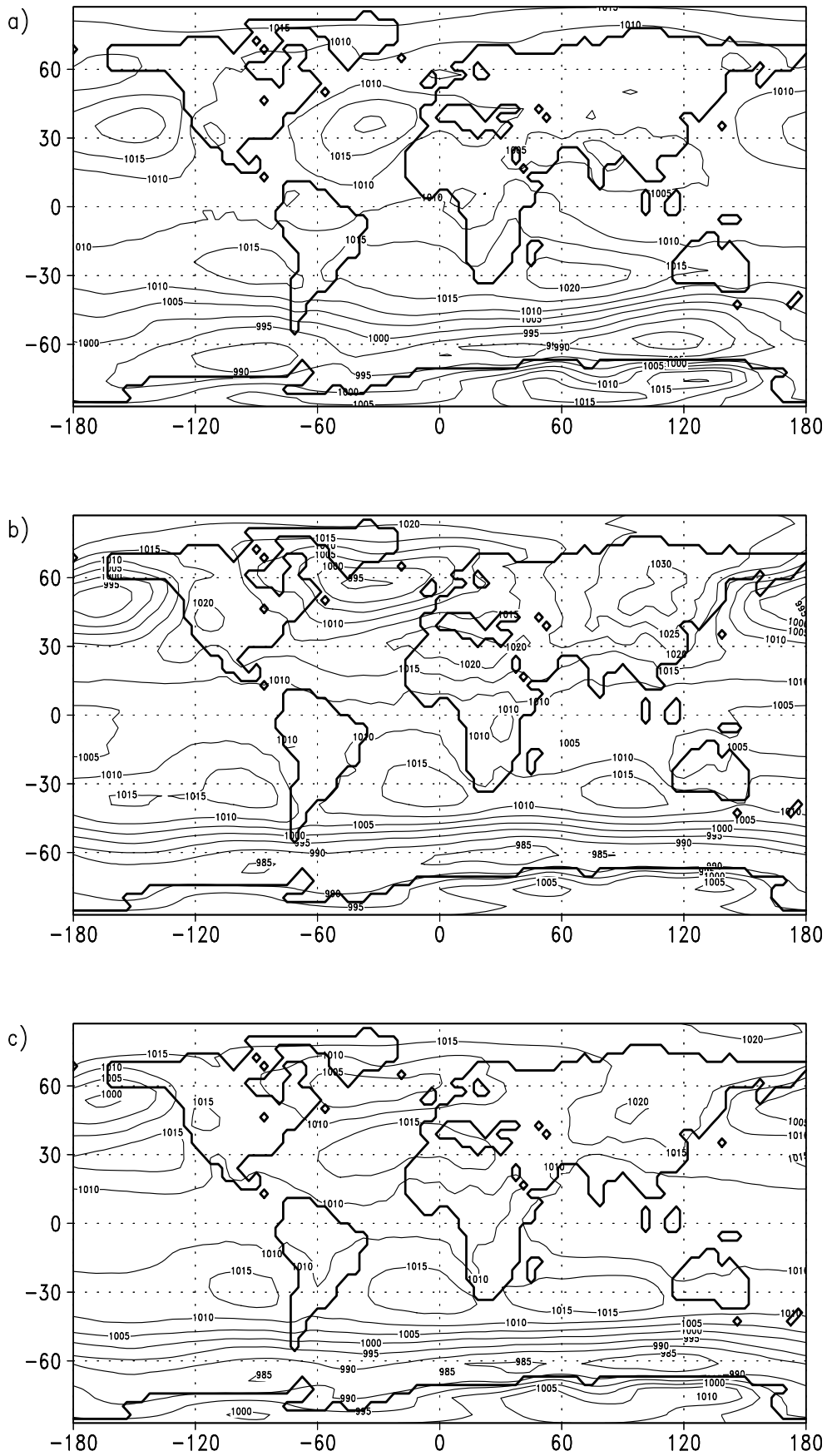

Figure B.4: *Surface pressure of Tortonian run in hPa for a) JJA b) DJF, and c) the year. Contour interval is 5 hPa.*

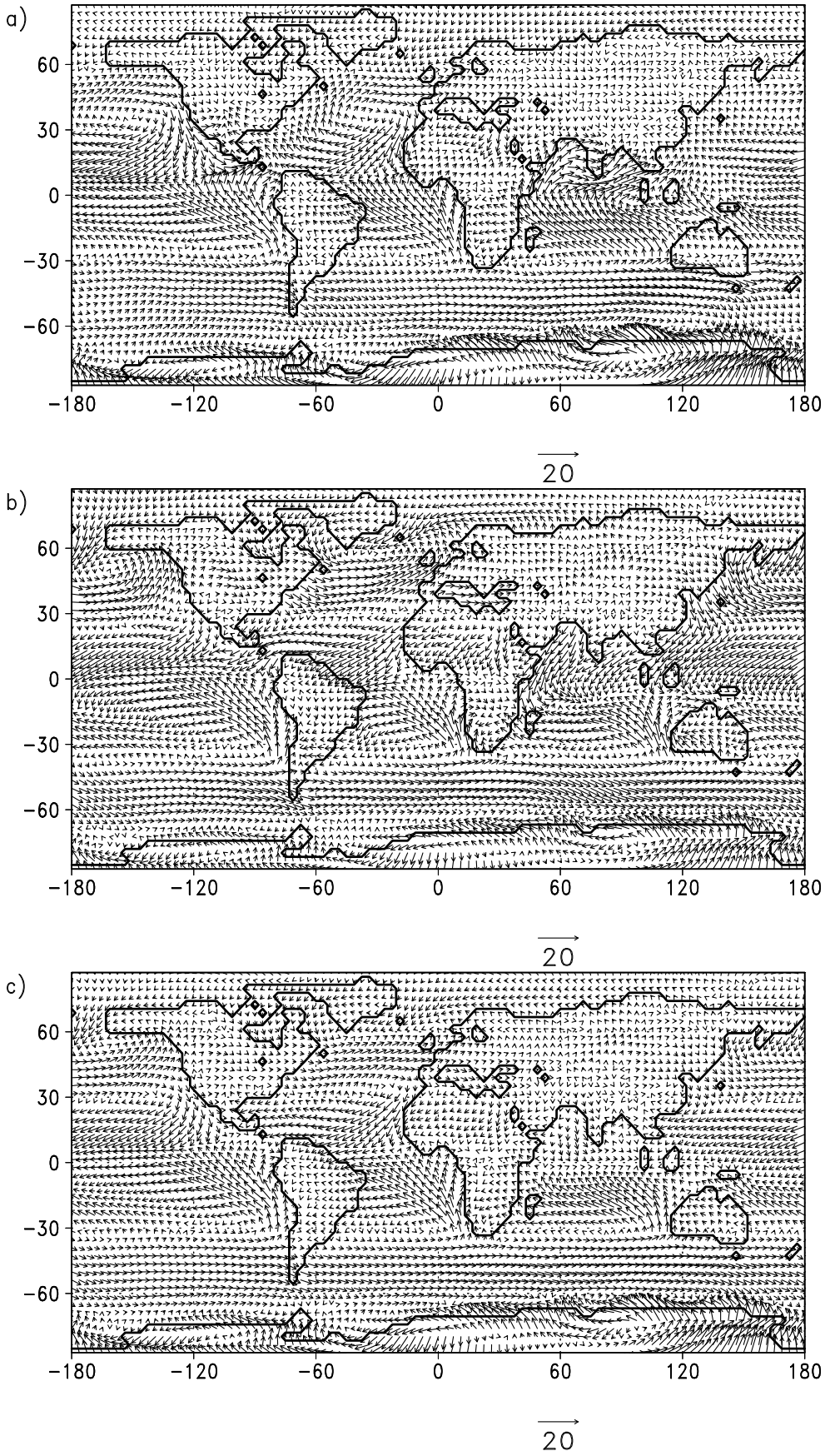

Figure B.5: *Wind field of Tortonian run in 10 m height for a) JJA b) DJF, and c) the year. Reference arrow indicate 20 m/s.*

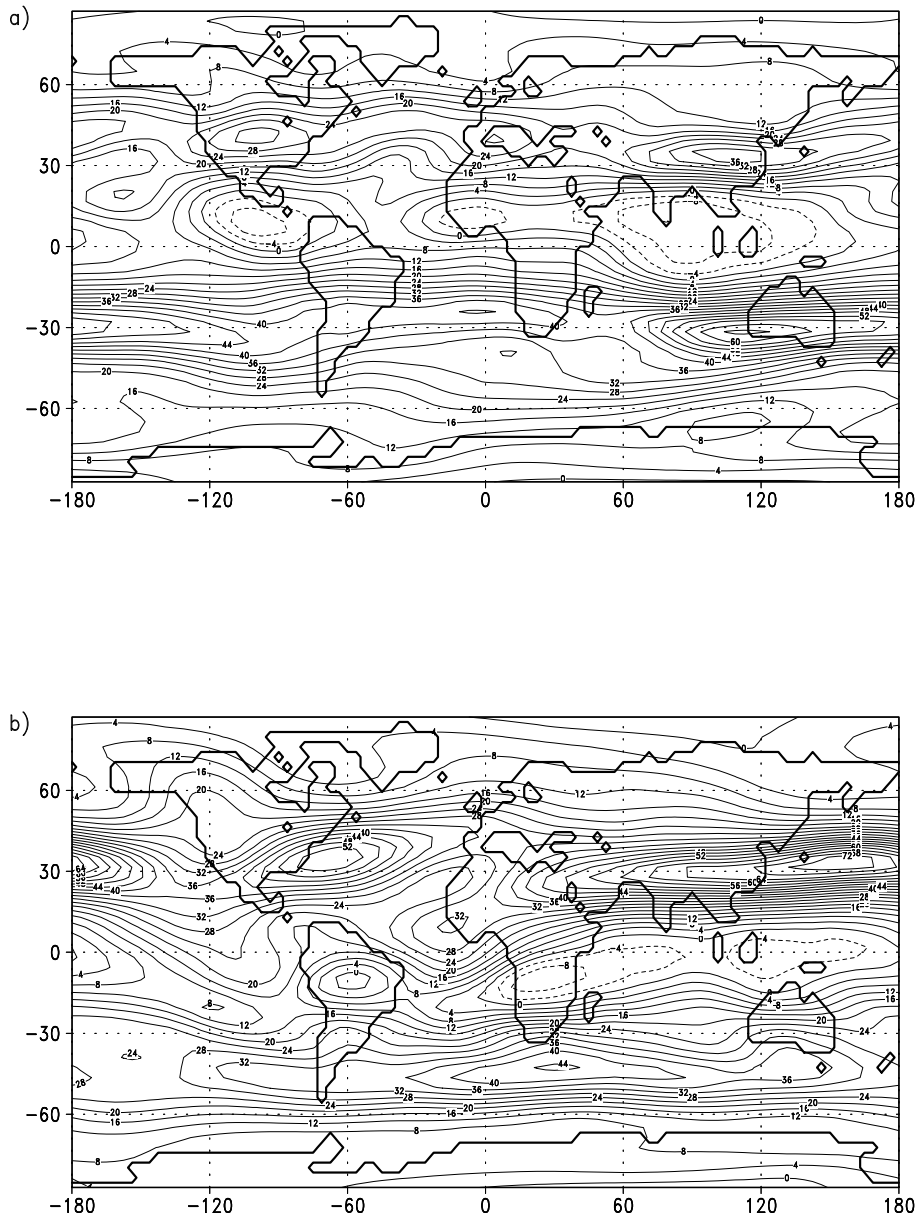

Figure B.6: *Zonal wind in 200 hPa height of Tortonian run for a) JJA b) DJF, and c) the year. Contour interval is 4 m/s.*

Appendix C

CLIMBER-2 - Standard Tortonian run

Figures C.1 to C.3 show the summer, winter, and annual means of the standard Tortonian run with regard to near surface temperature, total precipitation, and the oceanic streamfunction for the ocean basins.

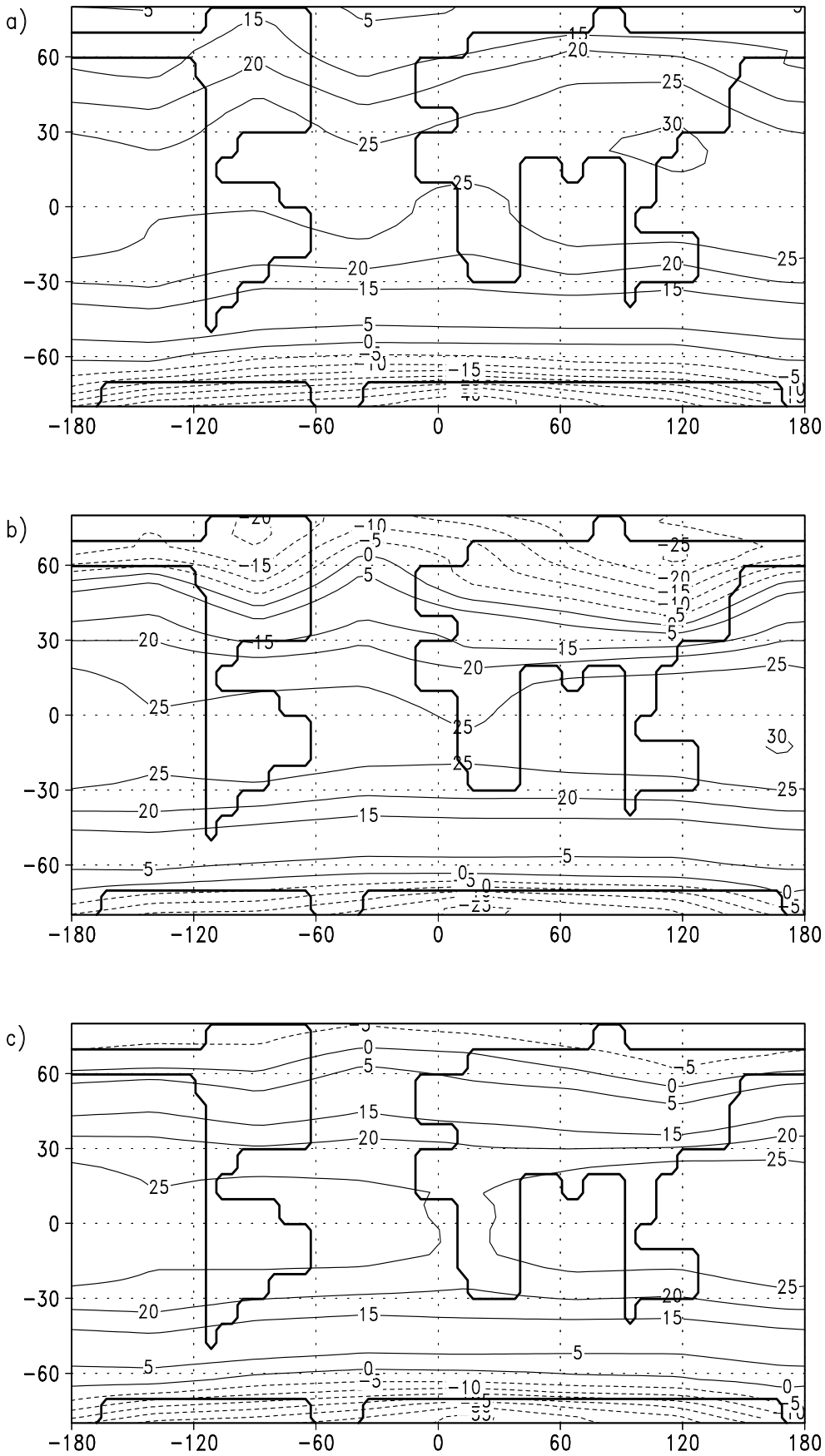

Figure C.1: *Near surface temperature of Tortonian run in ° C for a) JJA b) DJF, and c) the year. Contour interval is 5° C*

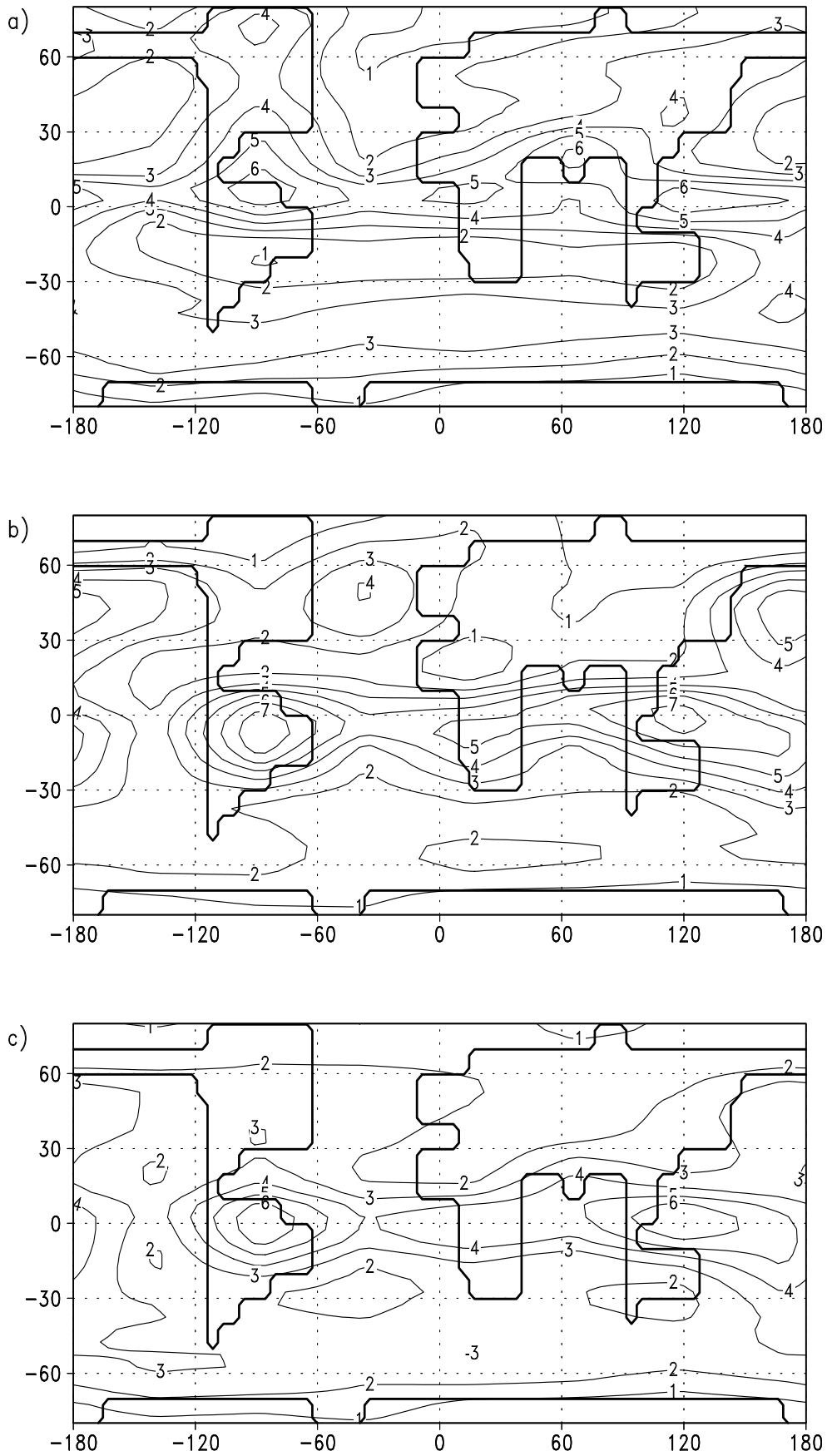

Figure C.2: *Total precipitation of Tortonian run in mm/d. a) JJA b) DJF, and c) the year. Contour interval is 1 mm/d.*

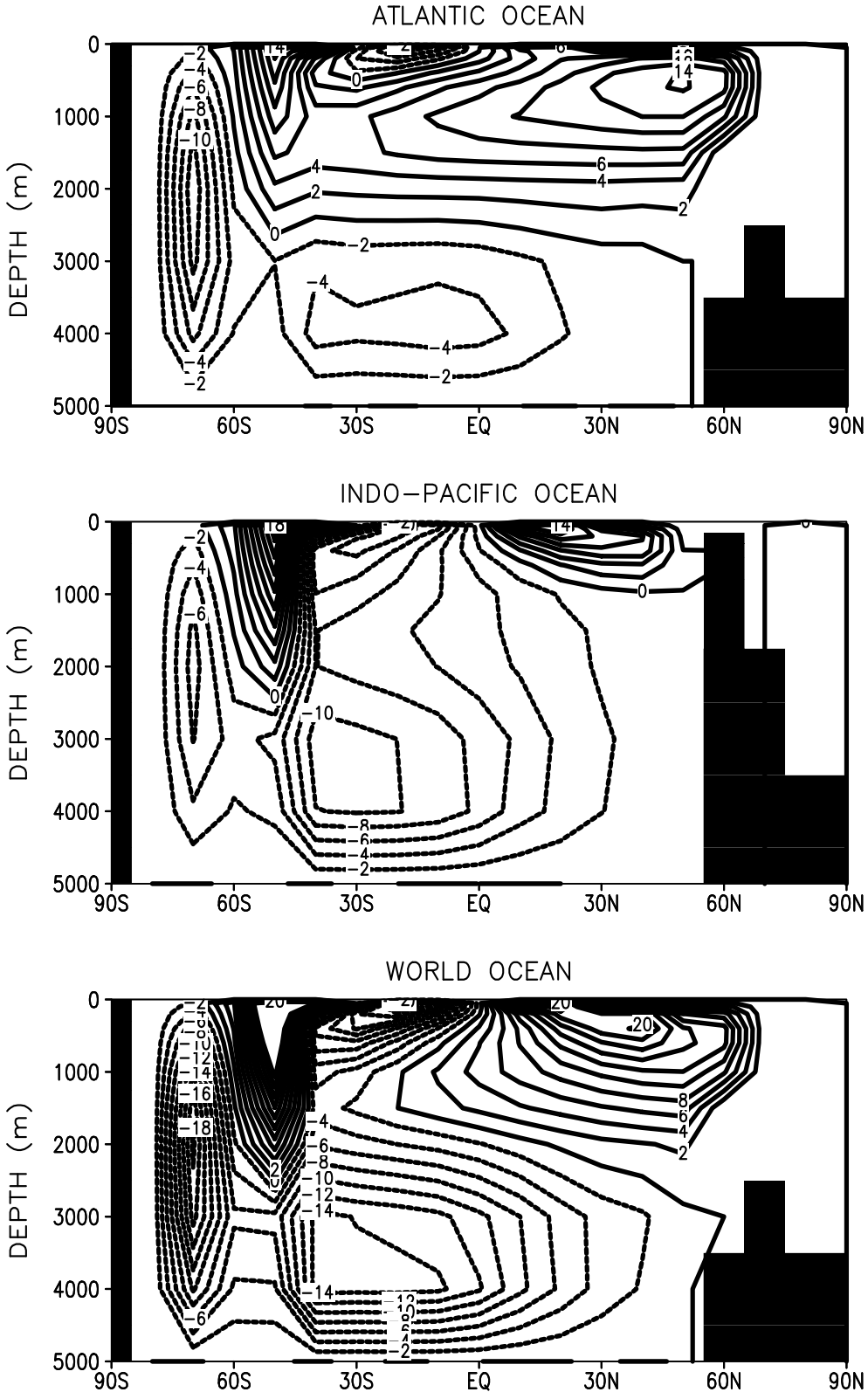

Figure C.3: *Streamfunction of Tortonian run in ° C for a) Atlantic Ocean b) Indo-Pacific Ocean, and c) the World Ocean. Contour interval is 2 Sv.*

Appendix D

List of Symbols

DJF		December, January, and February
c_o	J kg^{-1} K^{-1}	specific heat capacity of ocean water at constant pressure
C_o	J m^{-2} K^{-1}	effective heat capacity of the oceanic mixed-layer with depth h_o
$divT_o$	J m^{-2} s^{-1}	divergence of the oceanic heat transport corresponding to the depth h_o
f	s^{-1}	coriolis parameter
f_0		quotient of sea surface temperature gradients
FC	J m^{-2} s^{-1}	flux correction
$gradSST$	K m^{-1}	meridional sea surface temperature gradient
h_i	m	depth of ice sheet
h_o	m	depth of the oceanic mixed-layer
H_a	J m^{-2} s^{-1}	atmospheric heat flux at the sea surface
H_i	J m^{-2} s^{-1}	heat flux through the ice sheet of depth
JJA		June, July, and August
k	J m^{-1} s^{-1} K^{-1}	thermal molecular conductivity of the ice sheet with depth h_i
L_f	J kg^{-1}	latent heat of fusion of water
n		size of the sample of differences μ
p		significance level
R		measured isotope ratio
R_E	m	mean radius of the earth
S		sample variance of the differences μ

SST	K	sea surface temperature
t_S		Student t-Test Statistic
T	K	temperature
T_m	K	temperature of the oceanic mixed-layer
T_b	K	temperature at the bottom of the ice sheet
T_o	J m^{-1} s^{-1}	oceanic heat transport
T_s	K	skin temperature of the ice sheet
w_E	m s^{-1}	vertical velocity at the base of the Ekman-layer
x		longitudinal direction
y		latitudinal direction

β	m^{-1} s^{-1}	variation of Coriolis parameter with latitude
δ		reduced quotient of isotope ratios R
δ_c		δ^{18}O of carbonate relative to PDB
δ_w		δ^{18}O of ocean water relative to SMOW
λ	m	longitude
μ		mean difference of anomalous and control climate at one grid point
Ω	rad s^{-1}	earth's angular speed of rotation
ϕ	m	latitude
ρ	kg m^{-3}	density of atmosphere
ρ_i	kg m^{-3}	density of ice
ρ_o	kg m^{-3}	density of ocean water
τ	kg m^{-1} s^{-2}	wind stress
Ψ		horizontal streamfunction

Appendix E

List of CLIMBER sensitivity runs

Table E.1: *Short list of relevant CLIMBER runs. A=Atmosphere, O=Ocean, and V=Vegetation module (only selected runs are represented).*

time-slice	modules	CO_2 (in ppm)	"+" changed boundary conditions
Recent	AO	280	
Recent	AOV	280	
Recent	AO	353	
Recent	AOV	353	
Tortonian	AOV	280	
Tortonian	AO	353	
Tortonian	AO	$2 \cdot 353$	
Tortonian	AOV	353	
Tortonian	AOV	$2 \cdot 353$	
Tortonian	AO	353	boreal forests
Tortonian	AOV	353	Paratethys
Tortonian	AOV	353	Australian shift